

**MAGNETIC AND SEISMOLOGICAL INVESTIGATION OF RECENT EARTH
TREMOR IN PARTS OF NORTH CENTRAL NIGERIA**

BY

ALKALI, Aisha

PhD/SPS/2017/917

**DEPARTMENT OF PHYSICS
SCHOOL OF PHYSICAL SCIENCES
FEDERAL UNIVERSITY OF TECHNOLOGY,
MINNA**

MARCH, 2023

ABSTRACT

High resolution aeromagnetic data and Seismological data of parts of North Central Nigeria were analyzed and interpreted with the aim of detecting the source of the recent earth tremors in the area. The study area is bounded by latitude 9.00° to 10.00° N and longitude 7.00° to 9.00° E with an estimated total area of 24, 200km². The total magnetic intensity (TMI) of the study area was reduced to magnetic equator, Analytic signal and upward continuation techniques was applied to the RTE map. The TMI and the RTE map are characterized with high and low magnetic signature with the intensity ranging from 3377.1 to 33460.3 nT and 33094.659 to 32908.968 respectively with dominants structures trending NE-SW. Upward continuation techniques has been used in this study to locate prominent deep-seated anomalies, at 5 km the fault is deep-seated. The analytic signal reveals variations in the amplitude of the magnetic susceptibility of the rocks within the study area. Structural analyses (1VD, Horizontal, Tilt and CET derivative) were used in this study to locate the position of magnetic lineament (faults or fractures) within the area. Four major trends were observed NE-SW, NW-SE, E-W and NNE-SSW. The dominant trends are NW-SE and NNE-SSW within this area. The magnitude, epicenter and time of occurrence were determined using Seismological method. The origin time for the first event of Kwoi earthquake occurred on 11th September, 2016 at 12:28:16.50 seconds, the second event occurred on 12th September, 2016 at 03:10:48.80 seconds and the third event occurred on 12th September, 2016 at 03:11:20.00 seconds respectively. Magnitude of kwoi earth tremor was determined for three events, the first has a local magnitude of 2.8 and moment magnitude of 3.1, second event has local magnitude of 2.7 and moment magnitude of 3.0 and the third event has a local magnitude of 3.1 and moment magnitude of 3.1. The first and third event has a moment magnitude of 3.1. The epicentre was estimated to occurred at latitude 9.570° N and longitude 8.070° E for first event, latitude 9.640° N and longitude 8.180° E for second event and the third event at latitude 9.590° N and longitude 8.130° E. The magnitude of Abuja earth tremor was estimated with a main shock of local magnitude of 3.0, moment magnitude is 2.6. First and second aftershock, with a moment magnitude of 2.5 and local magnitude of 2.6, and a moment magnitude of 2.2 and local magnitude of 2.5. The epicenter for the first aftershock to be located at latitude 9.0339° N and longitude 7.5008° E. The Second aftershock was located at latitude 9.1620° N and longitude 7.4014° E. The main shock was located at latitude of 9.139° N and longitude 7.594° E. The origin time for the main shock of Abuja earthquake occurred in September and October 2018 at 5:11:32.60 seconds, the first aftershock occurred at 6:16:17.80 seconds and the second aftershock occurred at 7:12:18.40 seconds respectively. The Lineament map was superimposed on the epicenter map to identify the fault that coincides with the epicenter. Fault F5, F6 and F8 coincides with some of the epicenters corresponding to areas around Jaba, ZangonKataf, and part of Municipal area council. Fault F4 and F8 coincides with epicenter at Jema'a and Municipal area council, these are areas affected by earth tremor in 2016 and 2018. Therefore, the earth tremor activities within the study area are as a result of the effect of the emergence of these near surface faults

TABLE OF CONTENTS

Title	Page
Title page	i
Declaration	ii
Certification	iii
Dedication	iv
Acknowledgement	v
Abstract	vi
Table of Content	vii
List of Figures	viii
List of Plates	ix
List of Tables	x
CHAPTER ONE	1
1.0 INTRODUCTION	1
1.1 Background to the study	1
1.2 Location of the study Area	6
1.3 Statement of Research Problem	8
1.4 Aim and Objectives	8
1.5 Justification of the Research	9
CHAPTER TWO	10
2.0 LITERATURE REVIEW	10
2.1 Geology of Nigeria	10

2.2	The Basement complex of Nigeria	10
2.2.1	Rocks Types in Basement Complex	12
2.3	Geology of the study Area	12
2.4	Earthquake	14
2.4.1	Classification of Earthquakes	14
2.5	Faults	15
2.5.1	classification of Faults	15
2.6	Aeromagnetic Survey	16
2.6.1	The geomagnetic field	17
2.6.2	Earth's magnetic field	20
2.6.3	Data reduction	22
2.6.4	Application of magnetic surveying	22
2.7	Magnetic Lineament	23
2.8	Plate Tectonics	25
2.9	<u>Source parameters of earthquakes</u>	26
2.10	Seismic waves	27
2.10.1	Types of seismic waves	27
2.10.2	Phases of seismic waves	31
2.11	Geological Setting and Tectonic Activity	35
2.11.1	Significance of magnetic contours	36
2.11.2	Analysis of the magnetic Trends	36
2.11.3	Structural Trends	37
2.11.4	Previous Geophysics work in the Area	40

CHAPTER THREE	49
3.0 MATERIALS AND METHODS	49
3.1 Materials	49
3.1.1 Aeromagnetic Data Acquisition and Processing	49
3.1.2 Production of the unified Aeromagnetic map (Super map) of the study area	50
3.1.3 Seismological data acquisition and processing	50
3.2 Methodology	51
3.3 Explanation of Method	53
3.3.1 Production of the composite aeromagnetic map of the study area	53
3.3.2 Data Filtering	53
3.3.2.1 Reduction to magnetic equator	53
3.3.2.2 Upward Continuation	54
3.3.2.3 Horizontal derivatives	55
3.3.2.4 Vertical Derivative	56
3.3.2.5 Tilt Derivative	58
3.3.2.6 The Centre for exploration targeting (CET) grid Analysis	59
3.3.2.7 Analytical Signal	60
3.4 Seismic Instrumentation	61
3.4.1 Seismograph	62
3.4.2 Seismometer	64
3.4.3 Seismic Recorder	66
3.4.4 Seismic Signal Processing	68
3.5 Seismic Station Location	68

3.6	Seismic Data Analysis	69
3.6.1	Location of earthquake epicenter	69
3.6.2	Determination of magnitude	70
CHAPTER FOUR		
4.0	RESULT AND DISCUSSION	72
4.1	Results	72
4.1.1	Result of total magnetic intensity (TMI) map	72
4.2	Result of Reduced to equator (RTE)	75
4.3	Result of Upward Continuation	75
4.4	Result of Horizontal Derivative (Dx)	79
4.4.1	Result of Horizontal Derivative (Dy)	79
4.5	Result of First order Derivatives	86
4.6	Result of First order Derivative in Grey scale	86
4.7	Result of Tilt Derivative	89
4.8	Result of Centre for Exploration Targeting (CET) Grid Analysis	89
4.9	Result of Analytical Signal Map	92
4.10	Discussion	94
4.10.1	First vertical derivative (FVD) map compared with center for exploration Targeting (CET) map	94
4.10.2	Second vertical derivative map superimposed on the geology map	96
4.10.3	Structural geologic map compare with the center for exploration targeting map (CET)	96
4.10.4	Geology map compare with analytic signal map	99
4.10.5	Structural map superimposed on Lineament Map	99

4.11	Seismological Results	102
4.11.1	Source parameters of 2016 kwoi earthquake	102
4.11.2	Source parameters of 2018 Abuja earthquake	103
4.12	Discussion	103
4.12.1	Field site effects of the earthquake	103
4.12.2	Superimposing of lineament map on geology map showing the epicenter	104
CHAPTER FIVE		
5.0	CONCLUSION AND RECOMMENDATIONS	107
5.1	Conclusion	107
5.2	Recommendations	109
5.3	Contribution to Knowledge	108
REFERENCES		110
APPENDICES		116

LIST OF TABLES

Table		Page
1.1	Earthquake size classifications by magnitude	27
3.1	Earth model used for the location of the epicenter	70

LIST OF FIGURES

Figure		Page
1.1	Location map of the Area	7
2.1	Geological map of Nigeria showing the locations of seismological stations	11
2.2	Geological map of the Study Area	13
2.3	Elements of the Geomagnetic Field	18
2.4	Structural Geological map of the study area	24
2.5	Geological map of Nigeria showing the epicenters and fracture zones	28
2.6	Mode of Propagation of P-wave	30
2.7	Mode of propagation of S- wave	30
2.8	Mode of Propagation Rayleigh wave	32
2.9	Mode of Propagation of love wave	32
2.10	Ray path of seismic wave showing the various body wave phases	34
3.1	Seismogram of an earthquake recorded at IFE station	63
3.2	The principle behind the inertial seismometer	65
3.3	Schematic diagram of a digital process	67
3.4	Schematic diagram of a typical analog to digital conversion process	67
4.1	Total Magnetic Intensity Raster Map of the Study Area	73
4.2	Total Magnetic Intensity Map showing inferred fault lines	74
4.3	Total Magnetic Intensity Map of the study area-Reduce to Equator	76
4.4	2D (A and C) and 3D (B) Maps of Reduced to Equator shows a major	

	fault line cutting across the study area.	77
4.5	Upward continuation at 1 km	78
4.6a	Upward continuation at 2 km	80
4.6b	Upward continuation at 2 km in Grey-Scale	80
4.7	Upward continuation at 3 km	81
4.8a	Upward continuation at 5 km	82
4.8b	Upward continuation at 5 km in Gray-Scale	82
4.8c	Paleostructure zone's map	83
4.9a	Horizontal Derivative in x-direction map	84
4.9b	Horizontal Derivative in y-direction map	85
4.10a	First vertical derivative of the study Area	87
4.10b	First vertical Derivative in Grey-Scale	88
4.11	Tilt Angle Derivative of the Study Area	90
4.12	Center for Exploration Targeting (CET) map of the Study Area	91
4.13	Analytic signal map of the study Area	93
4.14	First vertical Derivative map compared with Center for Exploration Targeting (CET)	95
4.15	Geology map of the area on Second Vertical Derivative map	97
4.16	Structural Geologic map of the study area compared with the Center for Exploration Targeting (CET)	98
4.17	Geology Map compare with Analytic Signal Map	100
4.18	Structural map superimposed on lineament map	101
4.19	Superimposing of Lineament map on Geology map showing the	

Epicenter	105
-----------	-----

LIST OF PLATES

Plates	Title	Page
I	Damage caused by the 2016 Kwoi Earth tremor	3
II	Affected structures in Kwoi town, Nigeria, as a result of the 2016 earth tremor	4
III	Damage to buildings caused by an earthquake in Mexico earthquake	5
IV	Kaduna Seismological Station	52
V	Damage to a Mud Building in Kwoi town	106
VI	Collapse of Mud Building in Kwoi town	106
VII	Crack on a newly constructed building in Kwoi town	106

CHAPTER ONE

1.0

INTRODUCTION

1.1 Background of the Study

Seismology is defined as the study of the generation, propagation and recording of elastic waves in the earth and the sources that produce them (Stein and Wysession, 2003). It is the primary method for studies of earthquake and distribution of physical properties, which give detailed images of earth structure. It provides the basic data for understanding earth's dynamic history and evolution, including the process of mantle convection (Stein and Wysession, 2003).

An earthquake is the sudden release of built-up energy in the earth's lithosphere caused by movement of rocks along a fault (Lowrie, 2007). The energy released is in form of seismic waves which cause the ground to shake. Studies have shown that the greatest damage during an earthquake is usually around the epicenter which radiates seismic waves and travel throughout the earth (Stein and Wysession, 2003). Seismic wave is the transfer of energy through elastic earth materials by way of particle oscillation or vibrations which are generated at a source and can be natural, such as earthquake, or artificial, such as explosion. Earthquake is a global phenomenon experienced in many regions of the world; it is one of the most devastating natural disasters that pose threat and has the capability to impact negatively on human lives, economy and the built environment especially if the buildings are not designed to be earthquake-resistant. The impact of an earthquake in a nation can lead to a major setback in the development and economic status and this can even linger for years after the event had occurred (Akpan and Yakubu, 2010). Earthquake can be detected with modern instrument (seismometer)

mounted at a site on the globe known as seismic station for monitoring of earthquake. A seismogram is the record of the vibration of the ground resulting from the arrival of refracted, reflected and diffracted seismic waves at a receiver (Havskov and Ottemöller, 2010). Some of the causes of earthquake are: rupturing and shifting of rocks at tectonic boundaries, volcanic eruptions, landslides, mining-induced seismicity, underground nuclear explosions and nuclear tests (Thorne and Terry, 1995).

Over the years, several earthquakes occur throughout the world, varying in size from earth tremors that are perceptible only to sensitive instruments, to greater ones that cause considerable damage to buildings and injuries to humans. Earth tremors are earthquake of very shallow level. They cause minor damages such as the ones witnessed in Nigeria. The earthquakes that have so far occurred in Nigeria are earth tremors. The Nigeria landmass is not expected to be affected by naturally occurring earth tremors. This is because it is located far from the major earthquake zones of the world, as the nearest active plate boundary lies at the Mid-Atlantic Ridge (Osagie, 2008), and therefore considered a stable continental area. However, earth tremors have been felt over time in the country especially in the southwest part of Nigeria with magnitudes ranging from 4.3 to 4.5 (Akpan and Yakubu, 2010). The first widely reported occurrence of an earth tremor in Nigeria was in 1933 at Warri (Akpan and Yakubu, 2010). Earth tremors were also reported in 1939, 1963, 1964, 1984, 1990, 1997, 2000 and 2006 in the south-western and north-eastern parts of the country (Elueze, 2003; Akpan et al., 2014). Recently, earth tremor have been reported in Shaki town (2015) Elueze, 2003, and some towns in Rivers and Bayelsa States (2016) (Elueze, 2003). However, it should be noted that it was later discovered that some of these events were not earthquakes (Akpan et al., 2014).

In 2016 and 2018, earth tremors occurred in parts of North-Central Nigeria around Kwoi, Nok, SanbangDaji, and Chori Kaduna State and Gwarinpa, Wuse, Mpape,

Maitama areas of Abuja. Although the damage to structures were minor to moderate (plates I and II) when compared to earthquakes in other parts of the world (Plate III).



Plate I: Damage caused by the 2016 Kwoi earth tremor (Centre for Geodesy and Geodynamic, 2016)



Plate II: Affected structures in Kwoi town, Nigeria, as a result of the 2016 earth tremor

(Centre for Geodesy and Geodynamics, 2016).

An Earthquake Devastated Town



Plate III: Damage to buildings caused by an earthquake in Mexico earthquake (Osazuwa,
1985)

these earth tremors attracted the interest of researchers and policy makers as they were the first instrumentally recorded events within the continental landmass of Nigeria and occurred in areas where seismic activities were not expected. Therefore, the need to identify the sub-surface features responsible for the earthquakes using magnetic and seismological methods is the subject of this research work.

1.2 Location of the Study Area

The area where this study was carried out is located in north central part of Nigeria. It is bounded by latitude 9. 00° to 10. 00° N and longitude 7.00° to 9.00 ° E. The study area falls within parts of Kaduna, Nasarawa, Plateau, Niger States and the Federal Capital Territory (Figure 1.1). The study area is covered by eight (8) aeromagnetic data sheets of the Nigeria Geological survey Agency (NGSA) which include Bishini, Kachia, Kafanchaa, Naraguta, Abuja, Gitata, Jamaa and Kurra at a scale of 1:100, 000. The study area lies in the tropical climatic belt of Nigeria with distinct wet and dry seasons. The rainy season extends from March/April to around October/November the dry season starts around December to March. Average annual rainfall for Kaduna is 25.2 mm. Rainfall reaches a high peak in August. Temperatures vary between less than 15°C around December/January and 33°C in March/April. Vegetation consists of broad leaved savannah woodland. The land is open to the cultivation of vegetables and other food crops as well as for grazing by animals. The topography of the study area is characterized by pen plains with a landscape which is relatively flat and gentle slopes. Residents within this area are predominantly Jaba, Jema'a, Zangon Kataf, Kaura and Riyom their main occupations include farming, cattle rearing and trading across the area.

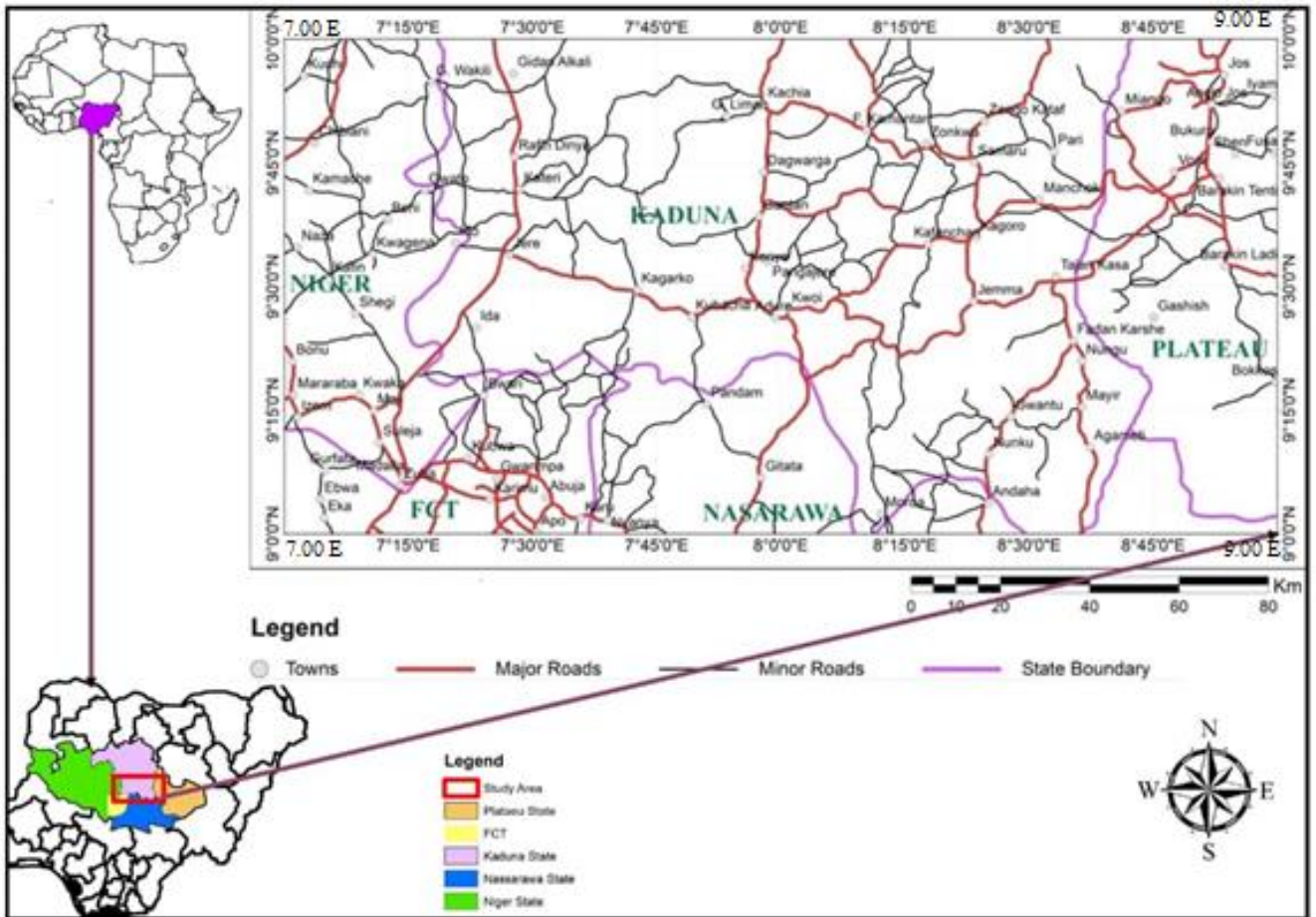


Figure 1.1: Location map of the study area

1.3 Statement of Research Problem

There was earth tremor in 2016 to 2018 in north central Nigeria which was the first intraplate earthquakes in Nigeria to be instrumentally recorded. It generated controversies on the likely causes of the tremors as they were attributed to a lot of factors which in some cases were not scientific. Though Nigeria does not lie on or near any plate tectonic boundary, there have been reports of seismic activities within the last 90 years especially in south-western part of Nigeria (Akpan and Yakubu, 2010). The installation of seismic equipment in some parts of Nigeria and availability of data has brought to the fore the need to carry out more research in earthquake seismology. Therefore, this research will attempt to properly identify the causes of these tremors.

1.4 Aim and Objectives

The aim of this research is to investigate the likely origins of the recent earth tremors in north central Nigeria using magnetic and seismological methods.

The objectives of the research are to:

- i. Produce the total magnetic composite map and perform upward Continuation of the total magnetic intensity map to locate prominent deep-seated anomalies within the study area;
- ii. Determine prominent structural trend and locate the position of magnetic lineament (faults or fractures) within the area;
- iii. delineate the paleo-fractures in the area;
- iv. Determine the magnitude, epicenter and time of occurrence of the earth tremors;
- v. Show the relationship between the fractures (faults) and epicenters of earth tremors in the area.

1.5 Justification of the Research

The occurrence of earth tremors in the study area caused wide scale destruction of properties and generated anxieties among the inhabitants of the area. This led to a major setback in the development and economic activities of the areas. It is therefore imperative that the subsurface structures in the study area be studied to ascertain the features that engender the earth tremors in the area. Therefore, this research will attempt to provide the required information to the relevant government agencies, policy makers and researchers with a view to mitigating the effects of this subsurface geohazard.

CHAPTER TWO

2.0 LITERATURE REVIEW

2.1 Geology of Nigeria

The geology of Nigeria is made of three major litho-petrological components, namely the Basement Complex, Younger Granites and Sedimentary Basins (Obaje, 2009). The Basement Complex, which is Precambrian in age, is made up of the Migmatite-Gneiss Complex, the Schist Belts and the Older Granites. The Younger Granites comprise several Jurassic magmatic ring complexes centered on Jos and other parts of North–Central Nigeria. They are structurally and petrologically distinct from the Older Granites. The Sedimentary Basins, containing sediment fill of Cretaceous to Tertiary ages, comprise the Niger Delta, the Anambra Basin, the Lower, middle and Upper Benue Trough, the Chad Basin, the Sokoto Basin, the Mid- Niger (Bida-Nupe) Basin and the Dahomey Basin (Obaje, 2009). The seismological stations used for this study are located in the basement complex and sedimentary basins. Figure 2.1 shows the location of seismological station in Nigeria.

2.2 The Basement Complex of Nigeria

The Nigerian Basement Complex forms part of the Pan African mobile belt and lies between the Congo Craton and south of the Taureg Shield (Obaje, 2009). The Nigerian Basement complex forms a part of the West African Congo Craton and underlies about 60% of Nigeria's land mass (Obaje 2009). Basement complex has been described by Rahaman (1988), as a heterogeneous assemblage which includes rocks of the migmatites, gneisses schists and a series of basic to ultrabasic metamorphosed rocks. Pan African Granites and other minor intrusions such as Pegmatite, Aplites dykes, basalt and quartz veins have intruded these rocks.

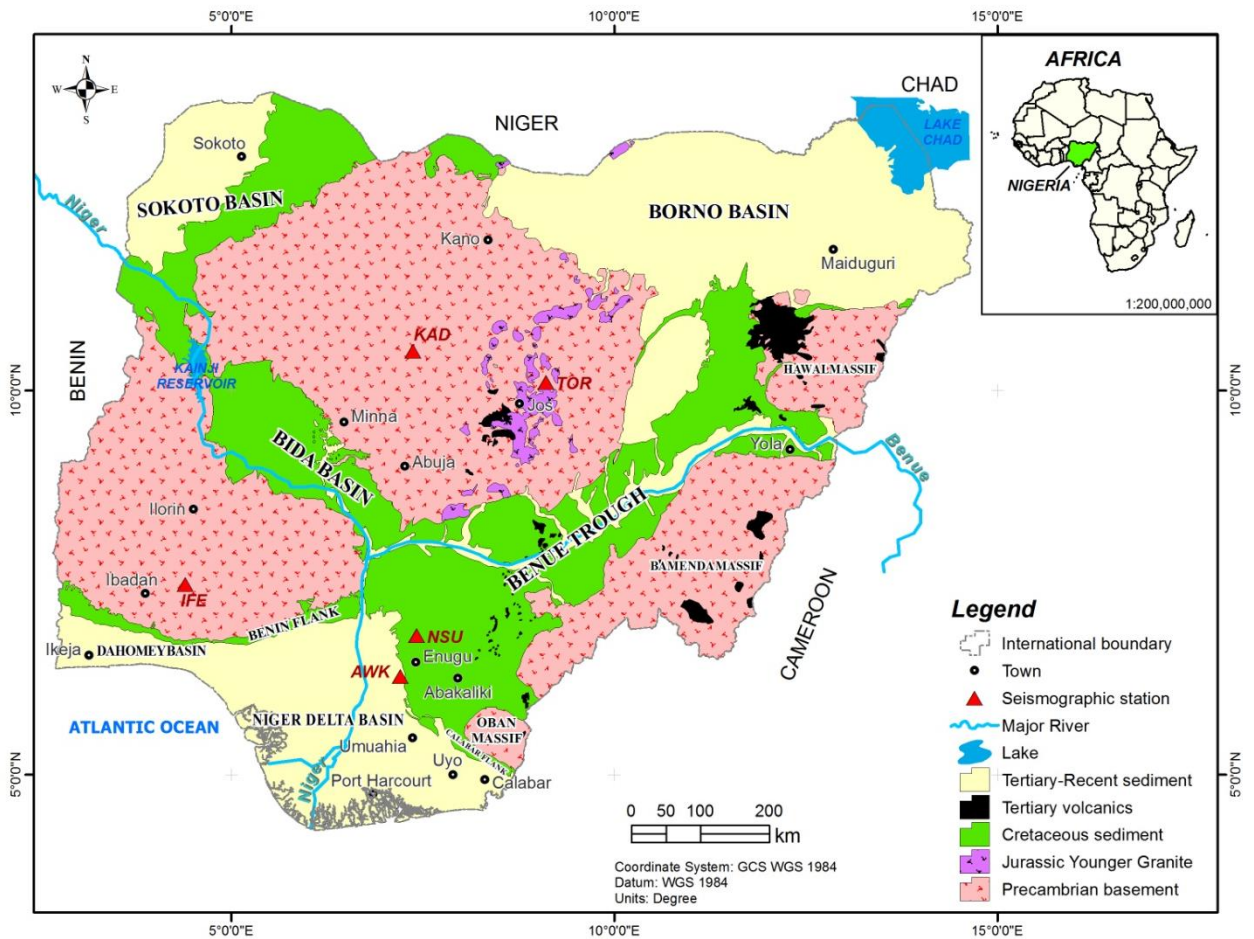


Figure 2.1: Geological map of Nigeria showing the locations of seismological stations (Nigeria Geological Survey Agency, 2009)

The Nigerian basement was affected by the 600 Ma Pan African Orogeny and occupies the reactivated region which resulted from plate collision between the passive continental margins (Burke and Dewey, 1972; Dada, 2006). The basement rocks are believed to be the result of at least four major orogenic cycles of deformations, metamorphism and remobilisation corresponding to the Liberian (1100 Ma), and the Pan African cycles (600 Ma) (Obaje, 2009).

The Pan African deformation was accompanied by a regional metamorphism, migmatitisation and extensive granitisation and gneissitisation which produced syntectonic granites and homogeneous gneisses (Abaa, 1983). Late tectonic emplacement of granites and granodiorites and associated contact metamorphism accompanied the end stage of this last formation. The Basement Complex is intruded by the Mesozoic calc-alkaline ring complex known as the Younger Granites.

2.2.1 Rocks types in basement complex

The Basement Complex of Nigeria comprises of four major petro-lithological units, namely:

- (1) The Migmatite-Gneiss Complex (MGC)
- (2) The Schist Belt (Metasedimentary And Metavolcanic Rocks)
- (3) The Older Granites (Pan African Granioid)
- (4) The Undeformed Acid and Basic Dykes

2.3 Geology of the Study Area

The study area Figure 2.2 lies entirely within the Basement complex Terrain of Nigeria. Migmatites are the most predominant rock types identified in the map which almost covered the entire area, with the undifferentiated Schists phyllites occurring around NE-SW of the study area. The Basaltic rock intruded into the porphyritic granite, coarse porphyritic biotite and biotite hornblende granite rock around the NE portion of the map.

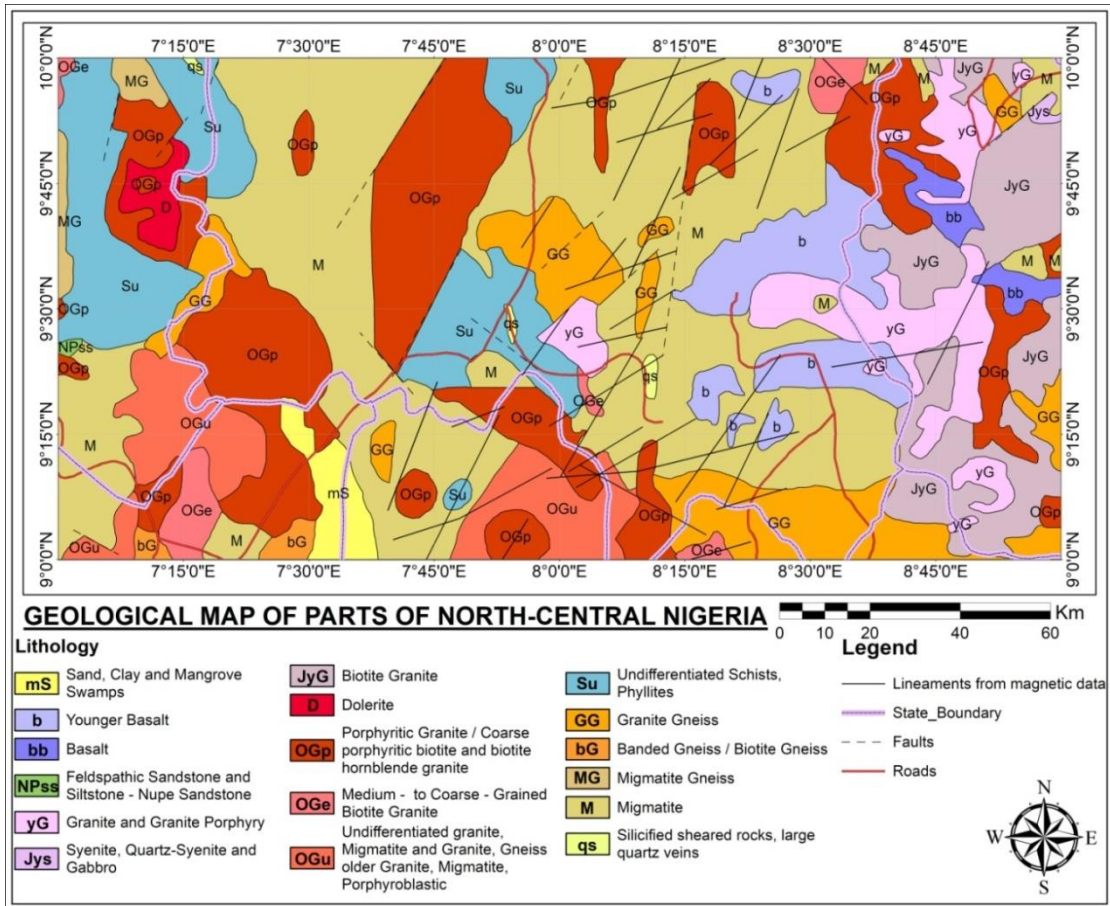


Figure 2.2: Geological Map of the Study Area (Adopted from Nigeria Geological Survey Agency, 2006)

Younger Basalt are found at the NE part of the map with isolated occurrence of other types of rocks which are undifferentiated older granite, Dolerite, Granite Gneiss, medium to coarse grained biotite granite. The structural elements in the map Figure 2.2 include faults, lineaments, some of the faults lines on the map are deep-seated in origin and ancient in age and was as a result of thermotectonic deformational events mostly of the Ebumean and Pan-African Orogeny. The domain structural trend in the basement is essentially NE-SW and follows the tectonic grain of the schist belt Olasehinde *et al.* (1990). Widespread fracturing occurs throughout the area and follows the orientation of the major faults generally intruded by the Pan African older Granite rocks, like Biotite Granite, medium - to coarse - grained biotite granite, undifferentiated granite, migmatite and granite, gneiss, Migmatite porphyroblastic and porphyritic Granite/coarse porphyritic biotite and biotite homblende granite. The rocks of the study area have undergone various episodes of deformation and have ages ranging from Precambrian to Pan African, the Basaltic rocks are the intruded rocks that have very high magnetic susceptibility.

2.4 Earthquake

An earthquake is the sudden release of built-up energy in the earth's lithosphere caused by movement of rocks along a fault (Lowrie, 2007).

2.4.1 Classification of earthquakes

Earthquakes can be classified as tectonic, volcanic, or man-made (Havskov and Ottemöller, 2010).

- (i) Tectonic earthquakes are by far the most devastating earthquakes and occur mainly at the boundaries of the world's major tectonic plates.
- (ii) Volcanic earthquakes are earthquakes that are triggered by volcanic eruption.

(iii) Human-induced earthquakes are those induced by human activities such as blasting of rocks, building of dams, nuclear explosions, mine burst, injection of fluid into oil wells.

Earthquake can also be classified based on focal depth as shallow, intermediate and deep earthquake (Havskov and Ottemöller, 2010).

1. Shallow focus earthquakes occur mainly in the ocean ridges, continental rifts and ocean trenches, focal depth is between 0-70 km. Shallow focus earthquakes account for about 85% of the total amount release of seismic energy. Oceanic ridges are responsible for about 10% of this amount while the ocean trenches accounts for the rest.
2. Intermediate earthquake occur in the ocean trenches, the focal depth is between 70 -300 km.
3. Deep earthquakes occur in the ocean trenches with focal depth of 300-700 km.

2.5 Faults

Faults can be divided into several different types depending on the direction of relative displacement or slip on the fault. Most faults make an angle with the ground surface, and this angle is called the dip angle. If the dip angle is 90° the fault plane is vertical. If the movement is lateral in the horizontal plane, then the fault is a strike-slip fault, where the hanging wall is lowered or downthrown relative to the footwall, the fault is a normal fault, the opposite case, where the hanging wall is upthrown relative to the footwall, is a reverse fault (Fossen, 2010).

2.5.1 Classification of faults

Faults can be divided into two major classes (Fossen, 2010).

- i. **Dip Slip Faults:** Dip Slip Faults are faults that have an inclined fault plane and along which the relative displacement or offset has occurred along the

dip direction. For any inclined fault plane the block above the fault is the hanging wall block and the block below the fault is the footwall block

- ii. Strike Slip Faults: are faults where the displacement on the fault has taken place along a horizontal direction. Such faults result from shear stresses acting in the crust.

2.6 Aeromagnetic Survey

The study of the earth's magnetism is the oldest branch of Geophysics. It has been known for more than three centuries that the earth behaves as a large and somewhat irregular magnet. Sir Williams Gilbert (1540 -1603) made the first scientific investigation of terrestrial magnetism. He showed that the earth's magnetic field was equivalent to that of a permanent magnetic lying in a general North-south direction, near the earth's rotational axis (Telford *et al.*, 2002).

The aim of a magnetic survey is to investigate earth subsurface on the basis of anomalies in the earth's magnetic field resulting from the magnetic properties of the underlying rocks. Magnetic survey can be carried out on land, at sea and in the air. Consequently, the technique is widely employed and the speed of operation of air borne surveys makes the method very attractive in the search for types of ore deposit or geological structures. Majority of the magnetic surveys are carried out in the air. Aeromagnetic surveying is rapid and cost effective, typically costing some 40% less per line kilometer than a ground survey (Kearey and Brookes, 1991). Vast areas can be surveyed rapidly without the cost of sending a field party into the survey area and data can be obtained from areas inaccessible to ground survey (Telford *et al.*, 2002). The most difficult problem in airborne survey is position fixing. The Electronic equipment used for positioning is the "ground positioning systems" (GPS) is available otherwise it is necessary to use aerial photography. Terrain photographs are taken simultaneously

with the magnetic readings so that the location can be subsequently determined by reference to maps (Siddorn, 2011).

2.6.1 The geomagnetic field

Magnetic anomalies caused by rocks are localized effects superimposed on the normal magnetic field of the earth (Kearey and Brookes, 1991). Consequently, the knowledge of the behavior of the geomagnetic field is necessary in both reductions of magnetic data to a suitable datum and in interpretation of the resulting anomalies. The geomagnetic field is geometrically very complex and exhibits irregular variations in orientation, magnitude, latitude, longitude and time.

At any point on the earth's surface, a freely suspended magnetic needle will assume a position in space in the direction of ambient geomagnetic field. This will generally be an angle to both the vertical and geographic north.

To describe the magnetic vector field, descriptors are used known as the geomagnetic elements (Figure 2.3). The total field vector F_e has a vertical component Z_e , and a horizontal component H_e (Separated into X and Y projections) in the direction of magnetic north. There are two important types of measurement relating to the earth's magnetic field as described below;

- (a) The angle of declination (D) which is the angle between observed compass reading (magnetic north) and the geographic longitude (true North).
- (b) The angle of inclination (I), which refers to the angle of dip of a magnetized needle relative to the horizontal. The angle varies from 90° at the magnetic poles to 0° at the equator. The geomagnetic field is often divided into three in relation to geophysics (Telford *et al.*, 2002). These three parts are:

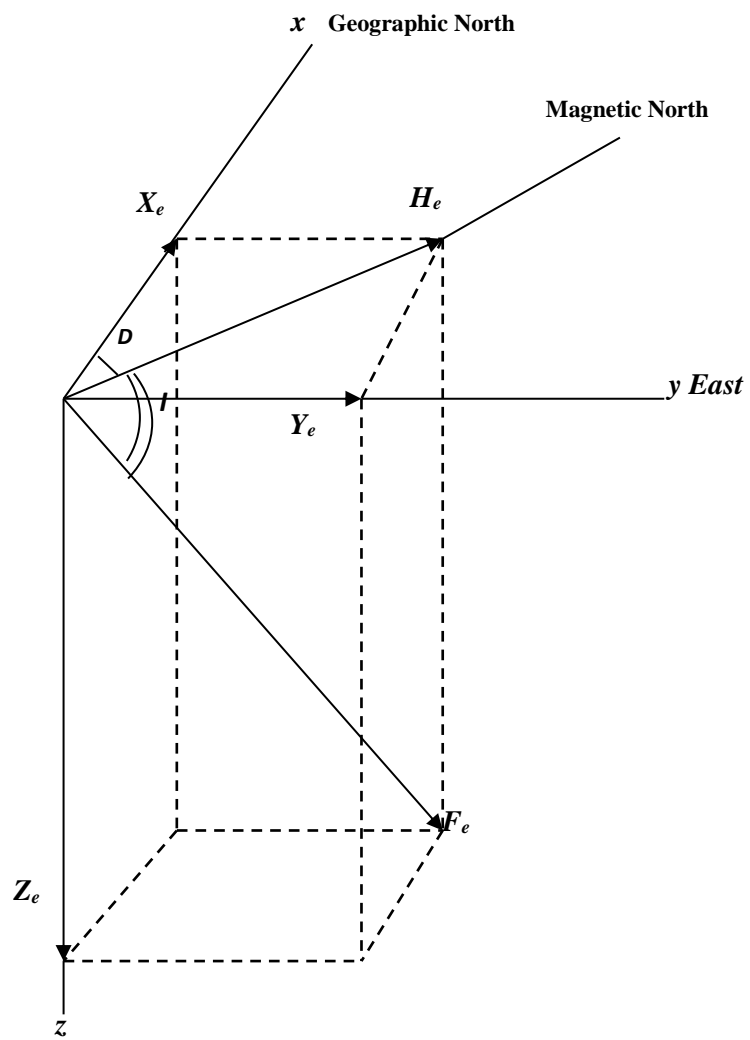


Figure 2.3: Elements of the Geomagnetic Field

The quantities X, Y, Z, D, I, H and F, are known as magnetic elements and are

$$H = F \cos I \quad (1.1)$$

$$Z = F \sin I \quad (1.2)$$

$$\frac{Z}{H} = \tan I \quad (1.3)$$

$$X = H \cos D \quad (1.4)$$

$$Y = H \sin D \quad (1.5)$$

$$\frac{X}{Y} = \tan D \quad (1.6)$$

$$H^2 + Z^2 = F^2 \quad (1.7)$$

$$H^2 = X^2 + Y^2 \quad (1.8)$$

$$F^2 = X^2 + Y^2 + Z^2 \quad (1.9)$$

Where F = Total field, Z = Vertical component of the geomagnetic field, H = Horizontal component of the geomagnetic field, F = Earth's main Magnetic Field

D = angle of declination and I = angle of inclination.

- i. **The Main Field:** This is the major part of the geomagnetic field. It accounts for about 95% of the total geomagnetic field. This field is not constant with time but the variation is very slow. Several theories attribute its origin to electrical currents circulating in the outer core of the earth and it accounts for large scale regional variation in intensity and direction.
- ii. **The External Field:** The external field is a small fraction of the main field, about 1-5% of the total geomagnetic field. It varies rapidly and sometimes randomly as compared with the main field. Its origin is outside the earth. Its variations include sunspot cycle (11 years), solar diurnal variation (about 24 hours with amplitude of about 30 gammas) and lunar diurnal variation (about 25 hours with amplitude of

about 2 gammas) (Telford *et al.*, 2002). It is also characterized by magnetic storm which is often transient and erratic with amplitude of up to 1000 gamma. It is thought to originate from the outside of the earth and it affects magnetic prospecting data (Telford *et al.*, 2002).

- iii. **Variation of the Main Field:** This is often called the anomalous field. Variation in the main field is said to be caused by variations in the mineral content of the near surface rocks (Telford *et al.*, 2002). These anomalies are usually smaller than the main field but may occasionally be large enough to double the main field. The variations are relatively constant in space and time and are restricted to the upper part of the crust since the temperatures at depth beneath the crust should be very much higher than their curie temperatures (Telford *et al.*, 2002). They do not persist over great distances. The variation in the main field is often the target of magnetic exploration in applied geophysics. In magnetic prospecting, instruments exist that can measure any of the components H_e or Z_e . Most aeromagnetic instruments measure the total field, F_e . These include the Proton Precession Magnetometer and the Optical Pump Magnetometers. In this aeromagnetic study, only the total field is dealt with.

2.6.2 Earth's magnetic field

The earth's magnetic field is generated in the fluid outer core by a self-exciting dynamo process produced by the circulation of charged particles in coupled convection cells within the outer fluid part of the earth's core (Campbell, 2003). The exchange of dominance between such cells is believed to produce the periodic changes in polarity of the geomagnetic field revealed by palaeomagnetic studies. The circulation patterns within the core are not fixed and change slowly with time. Electric currents flowing in the slowly moving molten iron generate the magnetic field. In addition to sources in the

earth's core the magnetic field observable at the earth's surface has sources in the crust and in the ionosphere and magnetosphere. The geomagnetic field varies on a range of scales and a description of these variations is now made, in the order low frequency to high frequency variations, in both the space and time domains. There are three major types of variations they are; Diurnal, Secular and Magnetic storms variation (Sharma, 1987)

- (i) Diurnal variation: Magnetic effects of external origin cause the geomagnetic field to vary on a daily basis to produce diurnal variations. Diurnal variation is smooth and regular and has an amplitude of about 20-80 nT, being at a maximum in polar regions such variation results from the magnetic field induced by the flow of charged particles within the ionosphere towards the magnetic poles. As both the circulation patterns and diurnal variations vary in sympathy with the tidal effects of the sun and moon.
- (ii) Secular variation: The circulation patterns within the core are not fixed and change slowly with time. This is reflected in a slow, progressive, temporal change in all the geomagnetic elements and is known as secular variation. Such variation is predictable and a well-known example is the gradual rotation of the north magnetic pole around the geographic pole.
- (iii) Magnetic storms: These disturbances are caused by the interaction of the solar wind, and disturbances therein, with the Earth's magnetic field. The solar wind is a stream of charged particles continuously emitted by the sun and its pressure on the earth's magnetic field creates a bounded comet-shaped region surrounding the Earth called Magnetosphere. When there is a disturbance in the solar wind the current systems existing within the magnetosphere are enhanced and caused magnetic disturbances and storms.

2.6.3 Data reduction

This is the removal of all other causes of magnetic variations from the recorded values other than that caused by the magnetic effect of the subsurface. Three kinds of corrections are normally carried out in a magnetic data. These corrections are diurnal variation correction. Geomagnetic correction, elevation and sometimes terrain correction. In addition, a model such as international geomagnetic reference field (IGRF) is used to remove the non-crustal effects from the data (Dobrin and Savit, 1988).

2.6.4 Application of magnetic surveying

The major use of magnetic surveying is to aid in geo- mapping. It can also be used to provide information on geological structures at all scales (Sharma, 1987) while Udensi (2001) outlined the roles of aeromagnetic survey as follows:

- i. Delineation of volcano-sedimentary belts under sand of other recent cover, or in strongly metamorphosed terrains when recent lithologies are otherwise unrecognisable.
- ii. Recognition and interpretation of faulting, shearing and fracturing not only as potential hosts for a variety of minerals, but also an indirect guide to epigenetic, stress related mineralisation in the surrounding rocks.
- iii. Identification and delineation of post-tectonic intrusive. Typical of such targets are zoned syenite or carbonite complexes, kinerlites, tin-bearing granites and mafic intrusions.
- iv. Direct detection of deposits of certain ores.
- v. In prospecting for oil, aeromagnetic data can give information from which one can determine depths to basement rocks and thus locate and define the extence of sedimentary basins.

2.7 Magnetic Lineament

Magnetic lineament is a major topographical feature or geological structure that could be of regional extent usually in linear or curvilinear, continuous or discontinuous over an entire length. It may be faults, joints, folds, contacts or other geological features, and are found in igneous, sedimentary and metamorphic rocks. While working on the central part of Nigeria, Ajakaiye *et al.* (1991) noted that magnetic feature in that area are mainly magnetic lineaments with definite characteristics which exist within the Nigeria landmass. The lineaments, they noted, coincided with the major structural trends such as the Benue Trough in Nigeria and fractures in the oceanic crust of West Africa. They stated that on-shore lineaments in the West Africa are extensions of St. Paul, Romanche, Chain, and Charcot fracture zones in the Mid-Atlantic Ocean. Lineaments are thus believed to be major zones of weakness in the crust that predate the opening of the Atlantic Ocean and were reactivated in the early stages of continental drift and early development of Atlantic fracture zones (Ajakaiye *et al.*, 1985).

The Geologic Structural Map of the study area is shown in Figure 2.4 where the major fracture/fault is trending along the NE-SW direction and most of the minor fracture is scattered throughout the map.

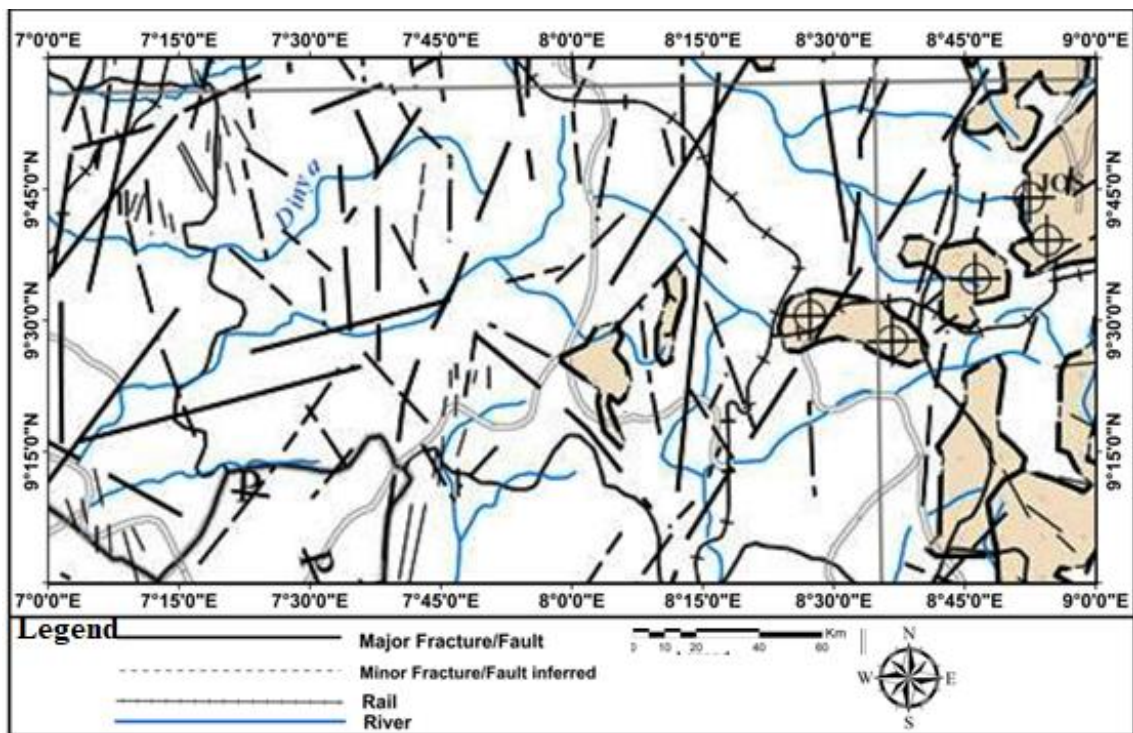


Figure 2.4: Structural Geologic Map of the study area (NGSA, 2006)

2.8 Plate Tectonics

Plate tectonics is related to earthquake in term of distribution and motion of the plate. The plates are rigid in the sense that little or no deformation occurs within them while deformations occur at their boundaries giving rise to earthquakes, mountain building, volcanism, and other spectacular phenomena (Stein and Wysession, 2003). The lithosphere, the rigid outermost shell of a planet (the crust and upper mantle), is broken into tectonic plates. The earth's lithosphere is composed of major plates describing the large-scale motion of large plates and the movements of a larger number of smaller plates of the Earth's lithosphere where the plates meet, their relative motion determines the type of boundary: convergent, divergent, or transform (Stein and Wysession, 2003). Earthquakes, volcanic activity, mountain-building, and oceanic trench formation occur along these plate boundaries (or faults).

The relative movement of the plates typically ranges from 0 to 100 mm annually. Tectonic plates are composed of oceanic lithosphere and thicker continental lithosphere. The lateral movement of the plates is typically at speeds of 0.66 to 8.50 centimetres per year. These plates move in relation to one another at the three plates boundaries.

The different types of plate boundaries are:

1. Convergent boundaries (or active margins) occur where two plates slide towards each other commonly forming either a subduction zone (if one plate moves underneath the other) or a continental collision- (if the two plates contain continental crust). Deep marine trenches are typically associated with subduction zones. Because of friction and heating of the subduction slab, volcanism is almost always closely linked. Such as Andes Mountain range in South America and the Japanese.

2. Divergent boundaries occur where two plates slide apart from each other and a new lithosphere is produced or an old lithosphere is thinned. (Examples of which can be seen at Mid- Ocean ridges and active zones of rifting (such as East Africa rift and continental rifts.
3. Transform boundaries occur where plates move past one another and the lithosphere is neither created nor destroyed. An earthquake activity on an oceanic ridge is confined almost entirely to the transform fault between ridge crests where the plates slide past each other. Examples are San Andreas Fault and Anatolia Fault.

2.9 Source Parameters of Earthquakes

Epicentre, magnitude, origin time and fault plane solution are important parameters reported after the occurrence of an earthquake (Havskov and Ottemöller, 2010). Generally, earthquakes are assumed to originate from a point some kilometres beneath the surface of the Earth (usually not more than 700 km) known as the origin, focus, or hypocentre (Lowrie, 2007; Kearey *et al.*, 2009). However, most earthquakes are initiated by movement along a fault; the focal area may extend for many kilometres (Lowrie, 2007). The epicentre is the point on the surface of the Earth (latitude and longitude) vertically above the hypocentre (Lay and Wallace, 1995; Lowrie, 2007; Havskov and Ottemöller, 2010). Magnitude is the relative size of an earthquake. Different types of magnitude are computed in an event depending on the type of event, there are classified as follows (Havskov and Ottemöller, 2010). : Local Magnitude M_L , Body wave magnitude M_b , Coda Magnitude M_c , Broad band body-wave magnitude M_B , Surface wave Magnitude M_s , Broad band surface- wave magnitiude M_S and Moment magnitude M_w . Table 1.1 describes the earthquake size and the magnitude.

Table 1.1 Earthquake size classifications by magnitude

Size Classification	Magnitude
Great	M.> 8
Large	M=6-8
Medium	M = 4-6
Small	M= 2-4
Micro	M<2

The time of occurrence of an earthquake is usually the time that an earthquake occurs. Figure 2.5 shows the geological map of Nigeria showing epicentres and fracture zones in Nigeria.

2.10 Seismic Waves

2.10.1 Types of seismic waves

Seismic waves are seismic energy propagated as waves caused by the sudden breaking of rock within the earth or an explosion (Lawrence, 2007). When an earthquake occurs, seismic waves generated at the origin, or hypocentre (the source) propagate through the medium (the Earth) and are recorded at the receiver (the seismological station) located at the Earth's surface (Stein and Wysession, 2003; Kearey *et al.*, 2009). A seismogram, the record of ground motion as a function of time at the receiver therefore contains information about the source, the medium of propagation and the receiver (Stein and Wysession, 2003). Body wave is a wave that travels through the Earth's interior and

consist of two types corresponding to the two ways in which a solid medium deforms (Kearey *et al.*, 2009). These include: the P-waves and S-waves.

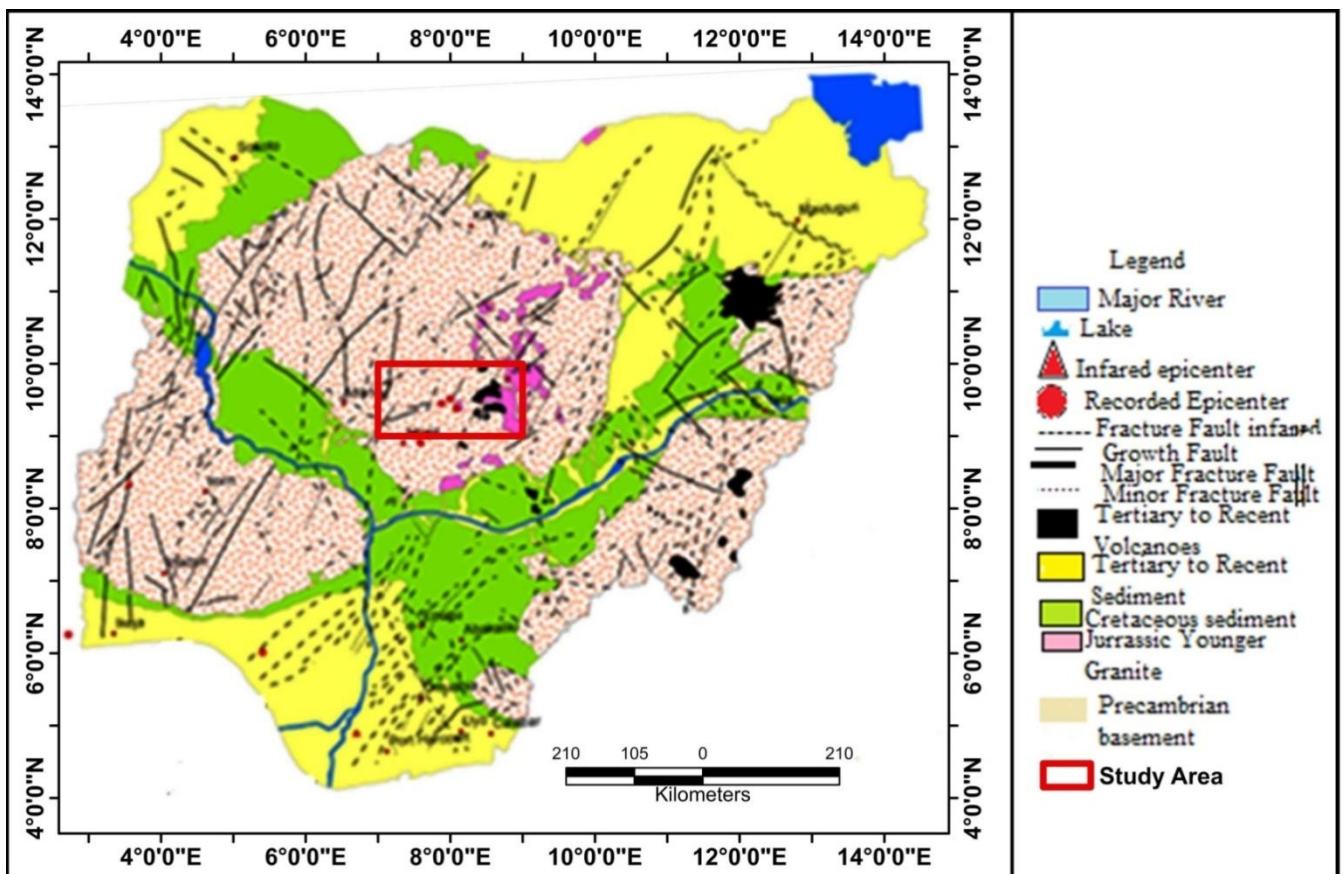


Figure 2.5: Geological map of Nigeria showing epicenters and fracture zones (Modified from Akpan and Yakubu 2010)

A P-wave (also called primary or longitudinal or compressional wave) corresponds to elastic deformation by compression and dilation. P-wave deforms or moves the ground in the same direction as the direction in which the wave travels (Figure 2.6). A P-wave can move through solid rock and fluids, like water or the liquid layers of the earth and travels faster than the other waves and is always the first to arrive a seismological station. The S-wave or transverse wave (also called secondary or shear wave) corresponds to elastic deformation of the transmitting medium by shearing without any volumetric change (Kearey *et al.*, 2009). The particle motion is perpendicular to the direction of wave propagation (Figure 2.7). S-waves cannot travel through fluids because fluids cannot support shear. The S-wave is the second wave to arrive a seismological station. Its speed is about 60 percent that of the P-wave. Surface wave is produced when body waves interact with the surface of the Earth, its travel path is restricted to the Earth's surface (Kearey *et al.*, 2009). Its mode of propagation is parallel to the surface of the Earth and the amplitude decreases with the distance from the surface (Udías, 1999). It travels at lower velocities than the body waves in the same medium and so arrive at a seismological station later than the body waves. Surface waves are classified into the Rayleigh wave and Love wave, which were named after the mathematicians who developed the early theoretical descriptions of the wave, Lord Rayleigh in 1885 and A. E. H. Love in 1911 respectively (Lay and Wallace, 1995; Lowrie, 2007).

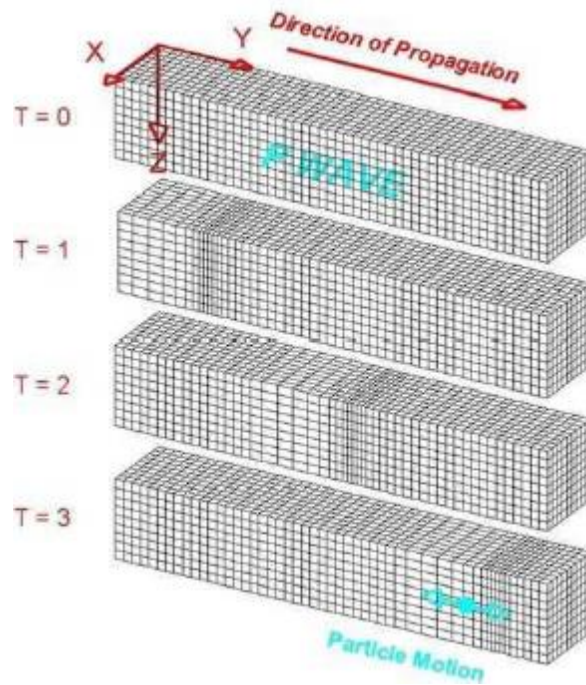


Figure 2.6: Mode of propagation of P-wave. The particle motion which comprises alternating compression [contraction] and dilation [expansion] is travelling in the direction in which the wave propagates) (Lay and Wallace, 1995).

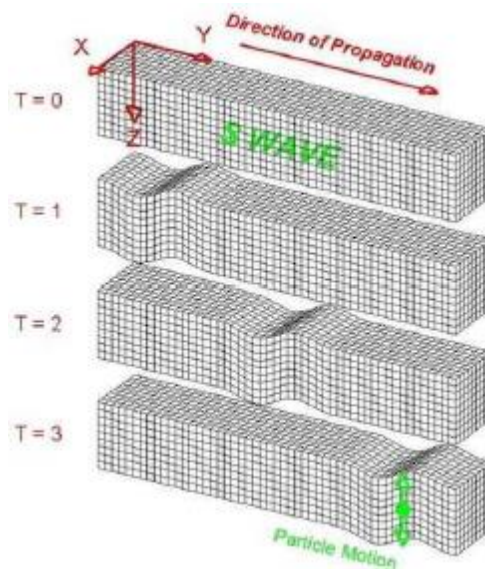


Figure 2.7: Mode of propagation of S-wave. (The ground motion which consist of alternating transverse motion is perpendicular to the direction in which the wave propagates) (Lawrence, 2007)

Rayleigh wave results from the interaction of incident P and SV (shear waves with displacement in a vertical plane, also called vertical shear) waves with the surface of the Earth (Lay and Wallace, 1995). The ground deformation produced by Rayleigh waves is similar to motions induced by the passage of an ocean wave before it breaks. The motion of the ground is up and down and is in the direction in which the wave is propagating such that the ground seems to move in a retrograde elliptical trajectory i.e. particles move in a direction opposite that in which the wave propagates Figure 2.8 (Lowrie, 2007; Kearey *et al.*, 2009). On the contrary, Love wave is an S-wave that vibrates the ground horizontally perpendicular to the wave direction Figure 2.9 (Stein and Wysession, 2003). It exists because the S-wave interacts with the surface of the Earth. It is essentially SH wave (horizontally polarized shear wave). A very important property of surface wave is its dispersion, that is, the different frequencies of the wave signal travel at different velocities; therefore, speed is a function of frequency or period.

2.10.2 Phases of seismic waves

Due to the spherical structure of the interior of the Earth, body waves propagate between the source and the receiver along multiple paths (Stein and Wysession, 2003; Havskov and Ottemöller, 2010). This result in the seismogram containing many arrivals or phases, which correspond to the different propagation paths (Stein and Wysession, 2003).

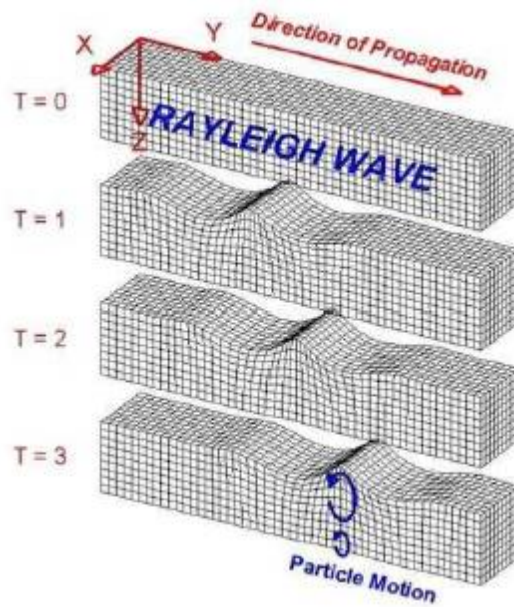


Figure 2.8: Mode of propagation of Rayleigh wave. (The ground moves in an elliptical path [generally retrograde elliptical], producing both a vertical and horizontal component of motion parallel to the direction of wave propagation. Amplitude decreases with depth) (Lay and Wallace, 1995).

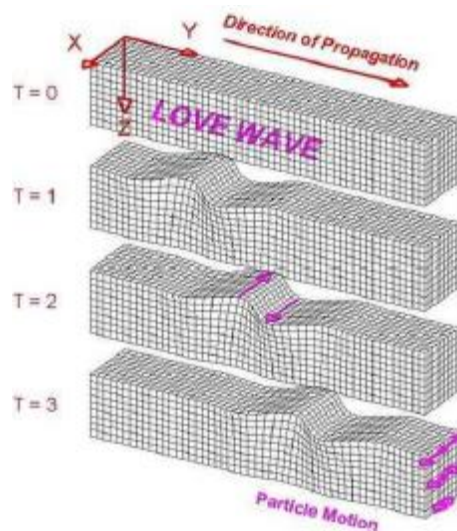


Figure 2.9: Mode of propagation of Love wave. (The ground motion is in the horizontal direction and perpendicular to the direction in which the wave propagates. The amplitude of the wave reduces with increasing depth) (Lay and Wallace, 1995).

The nomenclature of seismic phases depend on their propagation paths within the interior of the Earth (Figure 2.10) Stein and Wysession, 2003. P and S represent the direct compressional and shear waves respectively. Seismic phases which are reflected at the surface of the Earth are named in the following manner: the P-wave arrival representing one reflection at the surface is known as PP that for two reflections is called PPP, etc. In the same vein, SS represents one S-wave reflection at the Earth's surface while SSS denotes two reflections at the surface. Since P-wave can convert to S-wave when it is reflected at the Earth's surface, and conversely, P-wave that is converted to S-wave is called PS while SP is S-wave converted to P-wave. Seismic phases like the pP and pS denote P-wave up-going from the origin, reflected and converted respectively on reaching the Earth's surface. Similarly, sS or sP represent S-wave up going from the hypocentre, reflected and converted respectively at the Earth's surface. K denotes P-wave travelling through the outer core, P-wave travelling through the inner core is represented by I while c designate reflections at the Guternberg discontinuity. Hence, PKIKP trasverses the mantle, outer core and inner core. Every ray is refracted at its separate internal interface. PcP represents P-wave reflected at the Guternberg discontinuity. Reflection at the boundary of the inner core is represented by i, for example, PKiKP represent P-wave reflections from the inner core. PKJKP designates P-wave traversing the outer core as P and the inner core as S.

2.11 Geological Setting and Tectonic Activity

The Basement Complex covers about 50% of the total surface of Nigeria (Obaje, 2009). It is composed of the following litho structural units: The Migmatite - Gneiss complex (MGC), The Metasedimentary and Metavolcanic rocks (The Schist Belt). The Pan - African granitoids (The Older Granites), and the underformed acid and basic dykes. The Migmatite-Gneiss complex (MGC) has for long been regarded as basement sensu stricto (S.S.) (Obaje, 2009) and it is the most widespread of the main rock units in both Northwestern and Southwestern Nigeria (Obaje, 2009).

The term “Older granites” was introduced by Falconer (1911) who, on the basis of morphology and texture distinguished the Pan African Granitoid from the Jurassic anorogenic peralkaline “Younger Granites” of the central Plateau region.

The term Pan- African granitoids is preferred not only because of its merit on age, which was not available at that time, but because it covers several important petrologic groups formed at the same time (Falconer, 1911). They are composed of large volumes of granitic rocks, which intruded all pre-existing rocks including the gneiss-migmatite-quartzite complex and the schist belt. They were emplaced during the late Proterozoic to early Paleozoic (160+/-150My). These granites consist of porphyritic and non-porphyritic granites, granodiorites, adamallite, tonalite and quartz –diorite. They generally occur as inselbergs in the basement. Examples of such granite hills are the Olumo Rock in Abeokuta, Ogun State; Idanre Hills, Ondo State; Ikere Hills, Ekiti State. Aso Rock, Abuja. It is a heterogeneous assemblage including migmatites, orthogenesis, paragneisses and a series of basic and ultrabasic metamorphosed rocks Falconer (1911).

The various rock types in this complex are exposed in the north eastern, southwestern and a narrow zone parallel to the eastern boundary of the country, east of River Benue covering parts of Kaduna, Plateau, Bauchi, Kano and Sokoto States; southern Nigeria,

covering the greater parts of Kwara, Oyo, Ogun; and Ondo States; southeast Nigeria, spanning the northern parts of Cross Rivers State and as far north as Yola; and north of Benue River in Adamawa State. These crystalline basement rocks have been subjected to deformation of different intensities throughout the geological period. Consequently, North-South (N-S), Northeast-Southwest (NE-SW), Northwest-Southeast (NW-SE), North northeast-South southwest (NNE-SSW), North Northwest-South southeast (NNW-SSE) and to a lesser extent, East-West (E-W) fractures have developed Falconer (1911).

2.11.1 Significance of magnetic contours

Magnetic contours can look so deceptively similar to contours of subsurface structure that it can be easy for those not familiar with magnetic maps to interpret the magnetic features indicated by the contours as geomorphology. In areas where the hard rocks are shallow and uniformly magnetized, such an assumption might give useful qualitative information on the structure of the rock, particularly when linear trends are observed. Magnetic maps over sedimentary basins, where the magnetized rocks are deep can almost never be relied on for reliable information about the structure of the basement rocks (Dobrin, 1976).

2.11.2 Analysis of the magnetic trends

Over the years, researchers have tried to identify and establish the structural trends within Nigeria and beyond. Buser (1966) carried out one of the most intensive and far reaching of these studies covering Nigeria and the surrounding countries. He established the existence of paleostructures, which have directed events like tectonic movements, intrusions, metamorphism, sedimentation, mineralization, volcanism and drainage. He identified these paleostructures as striking in a NNE – SSW direction. These structures are in the form of culminations (crests) and regions to an approximate NE – SW direction. These paleostructures correspond to what Neev *et al.* (1982) have referred to as “lineament swarms” that exist within the ‘Pelisium line’. Their results were obtained

from an analysis of the extensive imagery supported by limited ground observations. They described the Pelisium line as a mega shear system with associated lineament swarms, which extends margin of the Mediterranean Sea and then curves NE-SW across central Africa from the Nile delta in the Gulf of Guinea. From there it continues across the Atlantic via the equatorial fracture zones, intersecting South America at the mouth of the Amazon in areas of predominantly arid climate; paleostructures to be observed on satellite image (Neev *et al.*, 1982). In wetter regions these features can be camouflaged by the effects erosion, sedimentation and other secondary features. In this case geophysical methods, especially aeromagnetic field studies can be used to establish the existence of structures and trends. A major contribution in this direction was made by Ajakaiye *et al.* (1991). In their interpretation of aeromagnetic data across the Nigerian continental mass, they identified the NE-SW trending anomalies as the dominant magnetic features of most of this shield area. The magnetic lineaments as seen as narrow belts represent major tectonic trends, which may also continue across the adjoining schist belt region. They further pointed out that this concentration of magnetic lineaments appeared to be connected with the occurrence of younger granites since because the trend is prominent in almost all known younger granite complexes. Udensi *et al.* (2001) also identified the existence of large-scale magnetic lineaments dominant in the NE-SW direction in Bida Basin.

2.11.3 Structural trends

Ajakaiye *et al.*, (1991) suggested that magnetic lineaments with definite characteristics exist within the Nigerian continental landmass. The lineaments, according to the authors, coincide with major structural trends such as the Benue trough in Nigeria, fractures in the oceanic crusts of the West African coasts, Eburnean syncline in Cote-D'Ivoire and can be traced to the lineaments in Guyana and eastern Brazil. They showed that the onshore

lineaments in West African are the extensions of the St Paul's Romanche, Chain and Charcot fracture zones are believed to be part of the major zones of weakness in the crust that predate the opening of the Atlantic Ocean and were reactivated during the early stages of continental rifting.

Falconer (1911), was the first to study the geology and geography of northern Nigeria where according to him, the area of study is underlain by the Basement Complex rocks which comprises migmatite and gneisses and is intruded by granites, which he calls 'Older Granite' to distinguish them from the Younger Granites. Falconer also described the Geology of the Plateau tin fields in his work where Keffi forms part of the pegmatites of central Nigeria which is located within the Basement Complex.

Jacobson and Webb (2021) also stated that the area is covered by undifferentiated migmatite including veins, banded and porphyroblastic gneiss, some schist and phylites.

McCurry (1976) reported about the geology of the Precambrian to Lower Paleozoic rocks of the NW Nigeria. She stressed the fact that Northern Nigeria is underlain by gneisses, migmatites and meta-sediments of Precambrian age, which are intruded by series of granitic rocks of the Late Precambrian to Lower Paleozoic age. The older rocks are represented by a series of older meta-sediments and gneisses believed to be of Birrimian age or older. These rocks have been variously metamorphosed and granitized through at least two tectono metamorphic cycles so that they have been largely converted to migmatite and granite gneisses.

The Early Archean (7.35Ga) to Late Archean (2.5-2.7Ga) Migmatite-Gneiss-Quartzite Complex forms the basement in this region. The Basement Complex rocks (granites, granite-gneiss, schist and migmatite,) have weathered to clayey-sandy cover and laterite cap (Obaje, 2009).

The general fold pattern consists of open and a symmetric flexure of low plunges to the north and northwest with fold axis of N-S strike pattern. The entire shield is a southern prolongation of the Pan African domain of the central Hoggar to the north whose geodynamic evolution has been linked to the continent-continent collision approximately 600Ma (Black, 1984 and Caby, 1989). The products of this event in Nigeria consist of granites, their associated intermediate (charnockitic, monzonitic syenite) rocks, acid and dolerites, as well as extensive migmatization and granitization of the Pan African Basement Complex.

Onyewuchi *et al.* (2012) stated that most mineral deposits are related to some type of deformation of the lithosphere and most theories of ore formation and concentration embody tectonic or deformational concepts. They also stated that some lineament patterns have been defined to be the most favourable structural conditions in control of major regional lineaments, the intersection of major lineaments or both major (regional) and local lineaments, lineaments of tensional nature, local highest concentration (or density) of lineaments between echelon lineaments associated with circular features. Linear features are clearly discernable on aeromagnetic maps and often indicate the form and position of individual folds, faults, joints, veins, lithologic contacts and other geologic features that may lead to the location of individual mineral deposits. They also indicate the general geometry of subsurface structures of an area thereby providing a regional pattern.

Yamusa *et al.*, (2018) reported about the geological and structural analysis using remote sensing for lineament and lithological mapping. The dominant rock types in the area are gneiss, granites and metasediments with minor lithologies such as aplite dykes, quartzofeldspathic and quartz veins, pegmatites and xenolith. Petrographic studies have shown that the granite comprises of porphyritic and medium to coarse grained varieties

that are composed mainly of quartz, feldspar, biotite ± muscovite. The metasediments include pelitic schist and composed of quartz, biotite, feldspar, ± muscovite, ± chlorite and quartzites. These rocks have been deformed, sheared and foliated. The dominant NW-SE to N-S structural trend, follows the general trend of structures resulting from both Pre-Pan-African and Pan-African Orogenies.

2.11.4 Previous geophysical studies

Studies have been carried out by different researchers using magnetic and seismological methods to delineate lineaments and earthquake investigations.

Udensi *et al.* (2003) carried out trend analysis of the total magnetic field over the Bida Basin, Nigeria. Two of the fracture zones, St Paul's and Romanche are believed to pass through the Bida Basin. The lineaments A-A^I and B-B^I are suspected to be continental extensions of St Paul's and Romanche fracture zones respectively. The St Paul's fracture zone maintained a NE-SW trend within the basin, the Romanche trends ENE-WSW.

Likkason *et al.* (2005) investigated some structural features of the middle Benue Trough, Nigeria modeled from aeromagnetic data, some digital processing tools were used in the analysis and these include analytic signal, filter (matched) and Forward and inverse modeling. Magnetic depth for the sedimentary cover was maximum of 3.30 km from the ground level. Results from matched filtering of the anomaly aeromagnetic data yielded three dipole equivalent source layers at 0.89, 4.33 and 18.22 km depth respectively. The depth of 4.33 km corresponds to the maximum thickness of sediments, that of 0.89 km may be attributed to effect of survey terrain clearance and other shallow plate sources, while that of 18.22 km correspond to the base of the curie depth in the area.

Anudu *et al.* (2012) analyzed aeromagnetic data over Wamba and its adjoining areas in North-central Nigeria. The study revealed that total magnetic intensity values in the basement part of the area varied from 7960 nT to 8020 nT, whereas residual magnetic intensity values ranged from 160 nT to 220 nT. They also used the residual aeromagnetic intensity anomaly data to produce the residual aeromagnetic intensity shaded relief maps of the area to delineate structural lineament trends. The trends generated and shown on the residual aeromagnetic intensity shaded relief maps of the area depicted the structural lineament trends on the magnetic basements beneath the area. The major structural lineament trends were NE-SW, NNE-SSW and NW-SE with minor ENE-WSW, E-W trends. Most of which correspond with previous work carried out in the Benue Trough and parts of the adjoining Basement Complex by Ajakaiye *et al.* (1986) and Olasehinde *et al.* (1990). They suggested that the NE-SW and NW-SE trending structures is the product of the Pan African orogeny event while the E-W trends are of pre-Pan African origin.

Anudu *et al.* (2014) used aeromagnetic data over the Cretaceous Middle Benue Trough to identify and delineate subsurface structures and volcanic rocks. The study revealed that edge enhancements of the aeromagnetic data is convenient, time saving and effective tool for mapping intra-sedimentary volcanic rocks and geological structures in areas with poor bedrock exposures, poor accessibility and paucity of rocks. The magnetic derivative maps of the area show a clear distinction between low amplitude anomalies associated with Cretaceous sedimentary rocks and high amplitude anomalies due to the intra-sedimentary volcanic rocks and structures. It shows high amplitude anomalies over the northern and south- eastern flanks of the area underlain by the crystalline basement rocks. The orientation of basement geological structures inferred from the magnetic maps suggests that are products of the Brasiliano/Pan- African orogeny (NE-SW, NW-SE and ESE-WNW tectonic trends).

Megwara and Udensi (2013) carried out lineament analysis of part of Southern Bida Basin and the surrounding basement rock using aeromagnetic data. Magnetic lineaments were inferred using Euler deconvolution and analytic signal techniques. The TMI values range from a minimum value of about 7630 nano tesla to a maximum value of about 7930 nano tesla. The zone coloured Euler Deconvolution and lineament maps were correlated on the bases of lineaments, both maps shows lineament trending in different direction.

The prominent trend directions common to both maps are the northeast-southwest and northwest-southeast orientations. Correlation of the zone coloured Euler Deconvolution and analytic signal maps shows magnetic lineaments trending in northeast-southwest and northwest-southeast directions. It is inferred that the northeast-southwest trending Romanche Fracture zone passed through the survey area.

Akpan *et al.* (2014) investigated an earthquake offshore south western Nigeria where it was shown that the fault which triggered the tremor ruptured at about 10 km within the upper crust local magnitude (M_L) of 4.5 and moment magnitude (M_w) of 4.1. The epicentre of the earthquake lies very close to one of the un-named fracture zone situated between the Romanche and Chain fracture zones which studies have shown to be extension of the Atlantic fracture zone into the continent.

Isogun and Adepelumi (2014) investigated seismic activities between 1990 and 2009 in the mid-Atlantic fracture zones (between latin America and west Africa). The analysis of the data showed that the epicentral locations of majority of the earthquakes were along, Romanche and Saint Paul fracture zones. The focal depth of the earthquakes is 10 km and their body wave magnitudes range between 3.5 and 6.3 with magnitude range of 4.0-4.4 and 4.5 -4.9 being dominant having 246 (36%) occurrences each. The surface wave magnitudes ranges between 3.0 and 7.0 with magnitude range of 4.0-4.4 being dominant

with 219 (32%) occurrences and moment magnitude ranges between 4.7 and 7.0 with 5.0-5.4 magnitude range having 91 (50%) occurrences. Empirical relationships between correlated magnitudes were $M_b = 0.701M_s + 1.544$, $M_w = 1.062 M_b - 0.205$ and $M_w = 0.711M_s - 1.997$. The yearly and monthly time occurrences of earthquakes did not show any clear characteristic period. The b-value for the year interval 1990- 2009 was 0.88. The result of b-values over two decades suggested that there was no likelihood of earthquake with surface wave magnitude > 7.0 before 2019.

Okpoli and Oladunjoye (2017) carried out a lineament study using aeromagnetic data over part of Ado-Ekiti region. The study revealed that various filtering methods such as reduction to pole, analytic signal, First Vertical derivative and first horizontal derivative were applied to the residual magnetic intensity. These filters helped to define lithological boundaries, intersection of geological structure, faults, folds and contacts. Reduction to the pole varied from -213.1 to 314.1 nT, Upward continuation at 100 m ranged from 156.1 to 142.4 nT and analytical signal varies from 0.0 to 0.4 nT. The magnetic intensity distribution was found to depend on the size, depth of burial, and the thickness of low susceptibility superficial material overlying the magnetite rich crystalline rocks. The Tilt derivative proved very useful in the delineation of lineaments which were in the form of contact, faults, folds and joint derivative map.

Ngama and Akanbi (2017) employed magnetic method to analyse the data set using different filters to enhance geological features within the study area. Analysis carried out using TMI, RTE, Upward continuation and First Vertical Derivative filter were helpful in identifying different magnetic anomalies within the area of study. The TMI map obtained has a magnetic intensity range of between - 696.9 to 599.2 nT/m, RTE varies from - 430.1 to 346.4 nT/m both showing anomalies in circular to near circular

closures which could be associated with granitic intrusions, long narrow features which could be dykes or long ore bodies and dislocations which could be due to subsurface fractures. Upward continuation map at 3 km deep revealed a basement trending in the NE-SW and ENE-WSW directions with the latter being the major trend direction. The rose diagram plot shows the dominant lineament trend to be in the NE-SW direction.

Adetona *et al.* (2018) carried out the trend analysis of the total magnetic field over eastern part of Benue Trough. The aeromagnetic data was reduced to pole. Vertical Derivative, Source Parameter Imaging and CET grid analysis was applied to the data to estimate depth to magnetic rocks and delineate the lineaments within the area. The first vertical derivative that sharpens the edges of the anomalies reveals that the Northern part of the study area consist of basement rock outcrops with various degrees of deformations as seen from the distortion to the magnetic signatures which represents the Granite Gneiss at Kwalla and the Migmatite Gneiss at Wamba. Depth to magnetic rocks estimates within the study area is generally shallow with a depth of 3 to 3.5 kilometers were obtained around Akira just above river Benue and below Akwana on latitude $7^{\circ} 30' N$. Lineament map obtained from CET shows linear structures that trend in the NW-SE and E-W directions and these could be veins that are host for minerals within the area.

Tawey *et al.*, 2019 investigated Gitata sheet to identify lineaments using derivative, Euler Deconvolution and Centre for Exploration Targeting (CET) techniques. The result revealed that the area is highly faulted with prominent trend in NE-SW and NW-SE direction. From 3D Euler Deconvolution, depths were divided and grouped at every 150 m and the result shows that the faults/fractures between the depths of 150 and 300 m dominate the study area. The fault pattern indicated by the FVD, CET and NE-SW trend alignment of many Euler solutions indicates that the study area has been seriously influenced by the NE-SW trend of a regional fault system.

Abraham *et al.* (2020) carried an investigation on recent tremors in Nigeria using Aeromagnetic and gravity data to investigate crustal depths. The result shows that the estimated depths to the bottom of magnetic crust was between 11.0 and 11.4 km at the Mpape region and decrease further southward towards Guabe town, which signifies the depth range of the active crust within the region. Deeper depths (15.0-16.2 km) were obtained at the locations farther from Mpape-Guabe towns at Nasarawa, Rubochi and Fuka regions, showing a more stable region away from Mpape region. Computed Moho depths from gravity data show deeper depths at the Mpape region (34.1 km) suggesting that the active crust exists in the upper crust. Two- dimensional modeling analysis along a profile taken across the Mpape regions shows a conspicuous subsurface basement intrusion at the Mpape region with deep faults and fractures reaching depths of 7-14 km. Shallow basal depths at the Mpape region resulting from significant subsurface intrusion and concentrated subsurface faults at the intruded region may be responsible for the instability of the Mpape region.

Goki *et al.* (2020) carried out an assessment of the geological evidence of the September 2016 Kwoi tremors. This involved systematic studies of the crack pattern and intensity on buildings, rocks and hanging walls of slopes around the area with the highest shock. Results show that the major evidence that proved a possible link to the area of highest impact is the tremor triggered displacement of a 4 by 3 m diameter rock boulder situated about a kilometer from the Kwoi town, some 3 km from the nearest epicenter that fell through a cumulative distance of 25 m, splitting the fresh granite boulder into two and creating a high impact scar on its path. Seismic vibrations that shock the residents of Kwoi and environs appear to have been generated and propagated laterally from the rocks along a northwest-southeast profile. Despite the non-homogenous strengths of the impacted buildings, the near- consistency of the E-W striking walls being the most

fractured gives a remote connection with the major 345° to 015° fracture patterns on the granitic plutons that shields Kwoi town to the north. Intensity of the fractures and collapse in the buildings increased south-westwards from the perceived area of highest impact.

Tawey *et al.* (2020) carried out assessment of structures and solid minerals to investigate subsurface structural characteristics and mineralization potential zones within part of North-Central Nigeria. Several filters such as Analytical signal, tilt derivative, First and Second vertical derivative and Euler deconvolution were applied to the aeromagnetic data. From the analytic signal map three magnetic zones were delineated. These are: low to relatively low magnetic zone (LM) with amplitude range from 0.003 to 0.009, moderate magnetic zone (MM) with amplitude 0.009 to 0.106 and those with high amplitudes above 0.106 are products of later magmatic intrusions into host rocks with fractures, faults and joints. Areas of high analytic signal are predominant within the central portion of the study area and span towards the western end of the map. Five tectonic structural trends in the directions ENE-WSW, NE-SW, NNE-SSW, NNW-SSE and WNW-ESE with ENE-WSW being the predominant or major structural trend.

Saleh *et al.* (2020) carried out delineation of structural geologic features and depth to magnetic sources over Allawa and its environs, North central Nigeria. The high resolution aeromagnetic data of Allawa and its environs was first reduced to the magnetic pole (RTP) to place the magnetic anomalies directly above their respective causative source. The residual magnetic intensity (RMI) derived from RTP was subjected to the shallow enhancement filters involving; First vertical derivative (FVD) and horizontal gradient magnitude (HGM). The FVD and HGM methods delineated series of linear geologic features which can be interpreted as faults, folds and fractures. The centre for exploration targeting (CET) in conjunction with constructed Rose diagram revealed that the study

region is dissected by series of major and minor deformations trending along the NE-SW, N-S, and NW-SE directions respectively, Afterwards, analytical method was also utilized to estimate the depth to the magnetic sources with values in the range of 108.4 to 322.4m. They concluded that the adopted methods have aided in unveiling the depths and pathways controlling the mineralization over the region.

Arogundade *et al.* (2020) used satellite imagery (Landsat-Z ETM+) and high-resolution aeromagnetic data to study the Zungeru-Kalangi fault zone in Nigeria. The N-S, NNE-SSW and NE-SW lineament trends are prominent on the landsat 7 ETM. The faults delineated from the aeromagnetic data showed that NE-SW trend is predominant. The results of the 2D models confirmed the existence of the Zungeru- Kalangi fault. Zone and other several new faults such as faults F3 (northern part), F4 (northeastern), F6 and F9 (northwestern) with their approximate source locations and dips were confirmed.

Abong *et al.*, (2020) investigated earthquake occurrences in Nigeria using the Weibull equations, historical and instrumental data recorded from 1933 to 2018. The Findings of the study revealed that the return period for an earthquake of magnitude 6.5 on Richter's scale is 86 years, an earthquake of magnitude 4.7 is 34.4 years, an earthquake of magnitude 4.2 is 17.2 years and earthquake of magnitudes 2-3.7 is between 5.56-14.3 years.

Egbelehulu *et al.*, 2021 investigated part of Gwagwalada, Abuja for potential mineral targets using derivatives filters. The application of vertical derivative enhanced shallow structures which trend NE-SW. Horizontal gradients along the x and y directions enhanced geological contacts attributable to blind faults. The tilt derivative (TD) accentuated fault lines which trend NE-SW. The main fault in the study area had the peak of the tilt angle amplitude and could be located within longitude $7^{\circ} 05' 00''$ N, 7°

08^I 30^{II} N and latitude 8 ° 58^I 00^{II}, 8 ° 59^I 00^{II}. These faults were identified as possible host for mineralization.

Hossain *et al.*, 2021 investigated the magnitude and focal depth of earthquakes in and around Bangladesh that have been felt from 2015 to 2019 having Richter magnitude more than 3. Maximum earthquakes with a magnitude of 3.0 to 4.9 have occurred at the northern side of Bangladesh whereas at the eastern side the values are between 4.0 to 5.9. It was seen that considerable earthquakes occurred in 2019 at the northern side of Bangladesh. The magnitude of 4.9 obtained indicates that a major earthquake may occur in this area from the stored energy and can cause a devastating effect. Focal depths have been found to be higher in 2016 related to other years.

Preliminary Report of the earth tremor in Southwestern Nigeria on 5th June, 2021 with estimated epicentral distance between 108 and 113 km, with local magnitude of 2.4 and moment magnitude of 2.6. Focal depth of 15.0 km and the fault that caused the earth tremor has a stress drop of 5.9 bar

In view of the reviewed previous studies in the study area and its environs, no research work using an integrated magnetic and seismologic method, which is novel for investigating the likely subsurface structures responsible for earth tremor occurrences in parts of north Central Nigeria, has been carried out. Therefore, this research be relevant in addressing this issue.

CHAPTER THREE

3.0 MATERIALS AND METHODS

3.1 Materials

During the research work, various materials such as Magnetic and Seismological Data, softwares for data analysis were used. The major materials used include:

- i. data from eight (8) aeromagnetic maps sheets 165 (Bishini), 166 (Kachia), 167 (Kafanchaan), 168 (Naraguta), 186 (Abuja), 187 (Gitata), 188 (Jamaa) and 189 (Kurra) covering the study area within parts of North Central Nigeria.
- ii. surfer package version 11
- iii. oasis Montaj version 8.4
- iv. seisan version 11.0
- v. arc GIS 10.5
- vi. geological map of study area

3.1.1 Aeromagnetic Data Acquisition and Processing

The study area (parts of North central Nigerian basement complex) is covered by eight aeromagnetic map sheet. These maps were obtained from the Nigerian Geological Survey Agency (NGSA) which was produced as part of the nationwide airborne survey carried out by Fugro and sponsored by Federal Government of Nigeria in the year 2009. The data were obtained at an altitude of 100 m along a flight line spacing of 500 m oriented in NW-SE and a tie line spacing of 2000 m. The magnetic data collected were published in the form of half-degree sheets in gridded format on a scale of 1:100,000. The actual magnetic values were reduced by 33,000nT before plotting the contour map. This implies that the value 33,000 nT is to be added to the contour values so as to obtain the actual magnetic field at a given point. A correction based on the International Geomagnetic Reference Field, (IGRF,) and epoch date January 1, 2010 was included in

all the maps. Eight sheets numbering 165,166,167,168, 186,187,188 and 189 were assembled for this work with each square block representing a map in the scale of 1:100,000. Each square block is about 55 x 55 km² covering an area of 24, 200 km². The digital data were acquired as merged unified block and were extracted from the map using Oasis Montaj software.

3.1.2 Production of the unified Aeromagnetic map (Super map) of the study area

The eight data sheets covering the entire study area was merge to form a single data base for the study. The grid was saved into the database, and new coordinate was projected into latitude and longitude in meters, thereafter, the database was re-gridded to produce the composite aeromagnetic map of the study area using bi- directional gridding method.

3.1.3 Seismological Data Acquisition and Processing

The seismological data used for this research are seismograms recorded by the five seismological stations in Nigeria that were functional at the time of occurrence of the 11th and 12th September, 2016 Kwoi earth tremors and 7th September, 2018 Abuja tremor. The stations located at Ile-Ife (IFE), Kaduna (KAD), Abakaliki (BKL) Nsukka (UNN) and Minna (MNA) are managed by an agency of the Federal Government of Nigeria, the Centre for Geodesy and Geodynamics Toro, Bauchi State. Each of the stations is equipped with the Eentec DR-4000 data acquisition system, three-component seismometers (Eentec EP-105 or Eentec SP-400) and Global Positioning System (GPS) timing signals. Each of them is powered by solar panels connected to a 200 Ah battery to ensure stable power supply. The data are recorded continuously in the MiniSEED format at a sampling rate of 40 samples per second (sps). The MiniSEED which is a sub-set of the Standard for the Exchange of Earthquake Data (SEED) is basically at archiving and exchanging seismological data and related metadata (Incorporated

Research Institution for Seismology, 2013). This data format is maintained and distributed by the Incorporated Research Institutions for Seismology (IRIS) which is an association of over one hundred universities and research institutes in the United States of America and other parts of the world responsible for operating scientific facilities used in acquiring, managing and distributing seismological data.

Plate IV shows Kaduna seismological station. The SEISAN earthquake analysis software version 11.0 was used in processing the data.

3.2 Methodology

The procedure that was adopted for processing the aeromagnetic data is outlined as follows:

Data acquisition

a. Data Filtering and Analysis

This is broken down into the following procedures.

1. Production of total magnetic intensity map (TMI) of the study area using Oasis Montaj softwares
2. Perform upward continuation of the (TMI) data; it separates a regional magnetic anomaly resulting from deep sources from the observed magnetic (residual) thereby enhancing large scale (usually deep) features in the study area (Telford *et al.*, 1990).
3. Apply derivatives to magnetic data to enhance the shallowest geologic sources in the data and map lineaments (Dobrin and Savit, 1988; Telford *et al.*, 2002).
4. Applying the Tilt derivative to magnetic data to determine structures, contacts and edges or boundaries of magnetic sources (Miller and Singh, 1994).
5. Applying Center for Exploration Targeting (CET) grid analysis to magnetic data to delineate fault lines within the basement rocks (Kovesi, 1997).



PLATE IV: Kaduna Seismological Station (KAD). (The seismometer [left] is installed in a vault beside the building and the data acquisition system [right] is placed inside the building. The solar panel at the top of the roof is connected to a battery [middle] which supplies power to the seismic equipment. In the background behind the building is an outcrop of quartz porphyritic granite of the Older Granite Complex).

3.3 Explanation of Method

3.3.1 Production of the composite aeromagnetic map of the study area

The aeromagnetic map of the study area was produced by merging the data sheets that was used to generate a single map of the study area. The grid was saved into database and new coordinate was projected to change the coordinate from x and y in meters (m) to latitude and longitude in degree. Thereafter, the database was re-gridded to produce the composite aeromagnetic map of the study area using bi-directional gridding method which can also be called the total magnetic intensity map of the study area. The magnetic intensity value was reduced by 33,000 Nt, this means that a value of 33,000 nT was added to produce the Total Magnetic Intensity contour map using Oasis Montaj software.

3.3.2 Data filtering

The early stages of magnetic data interpretation generally involve the application of mathematical filters to process data. The main goals of these filters vary, depending on the situation. The general purpose is to enhance anomalies of interest and/or to gain some preliminary information on source location or magnetization. Most of these methods have a long history, proceeding the computer age. Modern computing power has increased their efficiency and applicability tremendously, especially in the face of the ever-increasing size of digital data associated with modern airborne surveys. Some of the geophysical filters that was used in this study are Reduced to equator, reduced to Pole, Upward Continuation, First Vertical Derivative, Second Vertical Derivative, analytic signal, Tilt derivative and Centre for Exploration Targeting (CET).

3.3.2.1 Reduction to magnetic equator

The shape of a magnetic total intensity anomaly is affected by the directions (inclination and declination) of the magnetization and the earth's magnetic field vectors. Except

when inclinations of the vectors are either 90 or 0 degrees, the magnetic anomaly is not centered over the causative body. The process of reduction to the pole has been commonly used to remove this effect of inclination and declination and to center the anomaly over the body. It has been known for many years that the reduction-to-the-pole process cannot be applied to anomalies observed over regions in low magnetic latitudes. The process introduces errors and false trends to the reduced anomalies. An alternative approach is proposed for removing the effect of inclination and declination. The new approach reduces anomalies to the magnetic equator (0 degree inclination). It is a filtering process that recomputed the magnetic total intensity anomalies as if the causative bodies were magnetized in a horizontal direction. The reduced to magnetic equator is easy to implement and has been used for real data of low magnetic latitude areas.

Reduction to the equator has an amplitude component ($\sin(I)$) and a phase component ($i \cos(I) \cos(D-\theta)$). Reduction to Equator is given by equation (3.1)

$$L(\theta) = \frac{[\sin(I) - i \cos(I) \cos(D - \theta)]^2 X(-\cos^2(D - \theta))}{[\sin^2(Ia) + \cos^2(Ia) \cos^2(D - \theta)] X[\sin^2(I) + \cos^2(D - \theta)]}, \text{ if } (|Ia| < |I|), Ia = I \quad (3.1)$$

where

I = geomagnetic inclination

Ia = inclination for amplitude correction

D = geomagnetic declination

$\sin(I)$ is the amplitude component while $i \cos(I) \cos(D-\theta)$ is the phase component

3.3.2.2 Upward continuation

Upward continuations are processes by which potential field data from one datum are mathematically projected upward to level surfaces above or below the original datum. In

projecting to higher plane, we are suppressing the effect of the local (residual) anomaly and enhancing regional effects. Upward continuation helps to establish the regional trend, estimate the depth of a basin and establish if there exist any inter-layer structures. This is the calculation of the potential field at an elevation than at which the field is measured. The continuation involves the application of Green's Theorem and is unique if the field is completely known over the lower surface (which is usually true for magnetic fields) and where all sources above the lower surface are known (usually all are zero). Upward continuation is used to smooth out near surface effects. Upward continuation is a method used in geophysics to estimate the values of the magnetic field by using measurements at the lower elevation and extrapolating upward, assuming continuity (Telford *et al.*, 1990). The upward continuation (where z is positive upward) is given in equation (3.2)

$$F(x, y, -h) = \frac{h}{2\pi} \iint \frac{F(x, y, 0) \partial x \partial y}{\sqrt{(x-x')^2 + (y-y')^2 + h^2}} \quad (3.2)$$

where $F(x, y, -h)$ = Total field at the point P(x, y, -h) above the surface on which $F(x, y, 0)$ is known, h = elevation above the surface (Telford *et al.*, 1990).

3.3.2.3 Horizontal derivatives

Derivative tends to sharpen the edge of anomalies and enhance shallow features; the resultant map is much more responsive to local influence than to broad or regional deep-seated anomalies.

Derivative in the X direction is given by the algorithm,

$$L(\mu i)^i \quad (3.3)$$

n is the order of differentiation, and μ represents the X component of the wavenumber,

where $i = \sqrt{-1}$

while the derivative in the Y direction is given by

$$L(V) = (Vi)^n \tag{3.4}$$

where n is the order of differentiation V represents the Y component of the wavenumber and $i = \sqrt{-1}$

3.3.2.4 Vertical derivatives

Vertical derivatives of aeromagnetic are routinely used as an aid to the interpretation process because they enhance detail and sharpen geophysical anomalies. Vertical derivative (VD), known also as vertical gradients, accentuate or enhance short-wavelength (high wave- number) anomalies and suppress long-wavelength (low wave – number) anomalies in magnetic data (Dobrin and Savit, 1988: Telford *et al.*, 2002). Short- wavelength anomalies are always caused by surface and near-surface/shallow causative geological bodies, whereas long-wavelength anomalies are mainly due to deeper geological source bodies. Generally, vertical derivative tend to sharpen the edges of anomalies and enhance shallow features. The derivative maps are much more responsive to local influence than broad or regional effects and therefore tend to give sharper pictures than the map of the total field intensity. Thus, the smaller anomalies are more readily apparent in cases of long regional disturbances. In fact, the first derivatives (both horizontal and vertical) are used to delineate high frequency features more clearly where they are shadowed by large amplitude, low frequency anomalies. The enhancement sharpens anomalies over bodies and tends to reduce anomaly complexity, allowing clearer imaging of a causative structure. The transformation can be noisy since it will amplify short wavelength noise. First vertical derivative (FVD) data have become almost a basic necessity in magnetic interpretation projects. First Vertical Derivative emphasizes near surface features. To emphasize the effects of the geological contacts, critical for the

structural frame work of the area, the data processing involved accurate enhancement of the short- wavelength and linear features.

The enhancement of magnetic anomalies associated with faults and other structural discontinuities were achieved by the application of first vertical; derivative to the residual map. The derivative in the frequency domain are represented by the equation (3.5)

$$L(r) = r^n \quad (3.5)$$

where n = Order of differentiation and r = wave-number.

The FVD of the magnetic field is often computed by using the relation, (Telford *et al.*, 1990).

$$FVD = \frac{\partial T(x,y,z)}{\partial z} \quad (3.6)$$

where T is the total magnetic field at (x, y, z)

A Second vertical derivative of a magnetic field is a measure of the curvature of the field, that is, it is a measure of the rate of the change of non- linear magnetic gradients. In other to explain this, consider a plot of magnetic field versus distance along a profile. This is achieved by drawing a straight line along a magnetic contour map and plotting the result. Where the curvature of the line thus plotted is greatest (least radius), the second vertical derivative has its highest value. Where there is no curvature (infinite radius), the second derivative is zero.

Second Vertical Derivative (SVD) enhances the anomaly boundaries of near surface effects. They are a measure of curvatures and large curvatures are associated with shallow anomalies. The SVD is obtained from the differences between nearby first derivatives. These filters are considered most useful for defining the edges of bodies and for amplifying fault trends (Milligan and Gunn, 1997). In mathematical terms, a vertical derivative can be shown to be a measure of the curvature of the potential field, while zero SVD contours defines the edge of the causative body. Thus, the SVD is in effect a

measure of the curvature, which is the rate of change of non-linear magnetic gradients. The zero magnetic contours of the second vertical derivative often coincide with the lithologic boundaries while positive and negative anomalies often match surface exposures of the mafic and felsic rocks respectively. The second vertical derivative (SVD) has more resolving power than the first vertical derivatives (Milligan and Gunn, 1997). The SVD of magnetic field can be calculated by the equation (3.7) given below (Telford *et al.*, 1990).

$$SVD = \frac{\partial^2 T(x,y,z)}{\partial z^2} \quad (3.7)$$

where T is the total magnetic field at (x, y, z)

3.3.2.5 Tilt derivative (TDR)

The Tilt derivative filter, TDR (a very good edge-detection filter) brings out short wavelength anomalies and reveals the presence of magnetic lineaments. Verduzco *et al.* (2004) showed that the tilt derivative filter also performs an automatic-gain-control (AGC) filter, which tends to equalize the response from both weak and strong anomalies. Hence, the filter provides an effective way to trace out along striking anomalies. The tilt angle is defined as (Miller and Singh, 1994)

$$TDR = \tan^{-1} \left(\frac{VDR}{THDR} \right) \quad (3.8)$$

where VDR and THDR are the first vertical total horizontal derivatives, respectively, of the total magnetic intensity T.

$$VDR = \frac{dT}{dz} \quad (3.9)$$

And

$$THDR = \sqrt{\left(\frac{dT}{dx}\right)^2 + \left(\frac{dT}{dy}\right)^2} \quad (3.10)$$

The total horizontal derivative of the tilt derivative is defined as:

$$HD_THDR = \sqrt{\left(\frac{dTDR}{dx}\right)^2 + \left(\frac{dTDR}{dy}\right)^2} \quad (3.11)$$

By substituting (3.9) and (3.10) into (3.8), we have:

$$TDR = \tan^{-1} \left(\frac{\frac{dT}{dz}}{\sqrt{\left(\frac{dT}{dx}\right)^2 + \left(\frac{dT}{dy}\right)^2}} \right) \quad (3.12)$$

3.3.2.6 The centre for exploration targeting (CET) grid analysis plug-in for structures

The CET (Centre for Exploration Targeting) Grid Analysis extension consists of a number of tools that provide automated lineament detection of gridded data which can be used for first- pass data processing. The CET grid Analysis extension contains tools for texture analysis, phase analysis and structure detection. The aim of this structural analysis is to:

1. Locate the contact within the basement of the study area
2. Locate the extent and position of the outcrops and intrusive bodies into basement and sedimentary formations within the study area
3. Detect fracture or any fault that may exist within the area
4. Interpret the entire lineaments detected

Standard deviation provides an estimate of the local variations in the data at each location in the grid, it calculates the standard deviation of the data values within the local neighborhood. Features of significance often exhibit high variability with respect to the background signal. For a window containing N cells, whose mean value is μ , the standard deviation σ of the cell values x_i is given by:

$$\sigma = \sqrt{\frac{1}{N} \sum_{i=1}^N (x_i - \mu)^2} \quad (3.13)$$

When interpreting the output, values which approach zero indicate very little variation, whereas large values indicate high variation (Kovesi, 1997). The next stage is to apply Phase Symmetry; this property is useful in detecting line-like features through identifying axes of symmetry. It is also known that the symmetry of a signal is closely related to the periodicity of its spatial frequency. Consequently, it is natural to utilize a frequency-based approach to detect the axes of symmetry. This plug-in implements the phase symmetry algorithm developed by Kovesi (1997). The result from phase symmetry is passed through Amplitude Thresholding, in conjunction with non-maximal suppression (NMS). The NMS is useful for finding ridges since low values are suppressed whilst points of local maxima are preserved, it also takes into account the local feature orientation so that the continuity of features is maximized and can be used to remove noise and highlight linear features Finally Skeleton to Vectors is applied.

The Skeleton to Vectors plug-in is for vectorizing the skeletonized structures from the skeletonization plug-in via a line fitting method. The vectorized data can then be used as input to the structural complexity heat map plugins. For each structure in the grid, a line is formed between its start and end points. If the structure deviates from this line by more than a specified tolerance the structure is divided into two at the point of maximum deviation and the line fitting process is repeated on these two new structure segments. This process is continued recursively until no structure segment deviates from its corresponding line segment by more than the specified tolerance. These line segments form the vectorized representation of the structures within the grid (Kovesi, 1997).

3.3.2.7 Analytic signal

This is a filter applied to magnetic data and it is aimed at simplifying the fact that magnetic bodies usually have positive and negative peak associated with it, which in many case may make it difficult to determine the exact location of causative body.

Nabighian (1972) has shown that for two dimensional bodies, a bell-shaped symmetrical function can be derived which maximizes exactly over the top of the magnetic contact. The three-dimensional case was also derived by Nabighian (1984). This function is the amplitude of the analytical signal. The only assumptions made are uniform magnetization and that the cross section of all causative bodies can be represented by polygons of finite or infinite depth extent. This function and its derivative are therefore independent of strike, dip, magnetic declination, inclination and remanent magnetization.

The 3.D analytical signal A of a potential field anomaly can be defined (Nabighian, 1984) as:

$$A(x, y, z) = \left[\frac{\partial M}{\partial x} \right] x + \left[\frac{\partial M}{\partial y} \right] y + \left[\frac{\partial M}{\partial z} \right] z \quad (3.14)$$

where M = magnetic field

3.4 Seismic Instrumentation

Quantitative analysis of seismic disturbances requires that the earth vibrations be instrumentally recorded at observatories spread across the globe. The instrumentation must:

1. Be able to detect the transient vibrations within a moving reference frame (the instrument moves with the Earth as it shakes);
2. operate continuously with a very sensitive detection capability with precise timing so that the ground motion can be recorded as a function of time, producing a seismogram; and
3. have a fully known linear response to ground motion, or instrument calibration, which allows the seismic recording to be accurately related to the amplitude and frequency content of the causal ground motion. Such a recording system is called a

seismograph, and the actual ground-motion sensor that converts ground motions into some form of signal is called a seismometer in earthquake seismology, or a geophone in exploration seismology. The observatories are usually grouped together and this grouping is referred to as network. This is to enhance the data collection (Havskov *et al.*, 2002).

3.4.1 Seismograph

These are devices that make a records seismic waves caused by an earthquake, explosion, or earth-shaking phenomenon. Seismographs are equipped with electromagnetic sensors that translate ground motions into electrical charges which are processed and recorded by analog or digital instruments. A seismograph consists of seismometer (sensor) and recorder (digitizer and data logger). The record of the ground motion as a function of time is referred to as the seismograms.

The seismograms provide the basic data with which the seismologists study the elastic waves as they spread through the earth. (Figure 3.1) shows Seismogram of an earthquake recorded at IFE station. Three orthogonal components of ground motions (up-down, north-south, and east west) are shown as are needed to record the total (vector) ground displacement history; The Nigerian National Network of Seismic Stations (NNNSS), seismographic stations are equipped with state of the art seismic instruments, high efficient electrochemical seismometers, extremely low power consumption and one unit data acquisition system consisting of digitizer, data logger, communication accessories to ensure real time data transfer, connectors (input/output), trigger and event detection units (Havskov and Alguacil 2010). The seismograph stations are sited at remote locations away from sources of noise such as traffic, ocean waves, human activities.

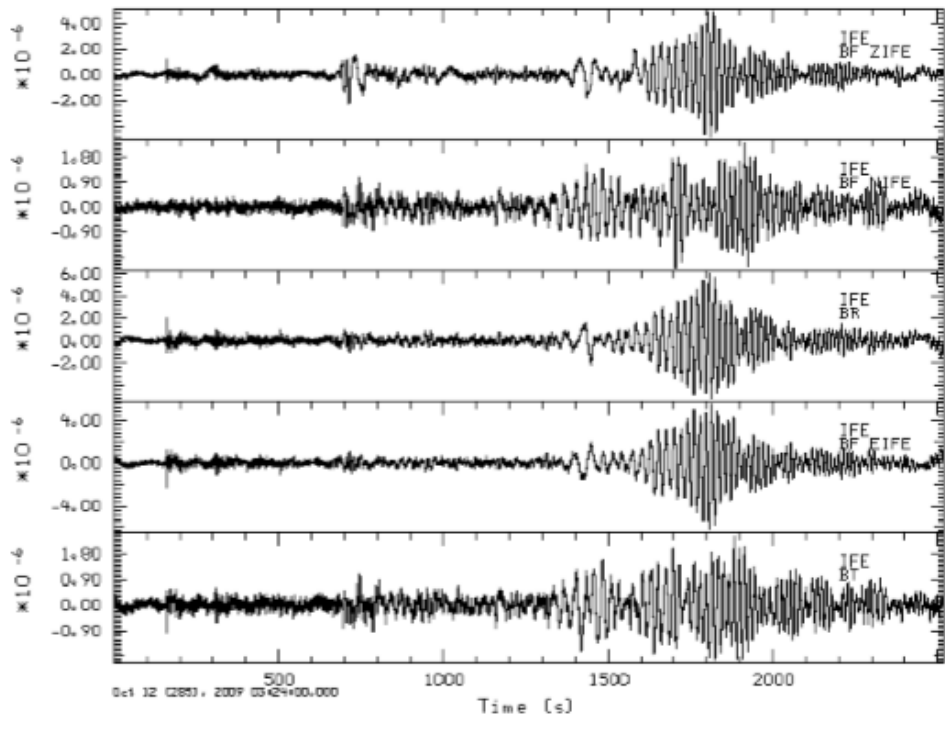


Figure 3.1: Seismogram of an earthquake recorded at IFE station (Centre for Geodesy and Geodynamics, 2016).

3.4.2 Seismometer

Seismometers, commonly called seismic sensors are instruments that measure motions of the ground, including those of seismic waves generated by earthquakes, nuclear explosions, and other seismic sources. This motion is dynamic and the seismic sensor or seismometer also has to give a dynamic physical variable related to this motion (Havskov and Alguacil 2010). Since the measurements are done in a moving reference frame (the earth's surface), almost all seismic sensors are based on the inertia of a suspended mass, which will tend to remain stationary in response to external motion (Havskov and Alguacil 2010). The relative motion between the suspended mass and the ground will then be a function of the ground's motion (Figure 3.2).

There are four basic types of seismometers, these are: short period (SP), long period (LP), broadband (BB) and very broadband (VBB)

1. The short period seismometers operate on frequency between 1 - 100 Hz and are constructed to have Dashpot, a very short natural frequency and a correspondingly high resonant frequency which is higher than most frequencies in a seismic wave. Examples are Mark Products L4-3D and Geotech S13.
2. The long period seismometer sometimes called displacement meter operates on frequency that is less than 1Hz with a very low resonating frequency. The lag between the seismometer and the ground motion becomes zero and the amplitude of the seismometer displacement becomes equal to the amplified ground displacement. Examples of LP are Streckeisen STS-1 and Geotech KS5400.
3. The broadband seismometer operates in a large band of frequency containing both SP and LP from 100 mHz to 50 Hz. They can be utilised for registering a very wide range of signals and the dynamic range extends from ground noise up to string

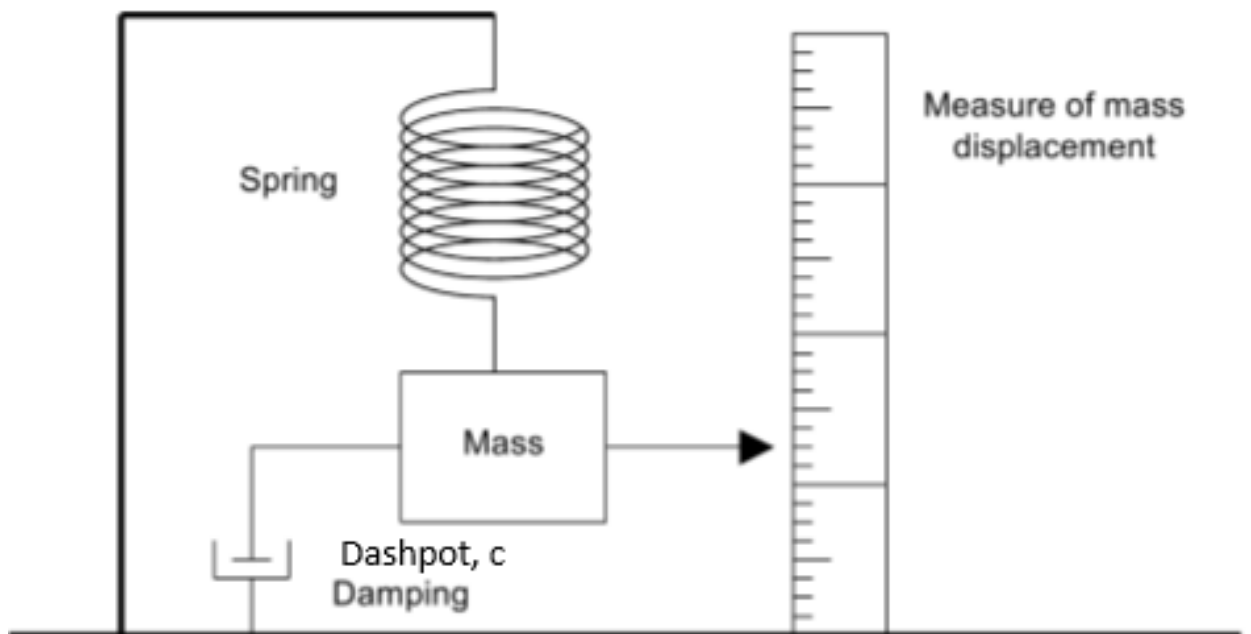


Figure 3.2: The principle behind the inertial seismometer

acceleration such as would come from a very major earthquake, and the periods that can be recorded range from high frequency body waves to the very long period oscillations associated with Earth Tides. Examples are Guralp 3T, Guralp 40T, Geotech KS2000, Nanometrics Trillium Compact, Eentec's EP105 AND SP400.

4. Very Broadband (VBB) operates in a large band of frequency containing both Short-Period and Long Period but a wider band than BB from 10 mHz to 50 Hz. Examples are Guralp 5T and Kinometrics.

3.4.3 Seismic recorder

The seismic recorder consists of the digitizer and the data logger. The digitizer consists of Analogue-to-Digital Converters (ADC) which is in-built in the seismic recorders and converts the analogue seismic signals to a sequence of digital samples for further processing and storage. There are two important aspects of the digitizer; these are the sample interval (step in time direction) and the resolution (step in amplitude direction), which corresponds to one step in the numerical output from the digitizer (Havskov and Alguacil 2010). A schematic diagram of a digitizing process is shown in Figure (3.3), while Figure (3.4) is a typical analogue to digital conversion process diagram (Havskov, 2002). Digitizers are usually classified as 12 bit, 16 bit or 24 bit signifying the number of discrete values of the digitizer uses. The data logger, also referred to as the recorder is the storage medium in form of a hard Disk where all the signals are stored. All recorders also have an additional facility for recording the time of event.

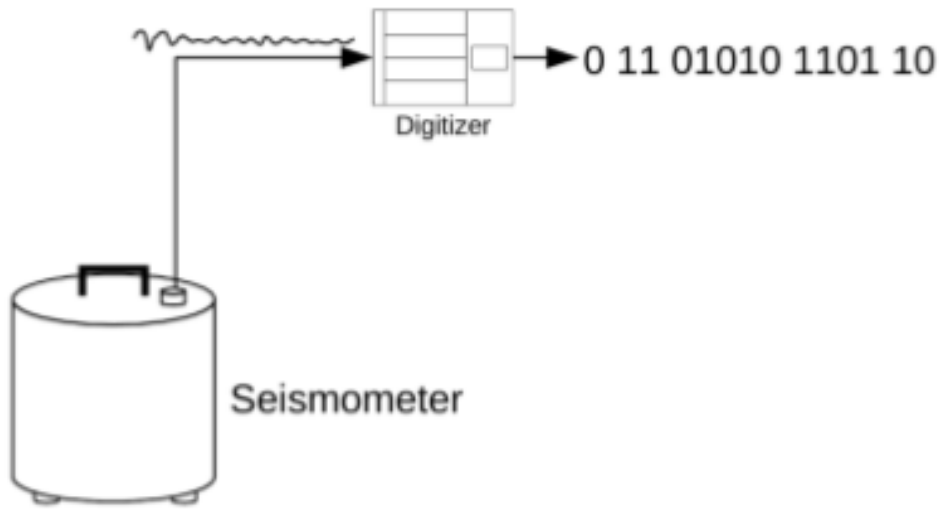


Figure 3.3: Schematic diagram of a digitizing process (Havskov and Alguacil 2010)

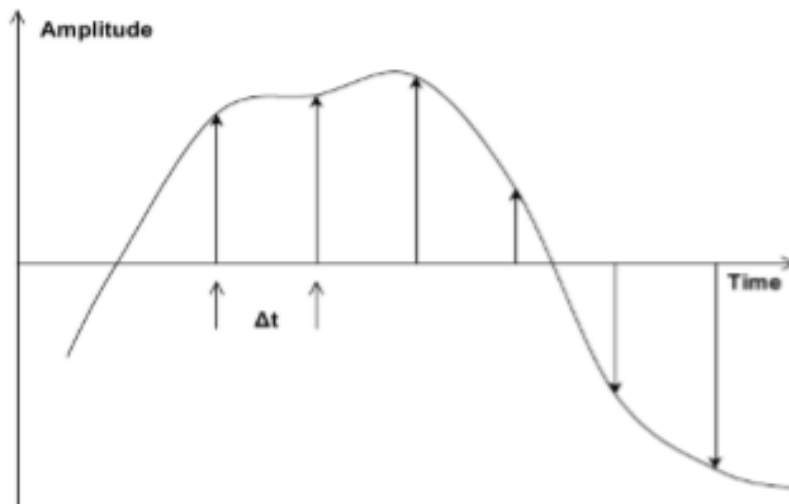


Figure 3.4: Schematic diagram of a typical analogue to digital conversion process.

(Havskov and Alguacil 2010)

3.4.4 Seismic signal processing

In the proceeding sections, seismic recording and seismic data storage technique were discussed. Seismic signals usually in digital form and this has afforded seismic data analyst many options for viewing the data in different ways and performing advance signal processing tasks. Signal processing is necessary because of the noise associated with most earthquake data and the contributions from the component elements of the seismograph. The following processes are the major techniques applied in the processing of earthquake data to obtain a noise free signal:

1. Filtering
2. Removal of instrument response
3. Rotation of seismogram component
4. Re-sampling
5. Correlation

3.5 Seismic station location

Seismic equipment is not just located anywhere outside on the field but requires a carefully selected site based on the aim and objectives or the subsequent uses of observed data. However, the main goal in station location is to achieve a sensor installation which is as insensitive to ambient noise sources (human and environment) as possible (Havskov *et al.*, 2002). This is to ensure that the sensitivity for earthquake generated signal is high. In other words, the station should be far from the oceans and human activities as much as possible. A new seismic station, can be either part of a local or regional network, or can be a stand-alone station which can be part of a global network. Stations that are part of a local network cannot be located anywhere, since the network must have some optimal configuration in order to best locate events in the

given region. Within the NNNSS networks, the stations are located in triangulations so as to be able to calculate earthquake epicenters once they occur. It is important to install all sensors on basement rock, if possible. The depth of the installation is then only important to the extent of eliminating low frequency noise caused mainly by temperature changes. Short period sensors are even sometimes installed in concrete over-ground bunkers, which at the same time serve as housing for equipment and a secure installation. If there is no hard rock within the area, it is always an advantage to put the sensor (any kind) few meters underground. Vaults are usually constructed for the sensor.

3.6 Seismic Data Analysis

3.6.1 Location of earthquake epicenter

The seismic database has been managed using SEISAN earthquake analysis software, version 11.0 (Havskov and Ottemoller, 2000). Data from the 5 stations were used for the location of the earthquake. The first arrivals of the P- and the S- waves were picked on each of the vertical components of the 5 stations (Figure 3.3). Although the velocity structure under the Nigeria crust has not yet been determined, for the location of the epicenter of this earthquake, a flat six-layered earth model was adopted (Table 3.1). The thickness of the crust was assumed to be 40 km which is the average value for proterozoic crust (Mooney *et al.*, 1998). The upper and lower crust were 23 km and 17 km thick respectively. The program HYPO- CENTER 3.2 (Lienert and Havskov, 1995) was used to locate the epicenter of the event.

Table 3.1. Earth model used for the location of the epicentre of the earthquake.

Earth layer	P-wave velocity (km/s)	Layer thickness (km)
Upper crust	6.2	12
	6.6	11
Lower crust	7.0	17
	8.0	10
Upper mantle	8.15	30
	8.5	

3.6.2 Determination of magnitude

Two types of magnitude were computed in this study, the local magnitude and the moment magnitude. The local magnitude (M_L) is an important parameter in earthquake hazard assessments both in terms of quantifying the rate and amount of seismicity and in understanding the attenuation of ground motion with distance.

M_L scales are typically based on amplitude measurements of high-frequency S waves. (Brazier *et al.*, 2008). The magnitude scale used for this study is expressed in equation (3.15)

$$M_l = \log A + a \log(r) + br + c \quad (3.15)$$

where M_l is local magnitude, A , is the maximum ground displacement (nm) measured in the frequency band 1.25-20 Hz, a , is the geometric spreading (0.776), r , is the hypocentral distance, b , is the attenuation (0.000902), c , is the base level (- 1.66), Langston *et al.*(1998).

The moment magnitude, M_w , of the earthquake will be computed using the expression of (Kanamori, 1983) given in equation (3.16)

$$M_w = \frac{2}{3} \log M_o - 10.73 \quad (3.16)$$

where M_w is the Moment magnitude, and M_o the seismic moment measured in dynes-cm. Equation (3.16) is equivalent to:

$$M_w = \frac{2}{3} \log M_o - 6.06 \quad (3.17)$$

where M_o is measured in Nm.

CHAPTER FOUR

4.0 RESULTS AND DISCUSSION

4.1 Results

4.1.1 Result of total magnetic intensity (TMI) map

The total magnetic intensity (TMI) anomaly map of the study area, Figure 4.1, reveals variation in magnetic anomaly within the study area. There are variations in magnetic intensity values which suggest a wide variety of different magnetic properties. These magnetic effects are due to the magnetic susceptibilities of different types of rocks, difference in the lithology, degree of strike and variation in depth to magnetic source within the area. The total magnetic intensity map shows both positive and negative anomalies with susceptibility values ranging from 33777.1 nT to 33460.3nT.

The high magnetic susceptibilities obtained were found around the North-eastern and North-western parts of the study area which corresponds to Lere, Kajuru, Toro, Bassa, Jema'a, Riyom, Barkin-Ladi and Zangon-Kataf areas. These anomalies could be due to the presence of basalt in the area as mapped by Figure 2.2. The low magnetic susceptibilities were found around the south-western corner of the area, corresponding to Gwagwalada, Abaji, Suleja, Gurara, Tafa, Bwari, Paikoro, Kagarko and Municipal area Council, due to the level of weathering of the basement rock and thick overburden. The area with low magnetic susceptibility values ranging between 33570.2 nT and 33632.4nT indicates alluvium deposit around Muya, Kokona and Akwanga areas. Figure 4.2 is the contour map obtained from Total Magnetic Intensity which shows line

of discontinuity inferred to be fault line label as (AA¹). Above and below this fault line are low magnetic closures.

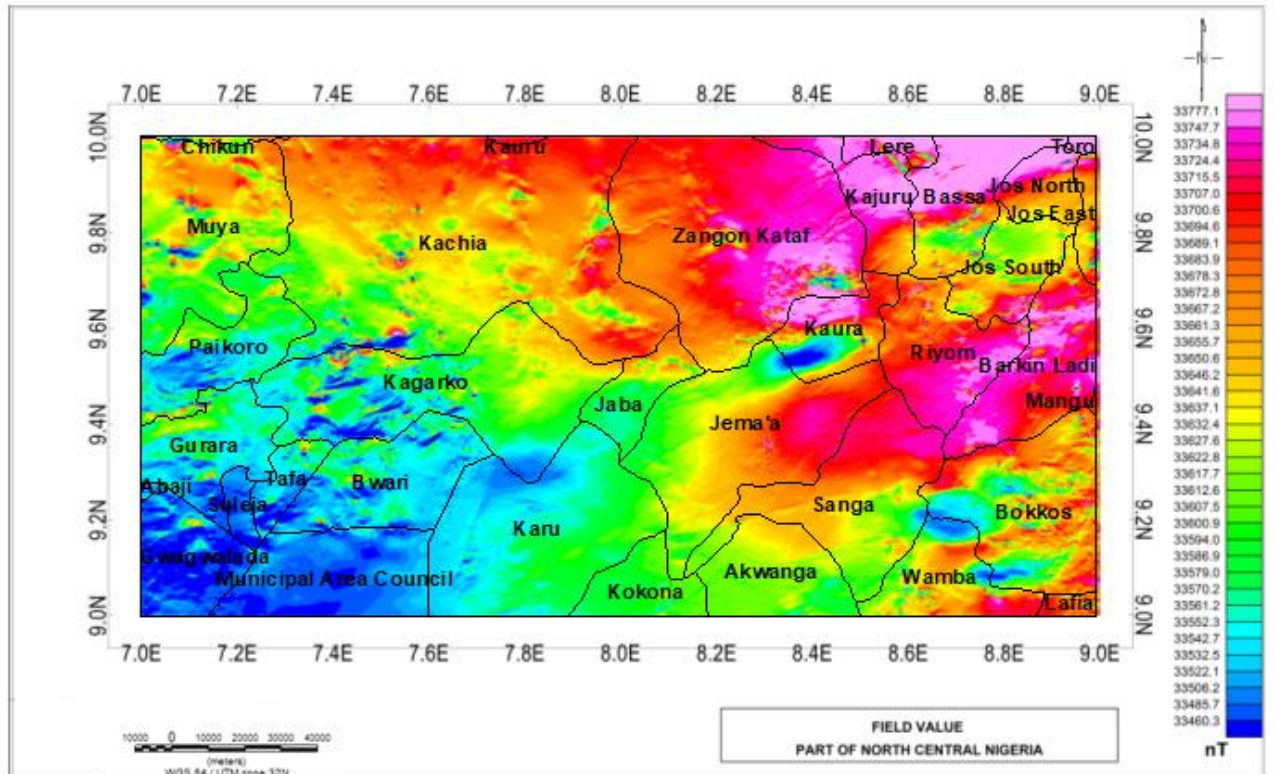


Figure 4.1: Total Magnetic Intensity Raster map of the study area

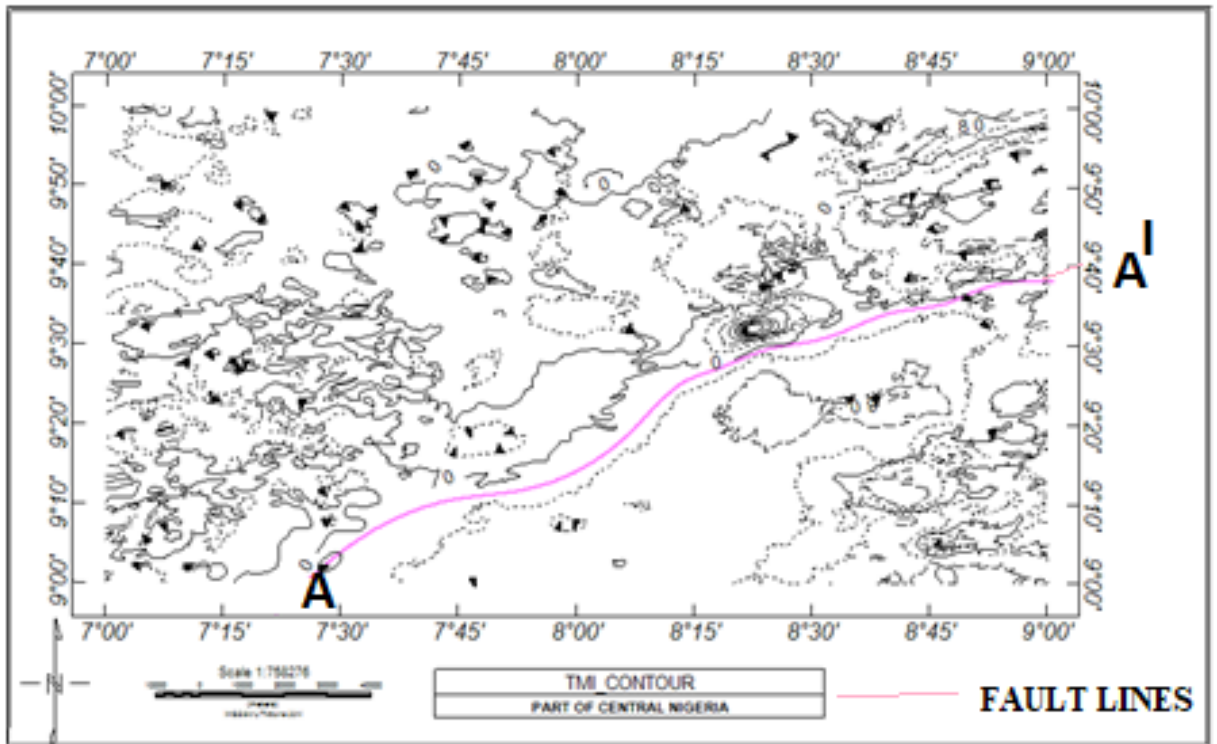


Figure: 4.2: Total Magnetic Intensity Map of the study area showing inferred fault lines

From the map (Figure 4.2), Fault line AA¹ was observed to pass through areas around Jema'a, Riyom, and Barkin-Ladi areas.

4.2 Result of Reduced to Equator (RTE)

RTE filtering was applied on the TMI of the study area in order to center the peaks and make magnetic anomalous bodies appear horizontally over their corresponding causative source bodies, Figure 4.3. Reduction to Equator was applied here because the data in Nigeria are low latitude magnetic data closer to the Equator than the Poles. The RTE map has magnetic intensity values ranging from 33094.659nT to 32908.968nT compared to TMI map where the magnetic intensity values are between 33777.1nT to 33460.3 nT. However, RTE map of the study area has high magnetic signatures trending NE-SW direction and extends to the central part of the map around Jema'a area, these could be due to basaltic rock found within the area (Figure 2.2). Low magnetic anomalies, lie within northeastern part of the study area, around Jos North, Jos East and Jos South and towards the central part around Kaura and Jaba area. Figure 4.4 is the 2-D and 3-D maps of RTE which shows a major fault cutting across the study area. The fault line is clearly designated as X-X¹ in the study area.

4.3 Result of Upward Continuation

The total magnetic field data of the study area reduced to magnetic equator was upward continued at the height of 1km, 2km, 3km, and 5 km so as to enhance and locate the deep-seated anomalies (long wavelength anomalies) within the study area and is shown in Figure 4.5, 4.6a, 4.6b, 4.7, 4.8a and 4.8b respectively. The upward continuation at the height of 1 km shows existence of a prominent fault trending NE-SW (Figure 4.5). The dominant structural trend NE-SW observed on the map (Figure 4.5) is related to the Pan African trending fault system and that of basement complex which follows the tectonic grain of the schist belt (Olasehinde *et al.*, 1990).

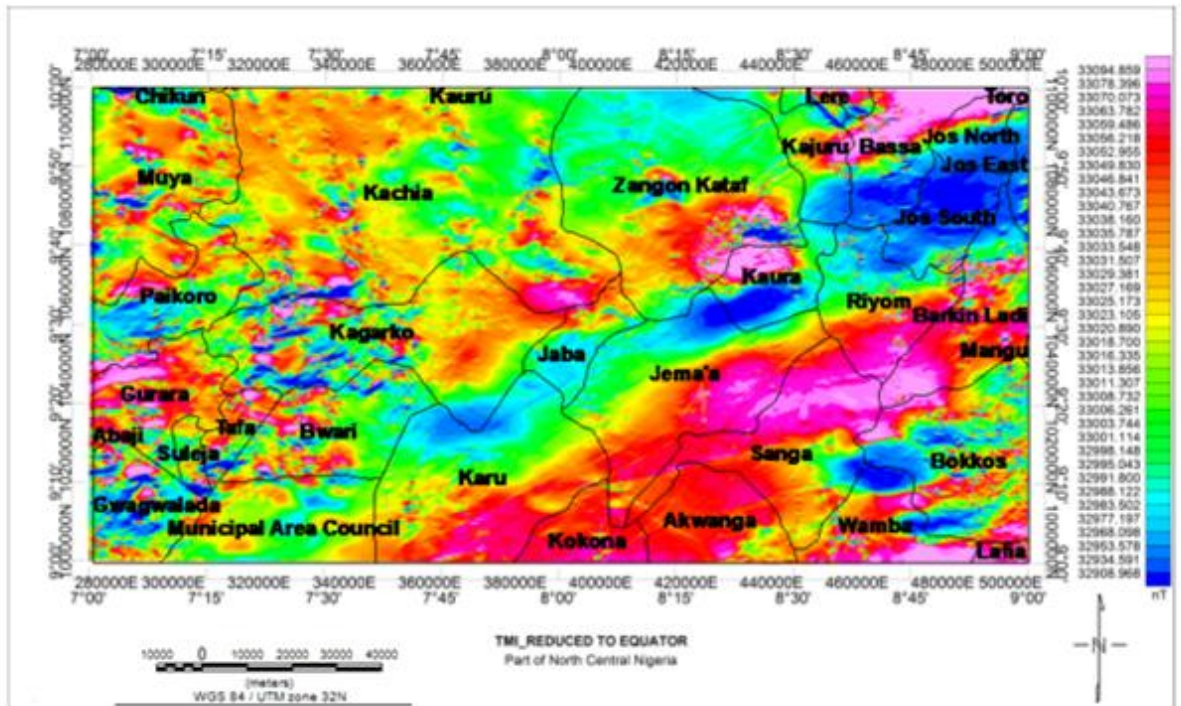


Figure 4.3: Total Magnetic Intensity Map of the Study – Reduced to Equator

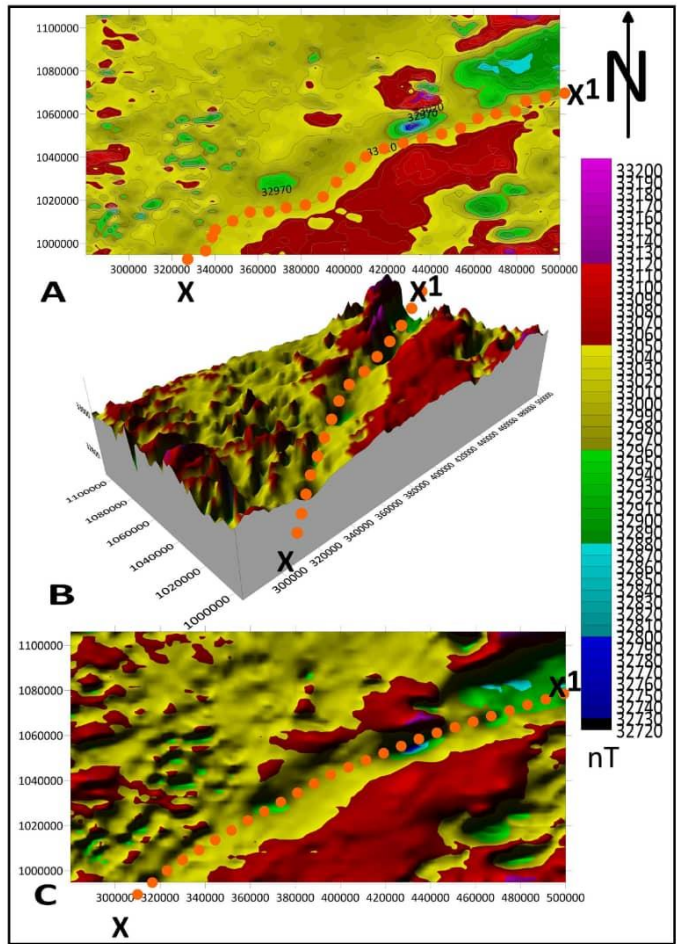


Figure 4.4: 2D (A and C) and 3D (B) Maps of Reduced to Equator shows a major fault line cutting across the study area.

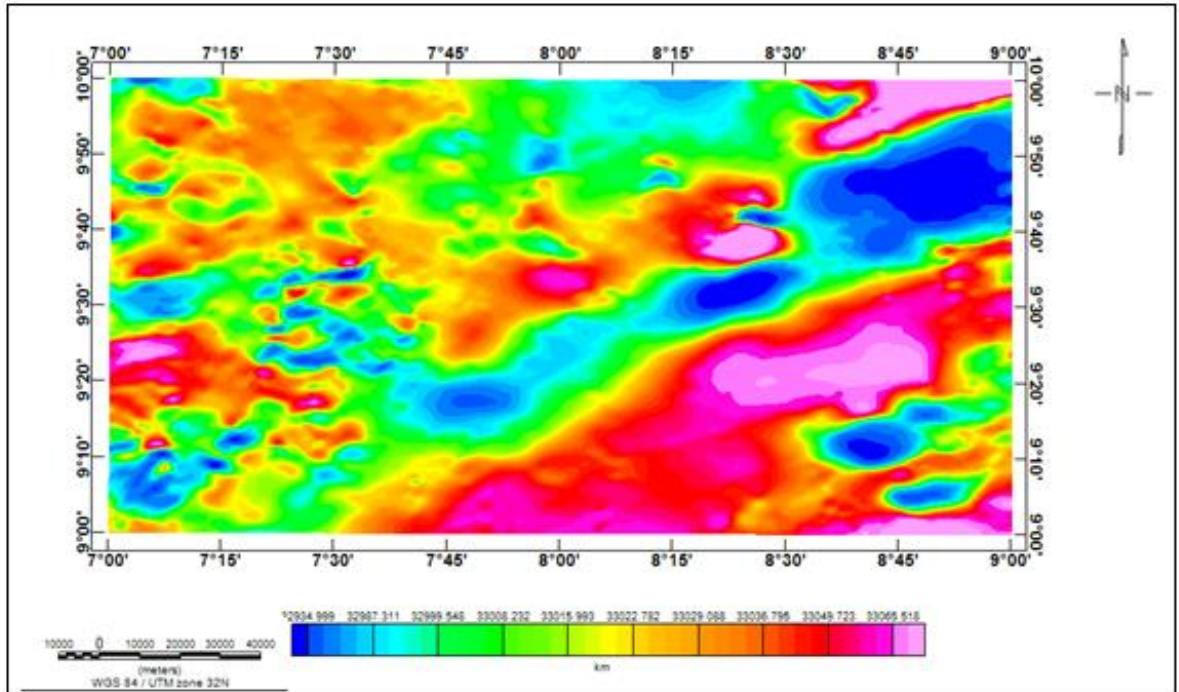


Figure 4.5: Upward`continuation at 1 km

The fault continues in upward continuation filtering at 2 km, 3 km and 5 km as shown in figures 4.6a, 4.6b, 4.7, 4.8a and 4.8b respectively. The grey-scale is presented in figure 4.6b and 4.8b showing the fault more clearly. The appearance of this fault at their depths shows that the fault is deep-seated. The fault line delineated in Figure 4.8b agreed with the fault lines delineated in Figures 4.2, 4.3, and 4.4. The inference is that this fault is a paleofracture zone, that some researchers like Megwara and Udensi (2013) and Tawey *et al.* (2020) have called Romanche fracture zone. Figure 4.8c is the Paleostucture zone's map.

4.4 Result of Horizontal Derivatives (Dx)

Figure 4.9a is the horizontal derivative (Dx) which estimates the rate of change of magnetic intensity in the E-W direction, thereby enhancing structures that are oriented N-S or sub parallel to the N-S. The horizontal derivative (Dx) map (Figure 4.9a) amplified (accentuate) short wavelength anomalies within the study area that trends NE-SW or NW-SE. from the map, these shallow seated anomalies which could be fault or fractures and are very dense around the western part to the end of the map around Gwagwalada, Abaji, Suleja, Bwari, Kagarko, Paikoro, Muya and Chikon areas (Figure 4.8a). Also, at the north eastern part of the map, short wavelength anomalies with edges trending northeast to southwest are observed around Bassa, Lere, Kaura, Bokkos, Jos South, Riyon and BarkinLadi.

4.4.1 Result of horizontal derivative (Dy)

Figure 4.9b is the horizontal derivative (Dy) which estimates the rate of change of magnetic intensity in the N-S direction, thereby enhancing structures that are oriented E-W or sub-parallel to the E-W. These fault lines identified trends in NE-SW and E-W trend direction (Figure 4.9b). Most of the high magnetic susceptibility identified is towards central part of the map around Jema'a and Karu areas.

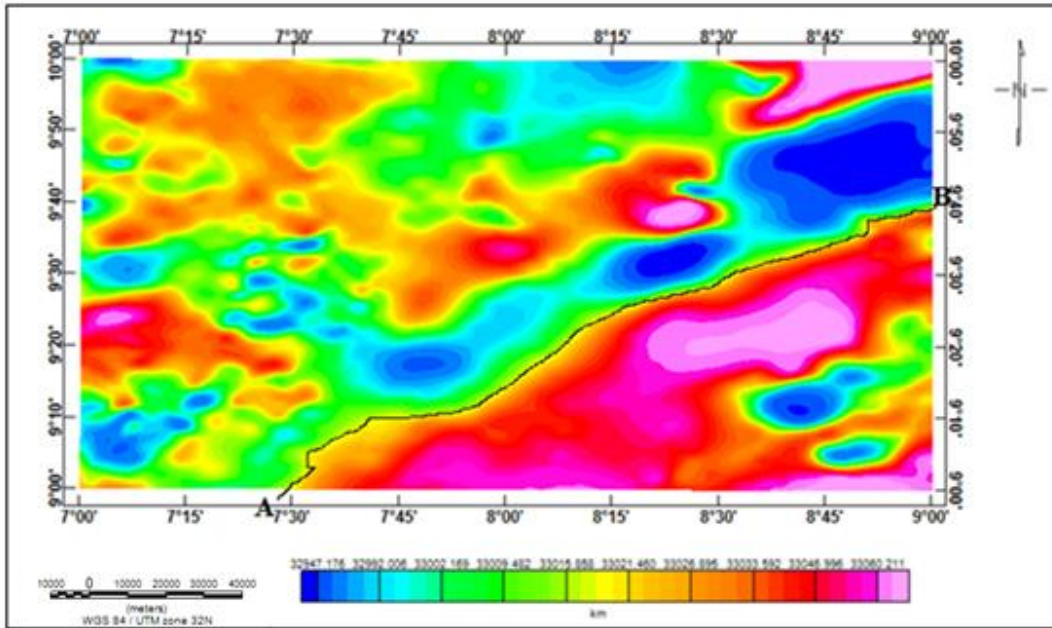


Figure 4.6a: Upward continuation at 2 km

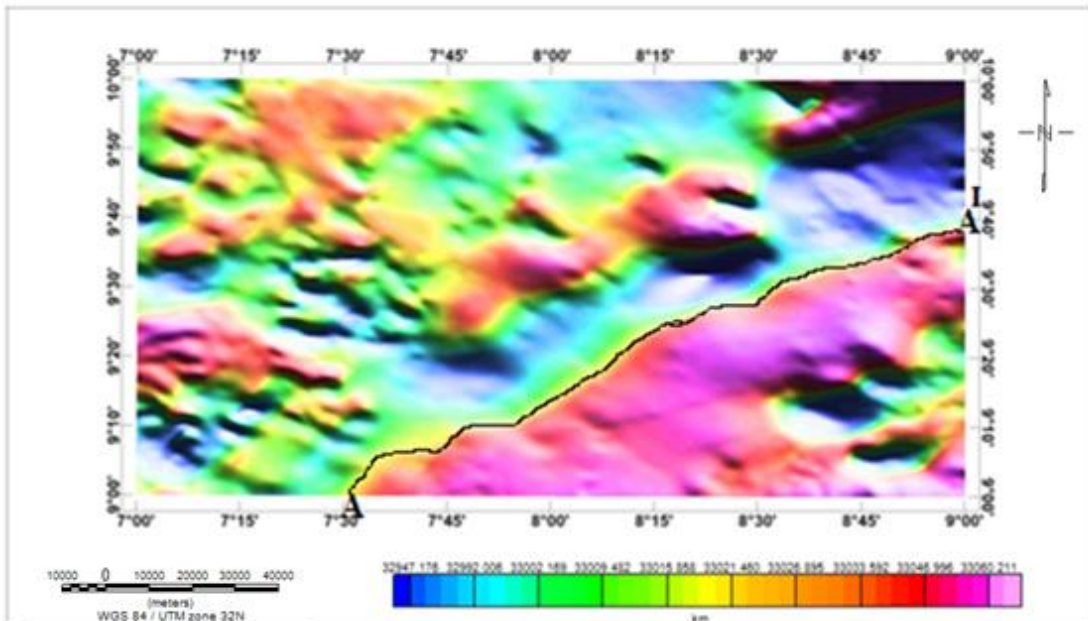


Figure 4.6b: Upward continuation at 2 km in Grey-Scale

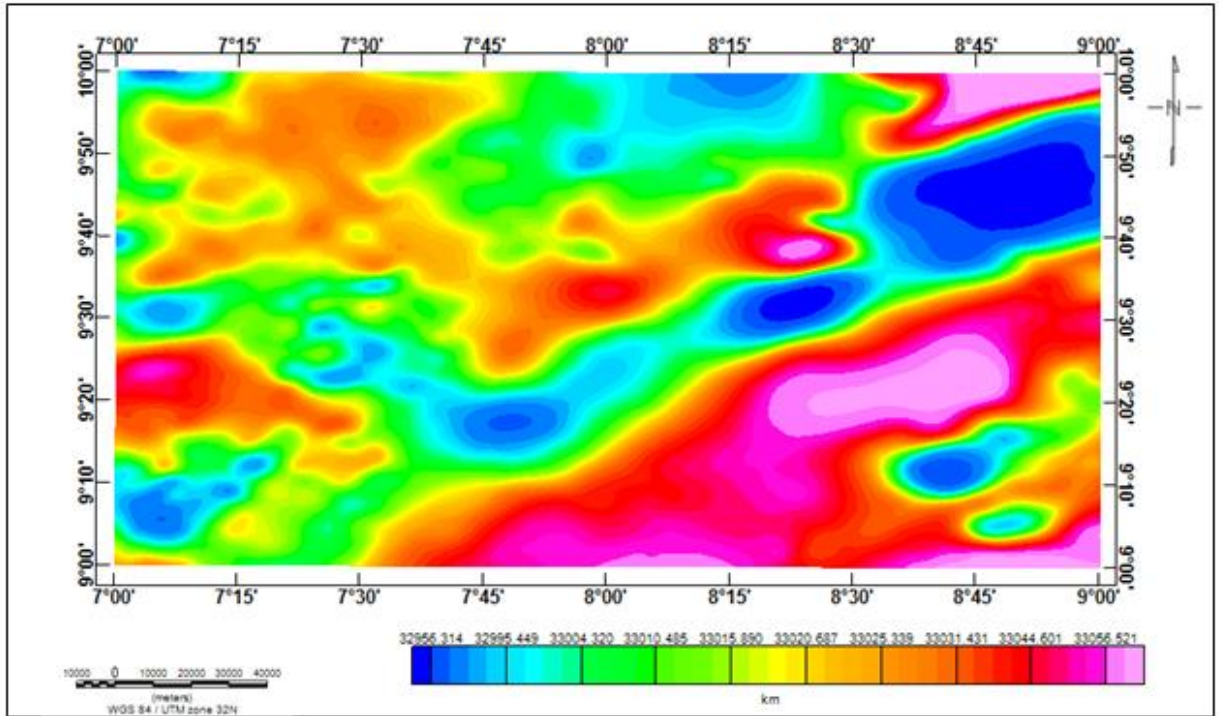


Figure 4.7: Upward continuation at 3 km

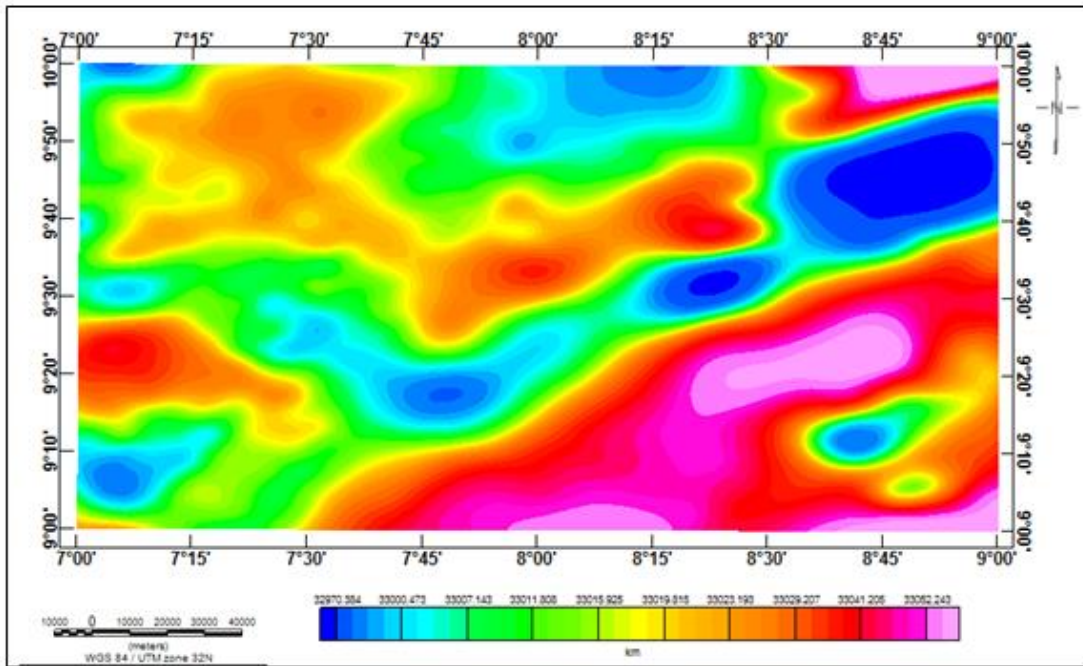


Figure 4.8a: Upward continuation at 5 km

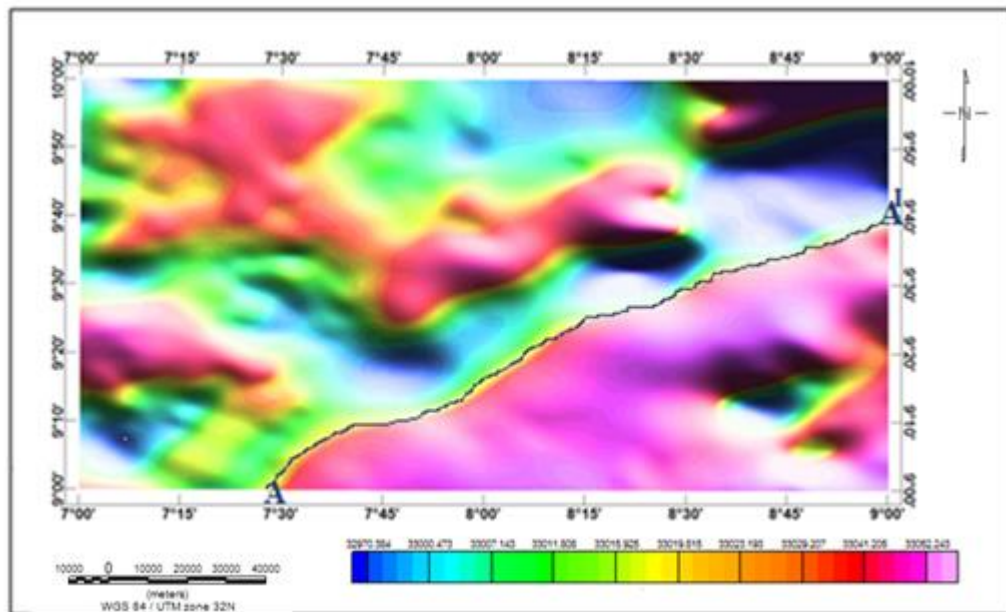


Figure 4.8b: Upward continuation at 5 km in Grey-scale

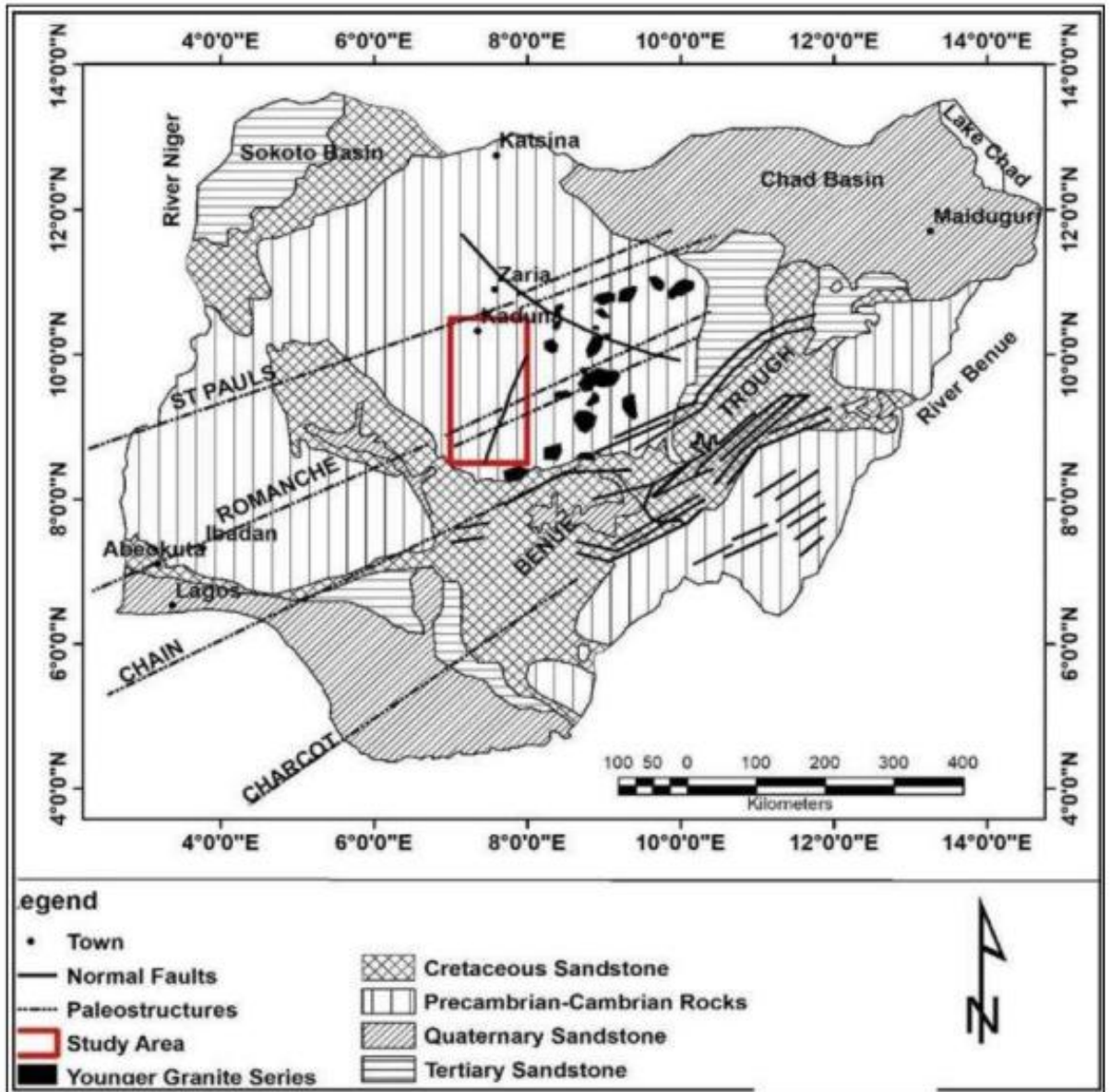


Figure 4.8c: Paleoproterozoic zone's map

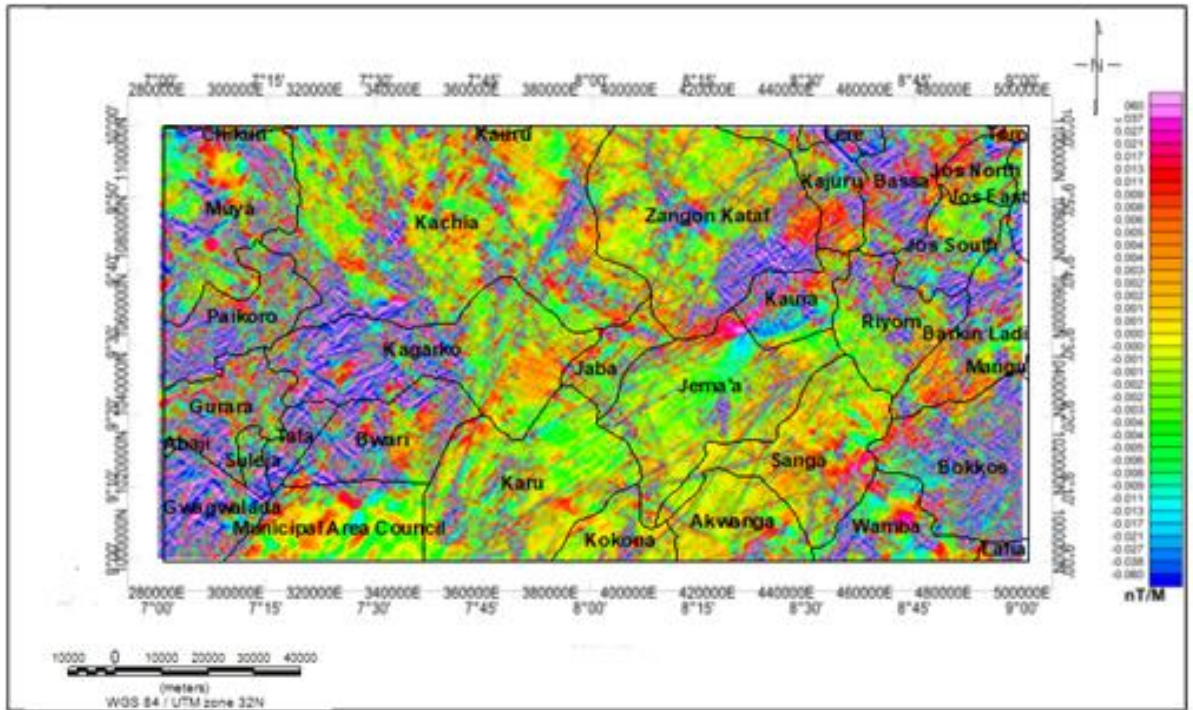


Figure 4.9a: Horizontal Derivative in x-direction Map

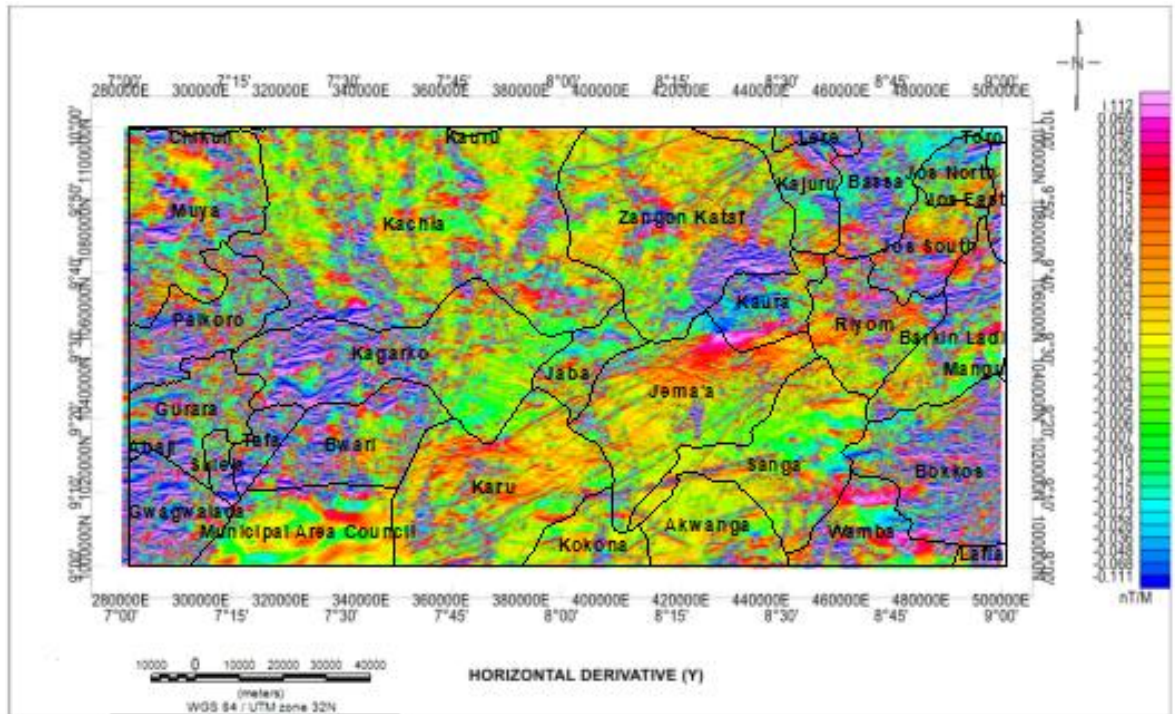


Figure 4.9b: Horizontal Derivative in y-direction Map

4.5 Result of First Order Derivatives

Figure 4.10a is the First Vertical Derivative Map which tend to amplify the high frequency short- wavelength anomalies that are associated with geological structures in the study area. The First vertical derivative of the field mapped several lineaments that are primarily fault lines within the study area, marked as F₁ to F₈. From the map, the map revealed high frequency (short wavelength) anomalies along north western part of the map, this short wavelength are also observed at the northeastern part of the map. The delineated lineament obtained from the map is trending in NE-SW, NW-SE, N-S and E-W. The dominant trend is NW-SE. The N-S trend defines the geological trend within this area. These trend directions correlate well with the mineral density map of Nigeria (NGSA).

4.6 Result of First Order Derivatives in Grey Scale

Figure 4.10b shows first vertical derivative in grey scale which intensify the lineament picture clearly and can easily identified minor fault, major fault lines which are fracture as well as lineament, the major fault is represented in red coloration trending in NE-SW and E-W direction which the trend direction is in agreement with First vertical derivative map (Figure 4.10 a) and the NE-SW trend is also in agreement with the geology map of the study area (Figure 2.2). The minor fault is represented in green colouration is also trending in NW-SE direction. Fold is seen in blue coloration and is trending towards the NE-SW and NW-SE directions. From the map, a prominent fault line, F₄ in Figure 4.10a which cut across the study area labeled AA', which is believed to be one of the continental paleostructure. This fault line was delineated by Megwara and Udensi (2013) and Tawey et al. (2020), as Romanche. This lineament agreed with the fault lines delineated by Figures 4.1, 4.2, 4.3 and 4.8b.

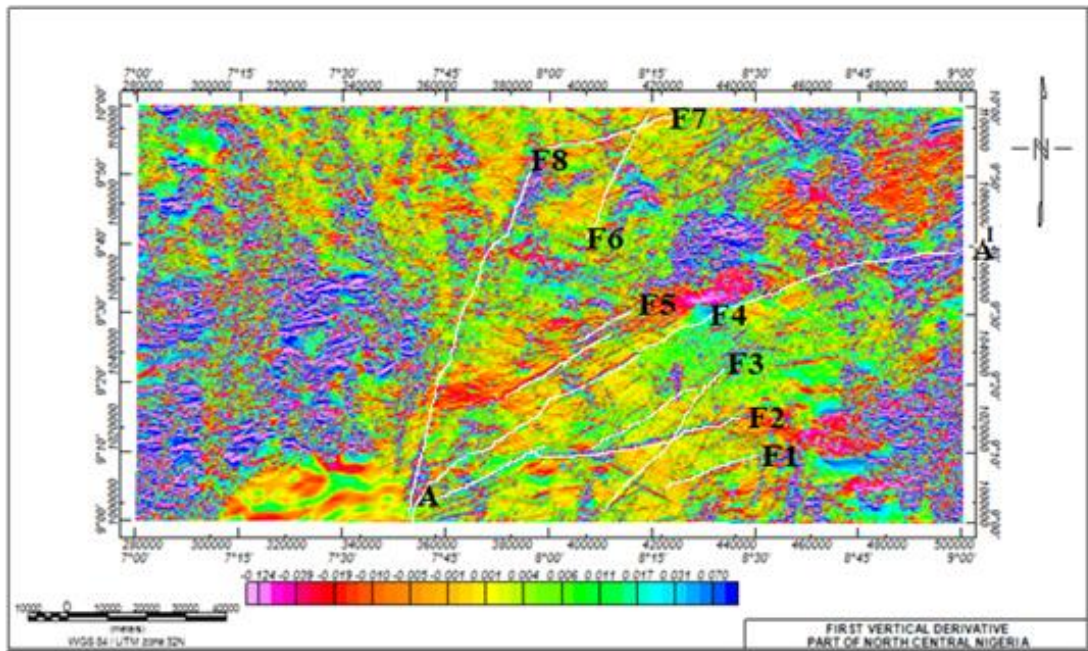


Figure 4.10a: First Vertical Derivative of the study area

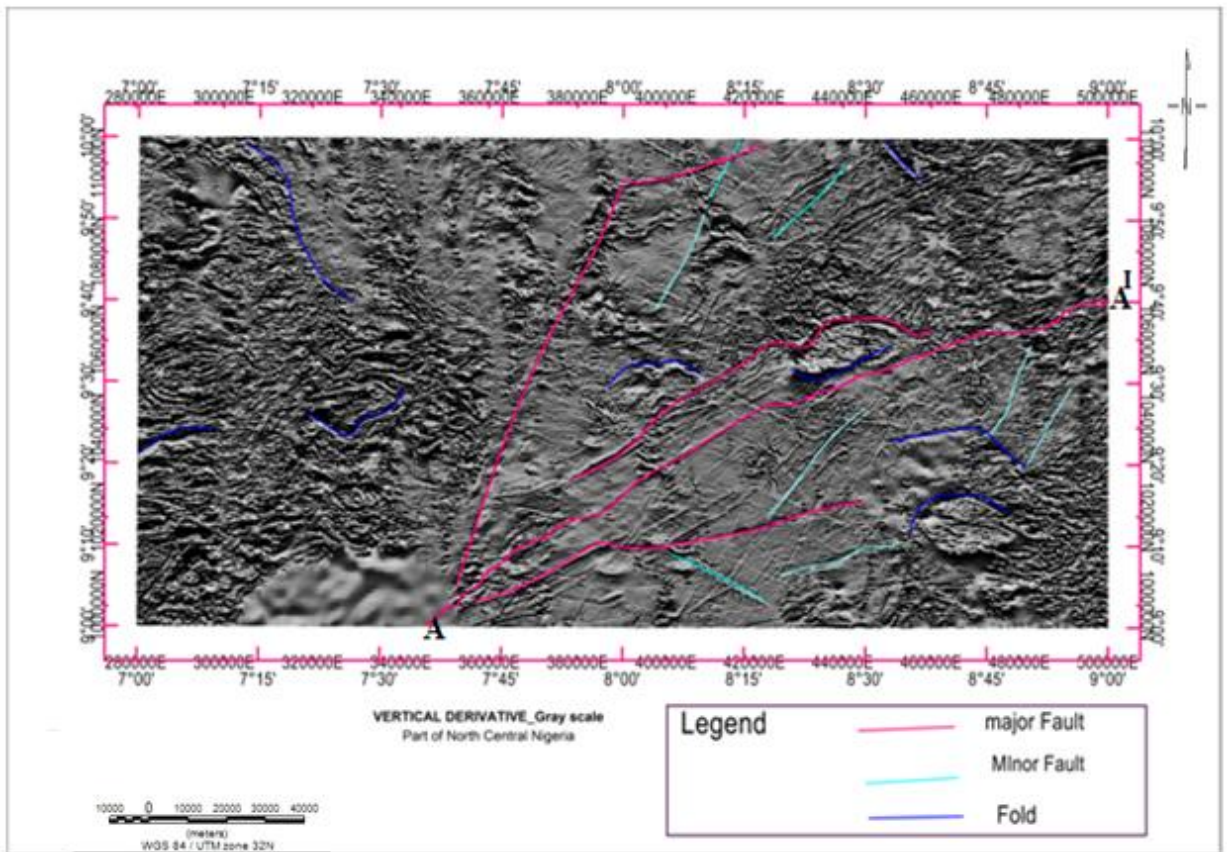


Figure 4.10b: First Vertical Derivative in Gray-Scale

Faults F1, F2, F3, F5, F6, F7 and F8 are emerging near surface fault lines, since they could not be captured by upward continuation at 5 km depth. Therefore, those fault lines are indications that the paleostructure (Romanche) is still active since those emerging fault lines are traceable to it.

4.7 Result of Tilt Derivatives

Figure 4.11 shows the Tilt derivative map, the Tilt derivative map has a magnetic intensity range between 1.3379 nT/m to 1.3847 nT/m. A1, A2, A3, A4, A5, A7 and A8 are indications showing regions with magnetic highs which are basically fresh basement outcrops. Older weathered outcrops are shown as regions with a mixture of highs and lows comprising of areas around Zangon-Kataf, Kaura, Jos south and Kachia areas. Generally, these regions are underlain by Precambrian and/or lower Palaeozoic Basement Rocks where younger granites intrude into the Older Basement Rocks. A1, A2, A3, A4, A5, A7 and A8 in the map trend in a NE-SW direction. This map is in agreement with Figure 4.1 in term of high magnetic susceptibility around northeastern region of the map.

4.8 Result of Center for Exploration Targeting (CET) Grid Analysis

Figure 4.12 shows the Center for Exploration Targeting Map (CET), the application of the center for exploration targeting (CET) grid image analysis technique was applied to the aeromagnetic data of the study area for rapidly locating regions of tectonic trend within the study area. The technique automatically delineates lineaments using several statistical steps including texture analysis, lineation detection, and vectorization. Figure 4.12 is obtained from CET shows linear structures that trend in the NE-SW, NW-SE and E-W direction which is in agreement with Figure 4.10a.

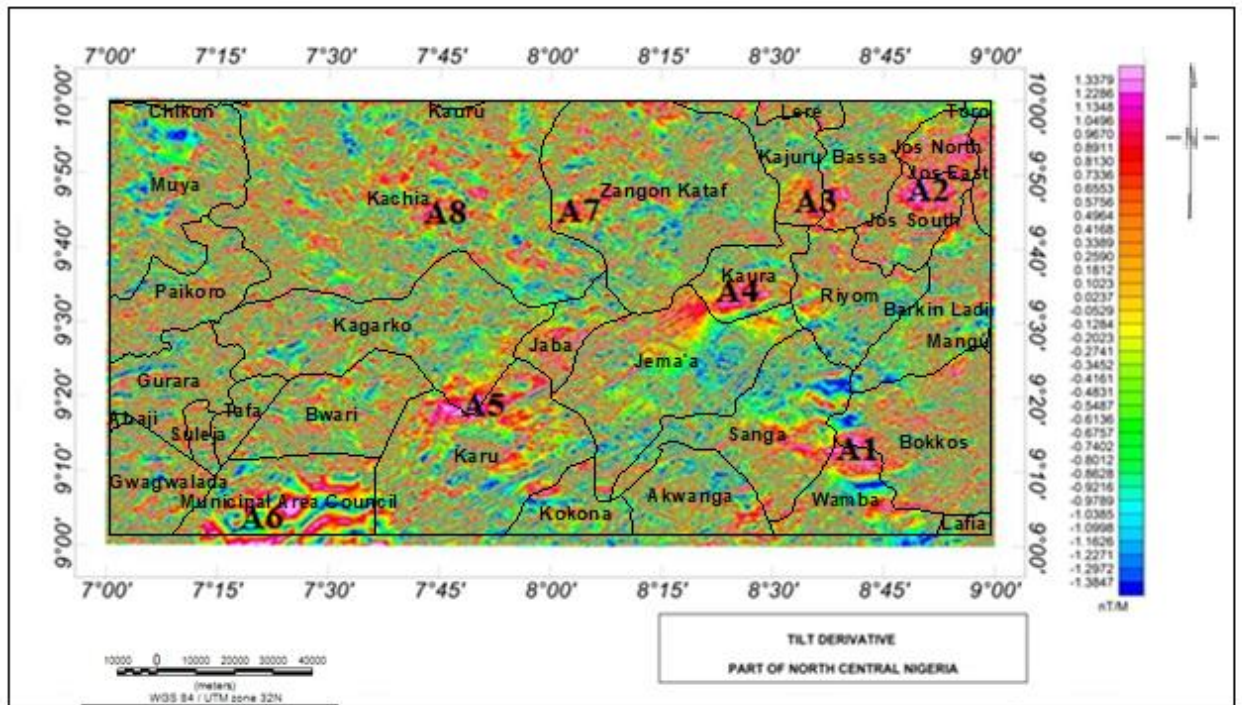


Figure 4.11: Tilt Angle Derivative map of the Study Area

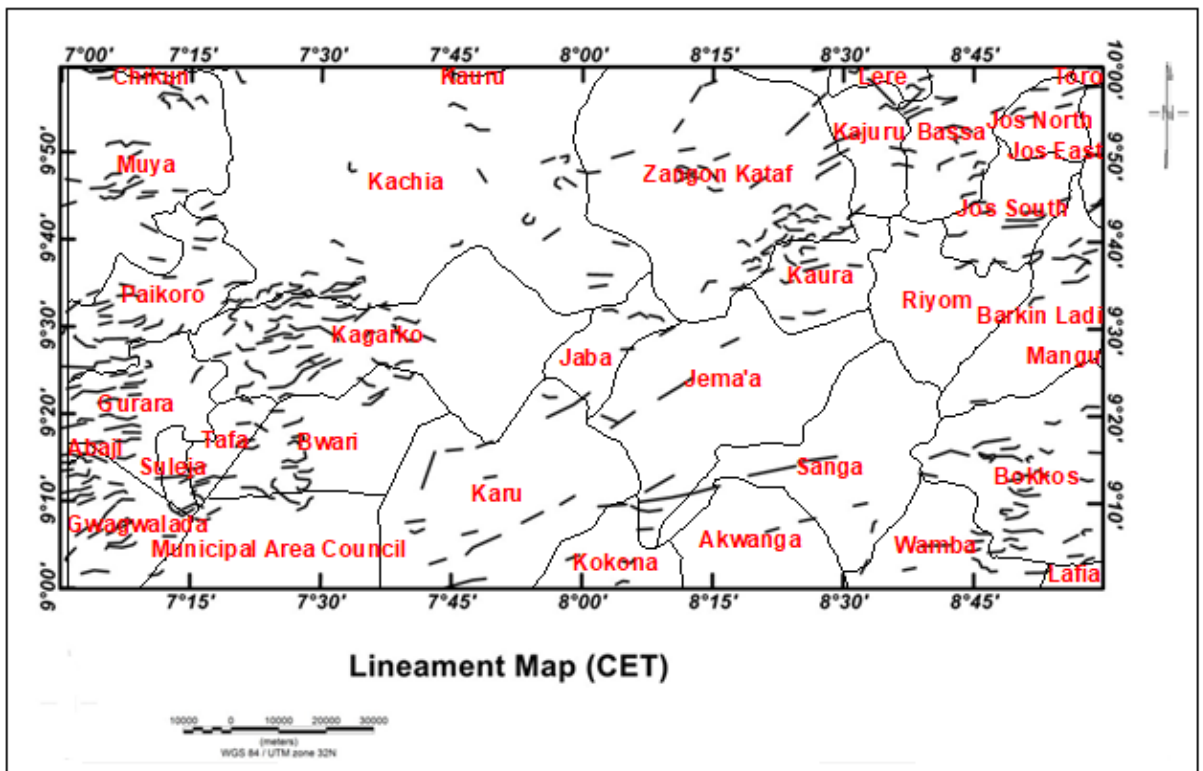


Figure 4.12: Center for Exploration Targeting (CET) map of the Study Area

4.9 Result of Analytical Signal Map

The analytic signal map (Figure 4.13) highlights the variation in the distribution of magnetic sources in the study area. The analytical signal map displayed high intensity amplitude from the north eastern part and also span towards the western end of the map and there are also isolated occurrences of high intensity around the north east and south west. The analytic signal amplitude maximizes over the edge of the magnetic structures as a result, the high magnetic anomalies zones are associated with high rich ferromagnesian-bearing rocks with minor felsic minerals (Telford *et al.*, 1990). Result of Analytical signal method indicates distinct variation in magnetic susceptibility between the older granitic basement rocks and the younger intrusive granitic and basaltic body. The analytic signal map has amplitudes ranging from 0.246 to -0.137nT/m within the study area. The alkaline igneous rocks (younger granite) depict higher amplitude of magnetic susceptibility compared to the older acidic basement rocks. Most of this high amplitude of magnetic susceptibility is situated around the Western, North-eastern and South-eastern part of the study area. Prominently within Abuja, Gwarinpa, Kubwa and Bwari within FCT, also around Jere, kateri, Kamancha, Zumkwa and Samaru in Kaduna State, they are equally sited within Bokos, Nungu and Mayir of Plateau state.

The analytical signal map is separated into Mafic and Felsic igneous rocks, where the felsic igneous rocks are characterized as having a lower iron content, as a result their magnetic susceptibilities are frequently smaller in comparison with the Mafic rock which has high iron content.

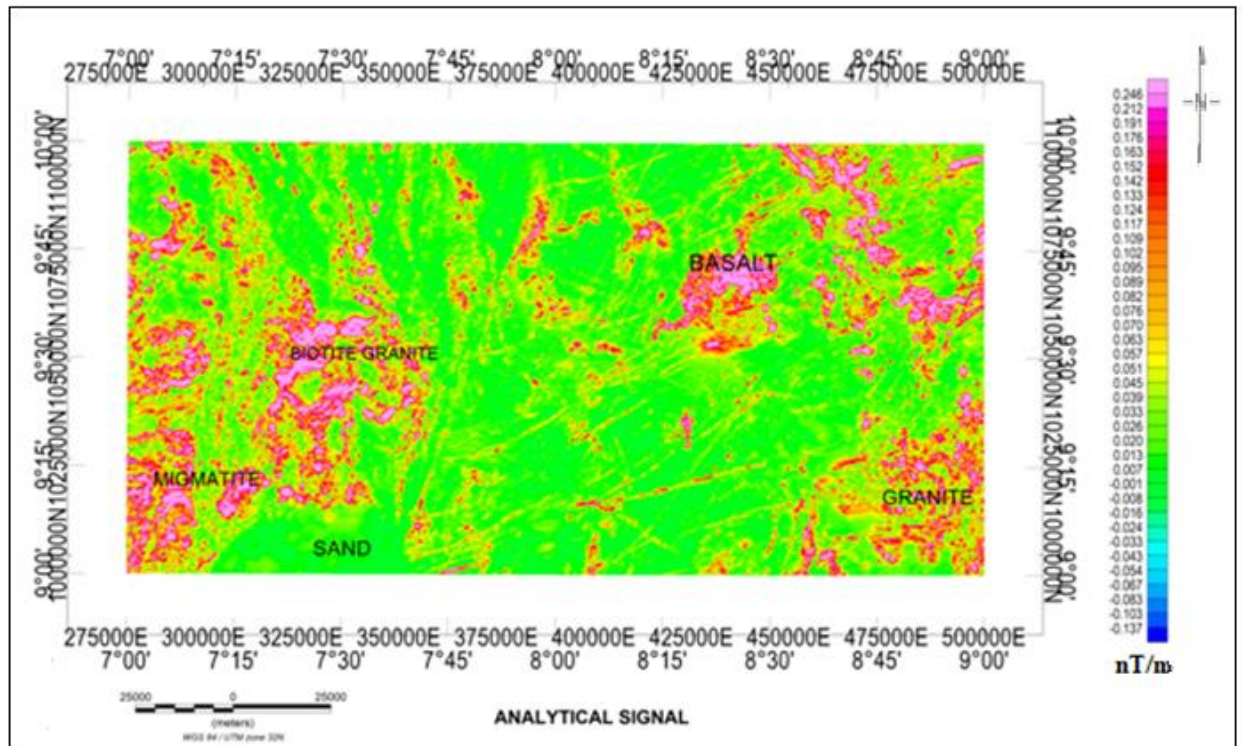


Figure 4.13: Analytic signal Map of the study area

4.10 Discussion

4.10.1 First vertical derivative (FVD) map compare with center for exploration targeting (CET) map

Figure 4.14 represents the First Vertical Derivative map and Center for Exploration Targeting (CET) Map. The correlation identified in both maps shows various lineaments trending in the same direction for both maps, with trending direction along NE-SW and NW-SE direction. This is in agreement with (Olasehinde *et al.*, 1990), who analyzed aeromagnetic data over central Nigeria's basement complex and concluded that the Nigeria basement complex's structural and tectonic framework comprises NE-SW and NW-SE lineaments superimposed on a dominant N-S trend. The relationship between the characteristics of magnetic lineament and that of CET map shows that most of the lineaments are trending in E-W direction areas around Barkin-Ladi, Mangu, Paikoro, Gurara and Abaji. It is interesting to note that structural features such as faults, joints and fractures are underlain by zones of localized weathering which increases permeability and porosity, thus the lineament map from IVD and CET could be a good target for prediction of underground water recharge flow.

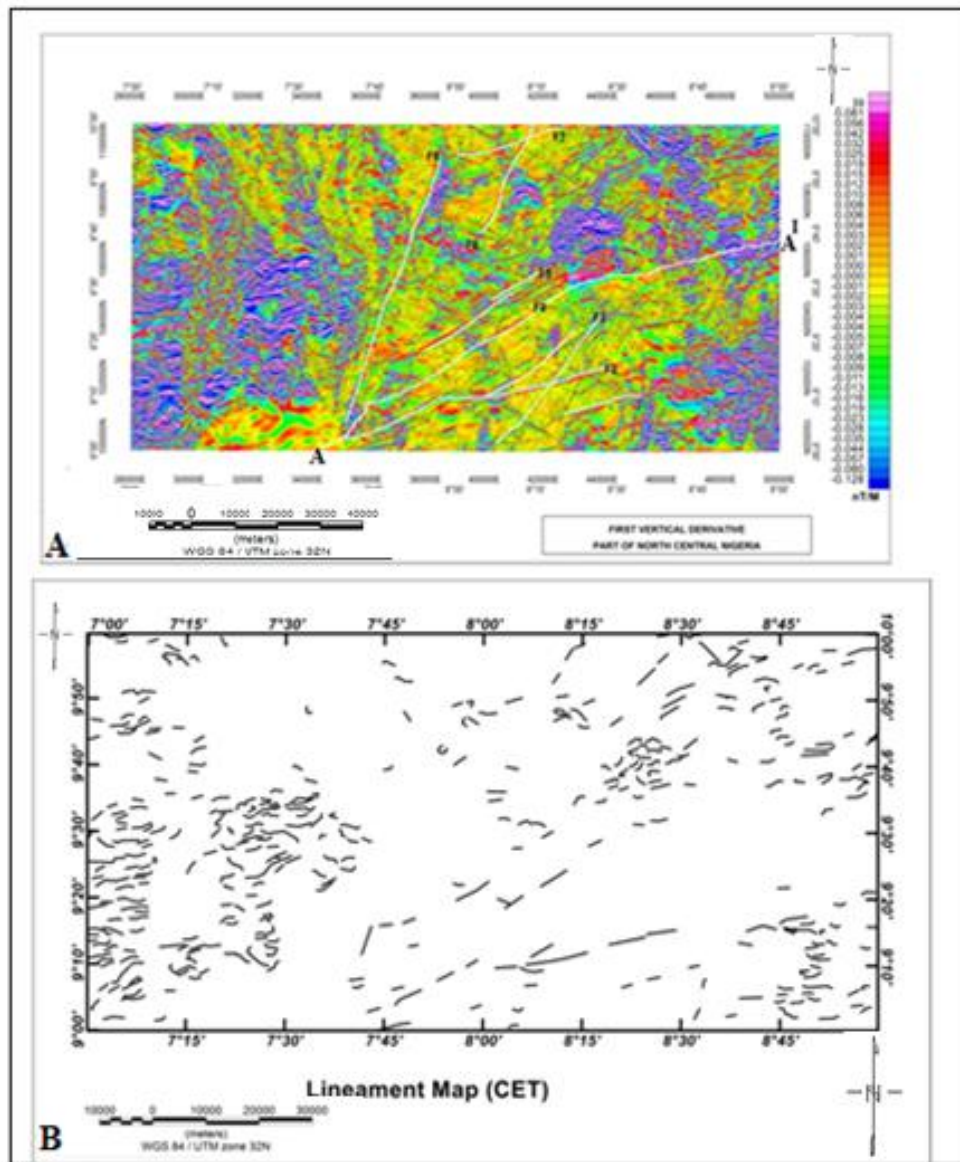


Figure 4.14: First Vertical Derivative (FVD) Map compare with Center for Exploration Targeting (CET) Map. First Vertical Derivative Map (A), and Centre for Exploration Targeting (CET) map (B)

4.10.2 Second vertical derivative map superimpose on the geology map

Figure 4.15 shows the Second vertical derivative map superimpose on the geologic map. The geologic map of the study area describes the rock types in the study area. The map shows the existence of both high and short wavelength which is high in occurrence especially along E-W direction which corresponds to the undifferentiated schist including phyllites porphyritic granite and migmatite-gneiss rock. A small closure at the north-central which correspond to younger basalt with granite and granite porphyry intruded into the basement rock. The structures identified in both maps are the same and is in NE-SW and E-W direction which is in agreement with Figure 4.12a.

4.10.3 Structural geologic map compare with the center for exploration targeting map (CET)

Figure 4.16 shows the lineament map of Nigeria compare with the Center for Exploration Targeting (CET) map of the study area. The major and minor faults are identified in both maps; the correlation identified in both maps shows various lineaments trending in the same direction for both maps the major fault observed in geological structural map is trending in NE-SW, E-W direction and same in Center for exploration targeting map. The trend direction of CET is in conformity with Figure 4.12a. The minor fault is observed to be scattered throughout the map of geological structural map and is the same with CET map.

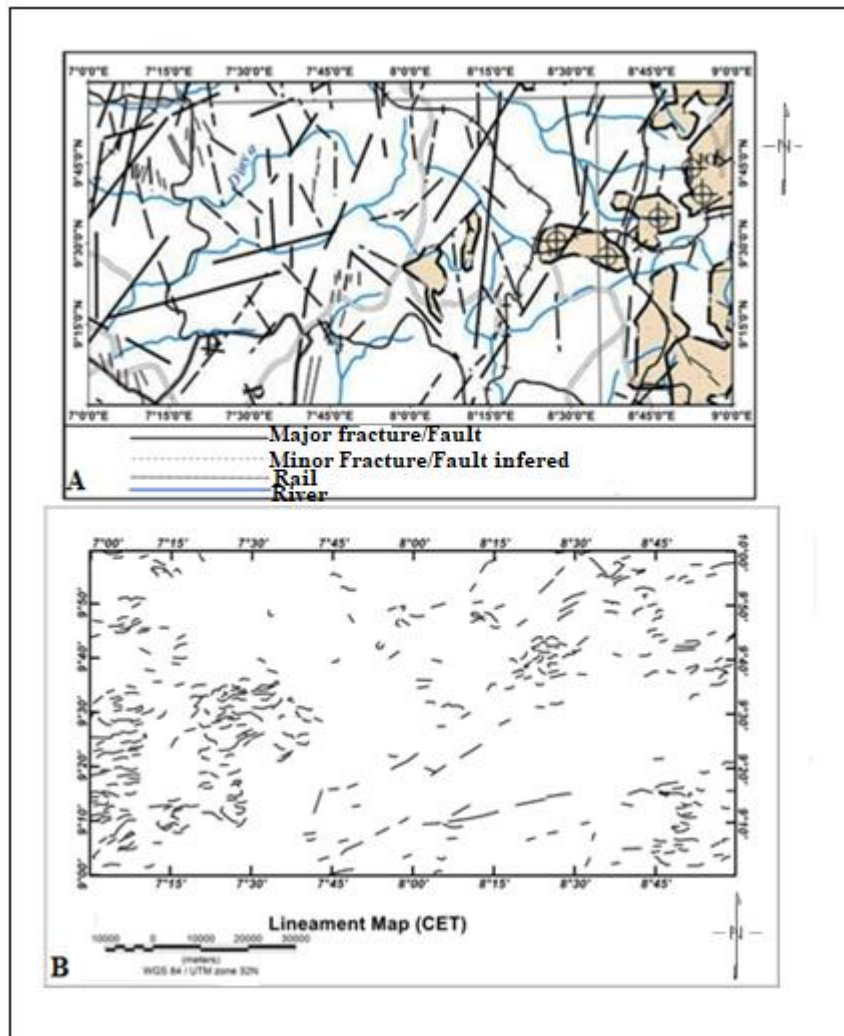


Figure 4.16: Structural Geologic map of the study area compared with the Center for Exploration Targeting Map (CET). Structural Geologic map of the study area (A), and Center for exploration targeting (CET) map (B).

4.10.4 Geology map compared with analytic signal map

Figure 4.17 shows the geology map of the study area compared with the Analytical Signal Map. The Analytical Signal map shows both high and low amplitude within the study area. It shows the high amplitude around the northeastern part and majorly around the western part of the study area. The high amplitude observed along the western part corresponds to undifferentiated schist including phyllites, porphyritic granite and undifferentiated older granites, while the low amplitude observed at the central part and at the southern edge of the map corresponds to silicified sheared rocks, large quartz veins, sand, clay and mangrove swamps mapped from Figure 2.1.

4.10.5 Structural map superimposed on lineament map

Figure 4.18 represent the structural map superimposed on the lineament map (FVD). The FVD map (Figure 4.10a) and structural map (Figure 1.2) were superimposed to ascertain significant similarities on both maps. Lineament with red colouration indicates lineament obtained from First vertical derivative map (Figure 4.10a) and black colouration indicates lineament from structural map (Figure 1.2). The 1VD map did not detect the structures trending in NW-SE directions. But is in agreement with structures trending in NE-SW and NNE-SSW. Some differ in location (coordinate) this is due to the fact that data used in for the present analysis has higher and better resolution compared to those used in mapping the structural map.

A major fault (F8) trending NE-SW situated at the middle of the study area enters through Karu village on Longitude 7.30 E and exist at Kachia on Longitude 8.00. Other set of lineaments labeled F2,F3, F4 and F5 are trending NNE-SSW are mapped between latitude $9^{\circ}.00$ to $9^{\circ}.40^{\text{I}}$ N and longitude 8.0 to $8^{\circ}.45^{\text{I}}$ E striking through Sanga, Jemma'a, Karu and part of Jaba areas. Fault label F7 and F8 correlates in location and direction with some fault in the Structural map of the area.

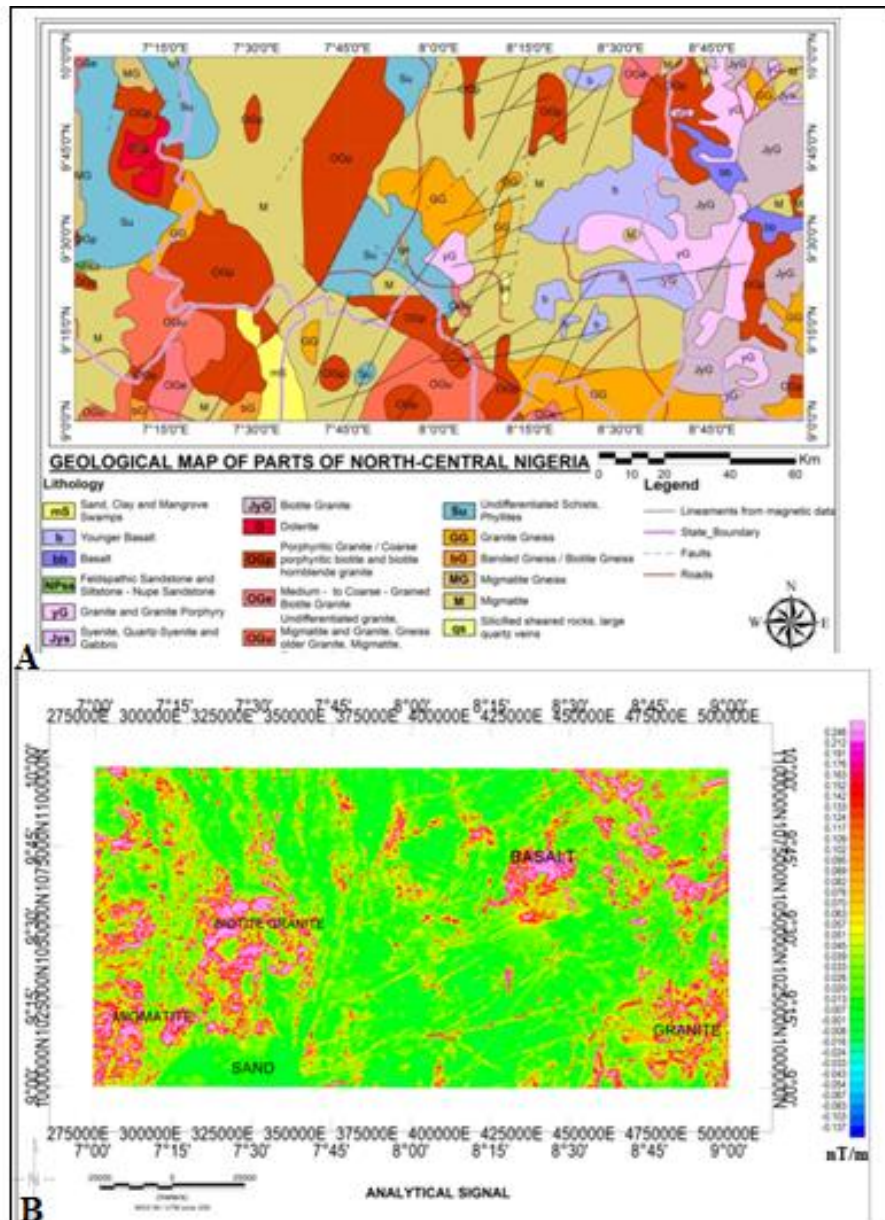


Figure 4.17: Geology map compared with Analytic Signal Map Geology map of the study area (A), and Analytic signal map (B)

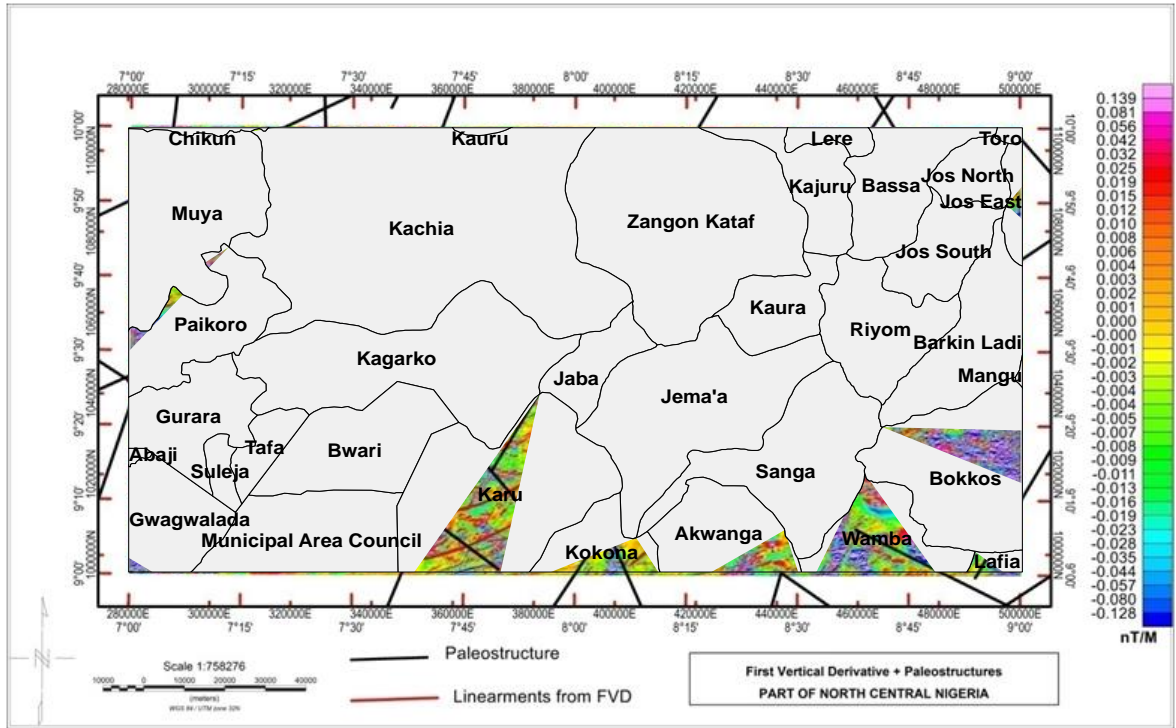


Figure 4.18: Structural map superimposed on lineament map

The trend direction NNE-SSW are in conformity with the NNE-SSW Ifewara fault in southwestern Nigeria, that disappear beneath Bida Basin but reappear at the Zungeru as transcurrent fault line above the Bida Basin. An extension of which has been mapped by Awoyemi *et al.* (2017), Anifowose *et al.* (2010). Others are Anka fault, Akko fault and Danbata Akko fault and Kalangai fault (Awoyemi *et al.*, 2017). Other minor subsidiary fractures are visible at the northern and south-eastern region of the study area, where intrusions of Basalt and younger granite is observed in the map. A detail observation of these fault and fracture density reveals that the major NNE-SSW structure is linked to the Ifewara fault line in southwestern Nigeria which is still active.

4.11 Seismological Results

4.11.1 Source parameters of 2016 kwoi earthquake

The magnitude, epicentre and origin time of the earth tremors in part of North central Nigeria were obtained. The first event occurred on Sunday, 11th September, 2016 at 12:28:16.50 seconds. The second event occurred on Monday, 12th September, 2016 at 03:10:48.80 seconds and the third event occurred the same day at 03:11:20.00 seconds. The difference between the second and third event is 1 minute 28 seconds.

The local magnitude of the first event was 2.8 and moment magnitude was 3.1, the local and moment magnitude of the second event was 2.7 and 3.0 respectively. The third event recorded local magnitude of 3.1 and moment magnitude of 3.1.

The focal depth of the Kwoi earthquakes is estimated to be 10 km. Seismograms of Kwoi earthquakes are shown in Appendice A1 to A4. Appendices B1 shows source parameter of Kwoi earthquake.

The epicenters of the Kwoi earthquakes are latitude 9.570°N and longitude 8.070°E for the first event, latitude 9.640°N and longitude 8.180°E for the second earthquake and latitude 9.590°N and longitude 8.130°E for the third event.

4.11.2 Source parameters of 2018 Abuja earthquake

The Abuja earthquakes occurred in September, 2018 and October 2018. The magnitude of the first, second aftershock and the main shock were determined as follows: the first aftershock had a moment magnitude of 2.5 and local magnitude of 2.6, the second aftershock had a moment magnitude of 2.2 and local magnitude of 2.5 while the main shock had a local magnitude of 3.0 and moment magnitude of 2.6.

The epicentre of the first aftershock was latitude 9.0339°N and longitude 7.5008°E, the second aftershock was located at latitude 9.1620°N and longitude 7.4014°E, while the main shock was located at latitude of 9.139°N and longitude 7.594°E.

The origin time for the first aftershock occurred at 6:16:17.80 seconds, the second aftershock occurred at 7:12:18.40 seconds and the main shock occurred at 5:11:32.60 seconds. Seismograms of the mainshock, first aftershock and second aftershock are listed in Appendices A5 to A7. Appendices B2 shows source parameter of Abuja earthquake.

4.12 Discussion

4.12.1 Field site effects of the earthquake

In the analysis of First Vertical Derivative map it was observed that the faults were too close to each other and was concluded that tremors could lead to other subsequent tremors of greater magnitude. This could be the reason why Abuja tremor closely followed the Kwoi event. The Kwoi earthquakes were felt in Kwoi, Nok, Sanbang Daji and Chori, all in Jaba Local Government Area, Kaduna State. The tremors were also felt in neighbouring communities about 20 km from Kwoi. The damage caused by the earth tremor ranged from few cracks on walls of buildings, falling down of ceilings and collapse of houses around Kwoi town (Plate V to VII). These were mainly seen in mud houses. However, in one newly constructed modern house where appropriate engineering design and materials were used, cracks were also seen in the walls and POP

ceilings in almost all the rooms. The residents of Kwoi and surrounding communities felt the tremors because the epicentres lie very close to the areas.

4.12.2 Superimposing of lineament map on geology map showing the epicenter

The Geological map showing the epicenter (Figure 1.3) was superimposed on the Lineament map, (Figure 4.18) to identify the faults that coincides with the related epicenters. Faults that are depicted by black colour are faults obtained from structural map while those depicted by white colour are faults obtained from lineament map. Epicenters are depicted by red circle and are seen at the central part and towards the southern part of the map. The epicenters are strongly related to the emerging faults delineated in this study. The superimposition between the two maps seems to agree in terms of the trend direction in a NE-SW and NNE-SSW direction. The major NNE-SSW trend is in conformity with the NNE-SSW Ifewara – Zungeru fault (Anifowose *et al.*, 2010, Awoyemi *et al.*, 2017). From the map, Figure 4.19, faults lines F5, F6 and F8 coincide with some of the epicenters corresponding to areas around Jaba, Zangon-Kataf and parts of Abuja Municipal area council. These Faults (F5, F6 and F8) seem to be tectonically active due to the closeness of the epicentre within that region. The earth tremor activities are therefore effect of the emergence of these near surface faults. Stress has been built up around those identified faults and this may also cause faults (F1, F2, F3 and F4) to be active and as a result could cause earth tremors within the study area. Fault line (F4) and F8 coincide with epicenter at Jema'a and Abuja Municipal area council, these are areas affected by earth tremor in 2016 and 2018. That the magnitudes of earth tremors are not high also shows the faults are not deep seated and that Nigeria does not lie on a plate boundary.

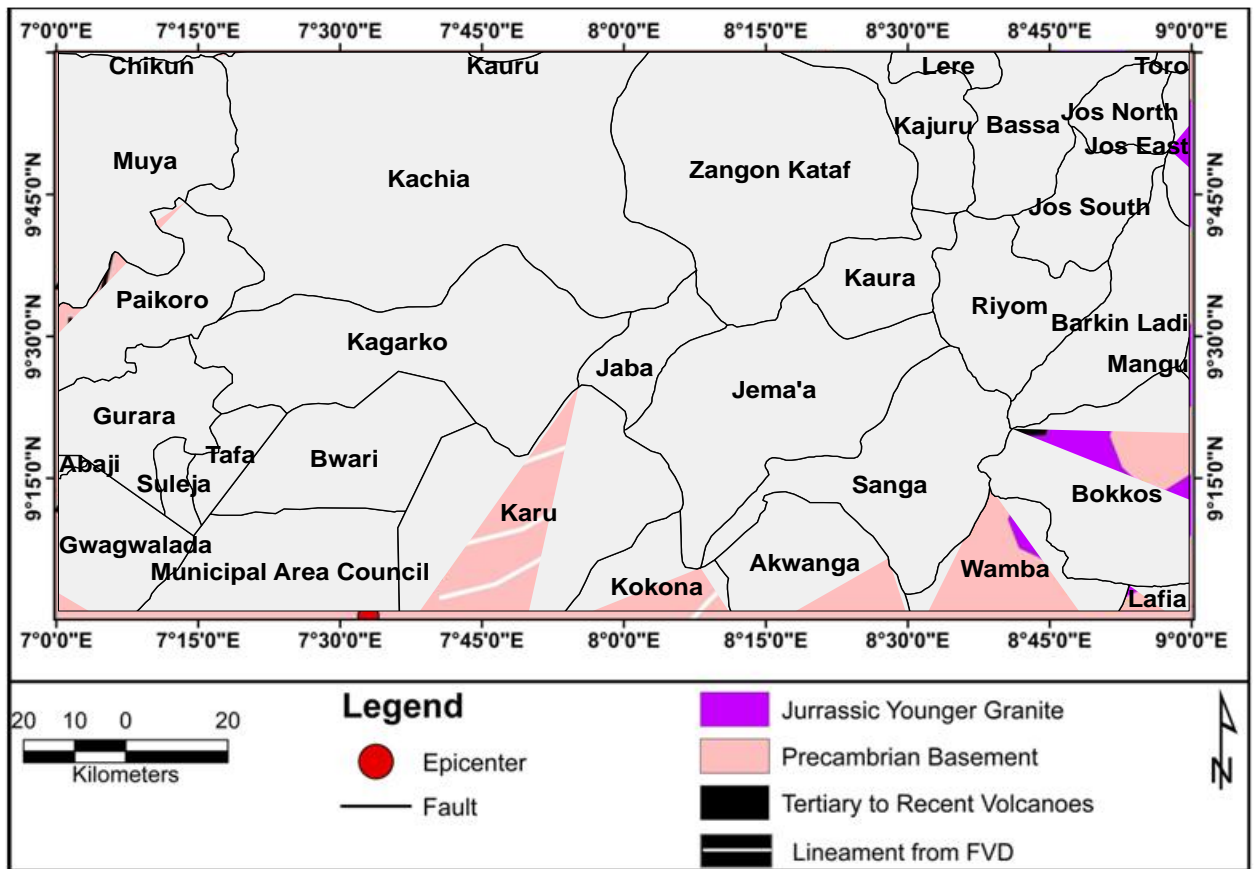


Figure 4.19: Superimposing of Lineament Map on Geology map showing the Epicenter

Map



Plate V: Damage to a mud building in Kwoi town



Plate VI: Collapse of mud house in Kwoi Town



Plate VII: Crack on a newly constructed building in Kwoi Town

CHAPTER FIVE

5.0 CONCLUSION AND RECOMMENDATIONS

5.1 Conclusion

The analysis and interpretation of the aeromagnetic data over the North central parts of Nigeria were successfully carried out using qualitative and quantitative methods with the aim of delineating prominent fault lines and locate the lineament, determine the magnitude, epicenter, time of occurrence of the earth tremors. The TMI-reduced to Equator was upward Continued to 1km, 2 km, 3 km and 5 km to enhance the deep-seated anomalies to be able to locate any fault deep inside the earth surface thereby suppressing the high frequent anomalies due to near-surface features. Upward continuation techniques have been used in this study to locate prominent deep-seated anomalies; at 5 km the fault is deep-seated.

Derivative analysis (1VD, Horizontal, Tilt and CET derivative) was used in this study to locate the position of magnetic lineament (faults or fractures) within the area. Four major trends were observed NE-SW, NW-SE, E-W and NNE-SSW. The dominant trends are NW-SE and NNE-SSW within this area, the first vertical derivative has been used to locate and delineate the location of Paleo-Fractures in the area, trending along NE-SW direction.

The magnitude, epicenter and origin time was determined for Kwoi and Abuja earth tremor. Magnitude for Kwoi earth tremor was determined for three events, the first magnitude has a local magnitude of 2.8 and moment magnitude of 3.1, the second event has magnitude of 2.7 and moment magnitude of 3.0 and the third event has a local magnitude of 3.1 and moment magnitude of 3.1. The first and third event have a moment magnitude of 3.1

The epicentre for Kwoi earth tremor, for the first event located at latitude 9.570°N and longitude 8.070°E , the second event at latitude 9.640°N and longitude 8.180°E and the third event located at latitude 9.590°N and longitude 8.130°E .

The origin time for Kwoi earth tremor for the three events. The first event occurred at 12:28:16.50 seconds, the second event occurred at 03:10:48.80 seconds and the third event occurred at 03:11:20.00 seconds.

The magnitude of Abuja earth tremor, the main shock has a local magnitude of 3.0 while the moment magnitude is 2.6. The First aftershock has a moment magnitude of 2.5 and local magnitude of 2.6, the second aftershock has a moment magnitude of 2.2 and local magnitude of 2.5.

The epicenter for Abuja tremor has an epicenter latitude of the first aftershock at 9.0339°N and longitude 7.5008°E . The Second aftershock was located at latitude 9.1620°N and longitude 7.4014°E . The main shock was located at latitude of 9.139°N and longitude 7.594°E .

The origin time for the main shock occurred at 5:11:32.60, for the first aftershock occurred at 6:16:17.80, and the second aftershock occurred at 7:12:18.40.

The Lineament map was superimposed on the epicenter map to identify the fault that coincides with the epicenter. Fault F5, F6 and F8 coincides with some of the epicenters corresponding to areas around Jaba, Zangon - Kataf, and part of Municipal area council. Fault F4 and F8 coincides with epicenter at Jema'a and Municipal area council, these are areas affected by earth tremor in 2016 and 2018. Therefore, the earth tremor activities within the study area are as a result of the effect of the emergence of these near surface faults

5.2 Recommendations

In view of repeated occurrences of earth tremors within the study area the following recommendations are made:

1. Ground magnetic survey should be employed to identify both the major and other minor faults that could be associated with earth tremor.
2. Weibull equations, historical and instrumental data should be used to investigate the earth tremor within the area to ascertain the present study.
3. Upgrade the infrastructure of the current seismic network to a state-of-the-art digital seismic network with real time telemetry capabilities.
4. Buildings and engineering infrastructure should be constructed within areas that are not connected with the active fault line.

5.3 Contribution to Knowledge

The study was able to identify the lineaments trends of the study area which are NE-SW, NW-SE, E-W and NNE-SSW. The study also identified emerging faults from the paleostructures thus indicating that the ancient faults might still be active. The study also determined the magnitudes of the earth tremor at Kwoi (Kaduna) and Mpape (Abuja) to be 2.7 to 3.0 and 2.6 to 3.0 respectively. The epicenters of the earth tremors at Jema'a (2016) and Municipal area council (2018) were observed to coincide with the emerging fault lines labeled F4 and F8 in the study area. This indicates that the tremors were of tectonic origin. Therefore, this study has identified that the earth tremor activities within Kwoi in Jema'a LGA of Kaduna State in 2016 and in Mpape in Abuja Municipal area Council in 2018 resulted from the effects of the emergence of the near-surface faults along the flanks of the Romache paleofault zone.

REFERENCES

- Abaa, S. I. (1983). The Structure and Petrography of Alkaline Rocks of the Mada Younger Granite Complex, Nigeria. *Journal of African Earth Science* 3, 107-113
- Abong, A. A., Asuquo, B.U and Ushie C.A. (2020) Appraisal of main Extreme Parameters of Earthquakes in Nigeria using the Weibull Equations. *Archives of Current Research International* 20 (6), 71-85
- Abraham, E.A., Elijah, E.N and Oeyekachi, E.I (2020). Integrated geophysical investigation of recent earth tremors in Nigeria using aeromagnetic and gravity data *Journal of Geophysics and Engineering* 192, 1-13
- Adetona, A.A., Salako., K. A and Rafiu. A. A. (2018). Delineating the lineaments within the major structures around Eastern part of Lower Benue Trough from 2009 Aeromagnetic Data. *FUW Trends in Science and Technology Journal* 3(1), 175-179
- Ajakaiye, D. E., Hall, D. H., Ashiekaa, J. A., and Udensi, E. E. (1991). Magnetic Anomalies in the Nigerian Continental Mass Based on Aeromagnetic Surveys. *Tectonophysics*, 192, 211-230
- Ajakaiye, D.E., Hall, D.H and Millar T.H (1985). Interpretation of aeromagnetic data across the central crystalline shield area of Nigeria, in Kogbe C.A (ed), *Geology of Nigeria Elizabethan publishing Co. Lagos*, 81-92
- Ajakaiye, D.E., Hall, D.H., Miller, T.W., Verhergen, P.J.T., Awad, M.B. and Ojo, S.B. (1986). Aeromagnetic anomalies and tectonic trends in and around the Benue Trough, Nigeria. *Nature*, 319, 582-584.
- Akpan, O.U., and Yakubu, T. A. (2010). A Review of Earthquake Occurrences and Observations in Nigeria. *Earthquake Sciences*, 23, 289-294
- Akpan, O.U., Isogun, M.A., Yakubu, T.A., Adepelumi, A.A., Okereke, C.S., Oniku, A.S and Oden.M.I (2014). An evaluation of the 11th September, 2009 Earthquake and its implication for understanding the seismotectonics of South Western Nigeria. *Open Journal of Geology*, 2014, 4, 542-550
- Anifowose, A.Y. B., Oladapo, M.I., Akpan, O.U., Ologun, C.O., Adeoye-Oladapo, O. O., Tsebeje, S.Y and Yakubu T. A (2010). Systematic multi-technique mapping of the southern flank of Iwaraja fault, Nigeria. *Journal of Applied Science and Technology* 15(1-2), 70-76.
- Anudu, G. K., Stephenson, R. A and Macdonald David I.M (2014). Using high-resolution aeromagnetic data to recognize and map intra-sedimentary volcanic rocks and geological structure across the cretaceous middle Benue Trough, Nigeria. *Journal of African Earth Sciences* 99, 625-636
- Anudu, G.K., Onuba, L.N., Onwumesi, A.G. and Ikpokonte, A.E. (2012). Analysis of aeromagnetic data over Wamba and its adjoining areas in North-central Nigeria. *Earth Science and Resistivity Journal*, 16 (1), 25-33.

- Arogundade, A.B., Awoyemi, M.O., Hammed, O.S., Flade, S.C and Ajama, O.D (2020). Structural investigation of Zungeru-Kalangi fault zone, Nigeria using Aeromagnetic and Remote Sensing Data ESSO/Ar/<https://doi.org/10.1002/essoar.10502472.2/cc>
- Awoyemi, M. O., Hammed, O.S., Falade, S.C., Arogundade, A.B., Ajama, O.D. and Iwalehin P. O (2017). Geophysical investigation of the possible extension of Ifewara fault zone beyond Ilesa area, southwestern Nigeria. *Arab Journal Geosciences*. 10 (27), 1-14
- Black, R. (1984). The Pan African event in the geological framework of Africa. *Journal of African Earth Science*, 4, 3-8
- Brazier, R. A., Miao, Q., Nyblade, A. A., Ayele, A., and Langston, C. A. (2008). Local Magnitude Scale for the Ethiopian Plateau. *Bulletin Seismological Society of America*, 98, 2341-2348. <http://dx.doi.org/10.1785/0120070266>.
- Burke, K. C. and Dewey, J. F. (1972). Orogeny in Africa: In Dessauvage T.F.J., Whiteman A.J. (Eds.), *African Geology* (pp.583-608). Ibadan: University of Ibadan Press.
- Buser, Hugo. (1966). Paleostuctures of Nigeria and adjacent countries. Publi, Johannesstr. 3A D-70176 Stuttgart, Germany. 24, 90-98
- Caby, R. (1989). Precambrian terrains of Benin-Nigeria and Northeast Brazil and the Late Proterozoic South Atlantic. *Fiti Geological Society of America, Special Papers* 230, 145-158
- Campbell, W. H. (2003). Introduction to Geomagnetic Fields (2nd Ed). Cambridge University Press
- Centre for Geodesy and Geodynamic (2016). The Technical Committee Report on Kwoi Seismic tremor of 12th September 2016
- Dada, S. S. (2006). Proterozoic Evolution of Nigeria. In: Oshi O (Ed.), *The Basement Complex of Nigeria and its Mineral Resources* (A Tribute to Prof. M. A. O. Rahaman), (pp.29-44.). Ibadan: Akin Jinad & Co.
- Dobrin, M.B and Savit, C.H. (1988). Introduction to Geophysical prospecting fourth ed. McGraw- Hill, New York 867.
- Dobrin, M.B. (1976). Introduction to Geophysical Prospecting. Mc Graw- Hill Book C.O. New york.
- Egbelehulu, P., Mallam, A., Osagie, A.U and Taiwo, A. (2021). Structural Exploration of Aeromagnetic Data over part of Gwagwalada, Abuja for Potential Mineral Targets using Derivatives filters. *Journal of Geological Research*. 03:03, 44-51
- Elueze, A.A. (2003). Evaluation of the 7 March 2000 Earth Tremor in Ibadan Area, South Western Nigeria. *Journal of Mining and Geology*, 39, 79-83.
- Falconer, J. D. (1911). *The Geology of Northern Nigeria*. London, MacMillan.

- Fossen, H. (2010). *Structural Geology*, Cambridge, University Press, 51-185
- Goki, N.G., Onwuka, S.A., Oleka, A.B., Iyakwari, .S., Tanko, I.Y., Kana, A. A., Umbugadu, A. A and Usman, H. O (2020). Preliminary geological evidence for multiple tremors in kwoi, Central Nigeria. *Geo-environmental Disasters* (2020) 7:22, <https://doi.org/10.1186/s40677-020-00156-w>
- Havskov, J and Alguacil G. (2010). *Instrumentation in earthquake seismology*. Springer, revised reprint, 358
- Havskov, J. and Ottemoller, L. (2010). *Routine Data Processing in Earthquake Seismology*. Springer, New York. <http://dx.doi.org/10.1007/978-90-481-8697-6>.
- Havskov, J., and Ottemoller, L. (2000). SEISAN Earthquake Analysis Software. *Seismological Research Letters*, 70, 532-534. <http://dx.doi.org/10.1785/gssrl.70.5.532>
- Havskov, J., Kvamme, L.B., Hansen, R.A., Bungum, H., and Lindholm, C. D. (2002). The Northern Norway seismic Network: Design, Operation and Results. *Bull. Seismic. Society. Am.* 82, 481-496.
- Hossain, A.F., Nusirat J. and Mehedi A.A (2021). A study on recent earthquakes in and around Bangladesh. *Malaysian Journal of Civil Engineering*.
- Incorporated Research Institution for Seismology, 2013
- Isogun, M. A and Adepelumi, A.A (2014). The review of seismicity of central Mid-Atlantic Fracture zones. *International Journal of Scientific & Engineering Research*, 5:10, 1309-1316
- Jacobson, R. E., and Webb, J. S. (2021). The pegmatite of Central Nigeria. *Geological Survey of Nigeria*. 17, 1-17
- Kanamori, H. (1983). Magnitude Scale and Quantification of Earthquakes, *Tectonophysics*, 93, 185-199.
- Kearey, P. & Brooks, M. (1991). *An Introduction to Geophysical Exploration*. Melbourne: Blackwell Publishers. 211-301.
- Kearey, P., Klepeis, K. A. & Vine, F. J. (2009). *Global Tectonics* (3rd ed.). London: Wiley-Blackwell.
- Kovesi, P. (1997). Symmetry and Asymmetry from local phase. A¹ 97, *Tenth Australian Joint Conference on Artificial Intelligence* 2-4 December 1997
- Langston, C. A., Brazier, R., Nyblade, A. A., and Owens, T. J. (1998). Local Magnitude Scale and Seismicity Rate for Tanzania, East Africa. *Bulletin of the Seismological Society of America*, 88, 712-721
- Lawrence, B. (2007). Upseis educational site. Michigan Technological University www.geo.mtu.edu/Upseis/index.html

- Lay, T. and Wallace, T. C. (1995). *Modern Global Seismology*. California: Academy Press.
- Lienart, B.R.E. and Havskov, J. (1995). A computer program for Locating Earthquakes Both Locally and Globally. *Seismological Research Letters*, 66, 26-36. <http://dx.doi.org/10.1785/gssrl.66.5.26>
- Likkason, O.K., Ajayi,C.O and Shemang, E.M (2005). Some structural features of the middle Benue Trough, Nigeria Modelled from aeromagnetic anomaly data. *Science forum Journal Pure & Applied Science*, 8, 100-125
- Lowrie, W. (2007). *Fundamentals of Geophysics*. First Edition, Cambridge University Press, 374
- McCurry, P. (1976). *The Geology of the Precambrian to Lower Palaeozoic Rocks of Northern Nigeria*. A Review in Kogbe CA (Ed.). *Geology of Nigeria*. 15–39 Lagos: Elizabethan Publishers.
- Megwara, J.U. and Udensi E.E (2013). Lineaments study using aeromagnetic data over parts of southern Bida basin, Nigeria and the surrounding basement rocks. *International Journal of Basic and Applied Sciences* 2(1), 115-124
- Miller, H.G. Singh, V.J., (1994), Potential Field tilt –A new concept for location of potential field sources. *Applied Geophysics*, 32, 213-217
- Milligan, P.R. and Gunn R.J. (1997). Enhancement and presentation of airborne geophysical data, Australian Geology Survey Organization *Journal of Australian Geology and Geophysics*. 17(2), 63-75
- Mooney, W.D., Laske, G. and Guy Masters, T. (1998), A global crustal model at 5°* 5°. *Journal of Geophysical Research*. 103(1) 727-747.
- Nabighian, M.N. (1972). The analytical signal of two- dimensional magnetic bodies with polygonal cross-section: its properties and use for automated anomaly interpretation. *Geophysics*. 37(3), 507-517.
- Nabighian, M.N. (1984). Toward a three-dimensional automatic interpretation of potential field data via generalized Hilbert transforms: Fundamental relations. *Geophysics*, 49(6), 780-786.
- Neev, D., Hall, J.K. and Saul, J.M. (1982). The Pelusium Megashear System across Africa and Associated lineament swarms. *Journal of Geophysical Research*, 87 (B2): 1015-1030
- Ngama, E.J., and Akanbi E.S (2017). Qualitative Interpretation of Recently Acquired Aeromagnetic Data of Naraguta Area, North Central Nigeria. *Journal of Geography, Environment and Earth Science International* 11(3), 1-14
- Nigerian Geological Survey Agency, (2006). *Geology and Structural Lineament Map of Nigeria*. Abuja: Nigeria Geological Survey Agency, Abuja.

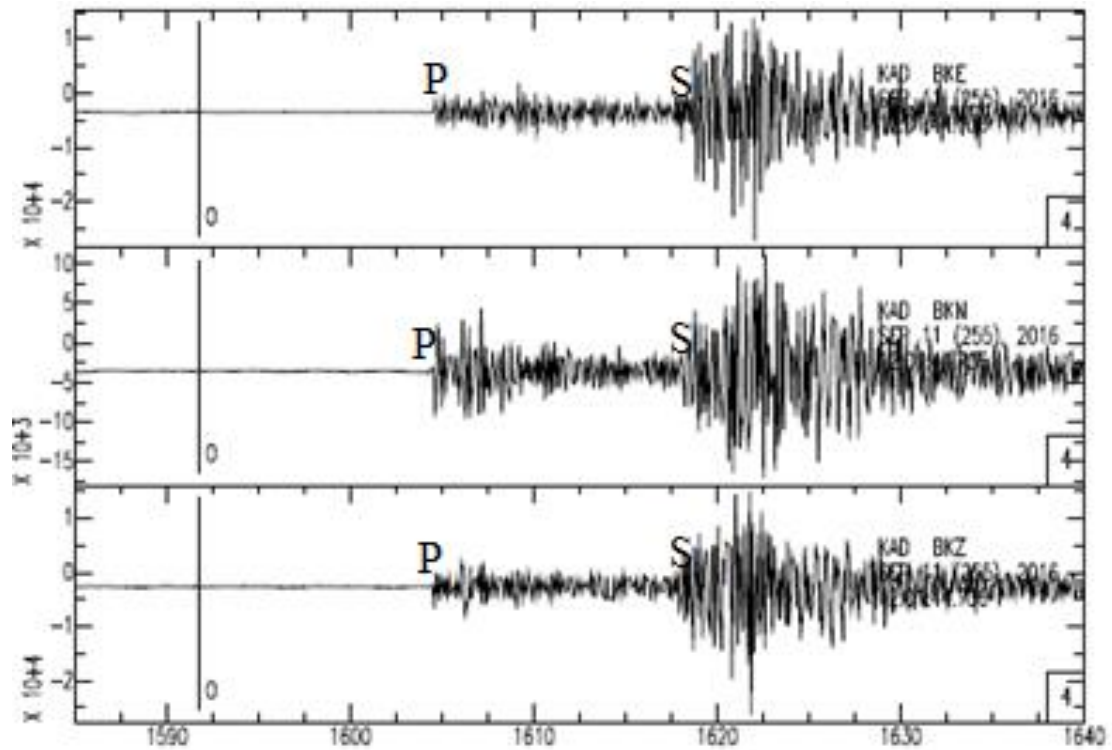
- Nigerian Geological Survey Agency, (2009). *Geological map of Nigeria on a scale of 1:2,000,000*. Nigeria Geological Survey Agency, Abuja.
- Obaje, N.G. (2009). *Geology and mineral resources of Nigeria*. Berlin: Springer-Verlag, Heidelberg, pp. 221. Hazards in Africa. *Nigeria Mining and Geosciences society Publication* Jos, 10-14.
- Okpoli C.C. and Oladunjoye M.A (2017). Precambrian Basement Architecture and lineaments Mapping of Ado-Ekiti Region using Aeromagnetic Data. *Geosciences Research* 2(1)
- Olasehinde, P. I., Pal, P. C., and Annor, A. E. (1990). Aeromagnetic Anomalies and Structural Lineaments in the Nigerian Basement Complex. *Journal of African Earth Science*, 11, (3/4), 351 – 355
- Onyewuchi, R. A., Opara, A. I., Ahirakwem, C. A., and Oko, F. U. (2012). Geological interpretations inferred from airborne magnetic and Landsat data: Case study of Nkalagu area, Southeastern Nigeria. *International Journal of Science and Technology* 2(4), 56 – 66
- Osagie, E. O. (2008). Seismic Activity in Nigeria. *The Pacific Journal of Science and Technology*, 9, 1- 6.
- Osazuwa, I. B., (1985). On the application of microgravity techniques for the monitoring of possible Earthquake occurrences in Nigeria, *Proceedings of National Seminar on Earthquakes in Nigeria*, 63 – 76.
- Saleh, A., Qudus, B., Magawata, Z. U., and Augie, A.I. (2020). Delineation of structural geologic features and depth to the magnetic sources over Allawa and its environs, North-central Nigeria. *International Journal of Advances in Engineering and Management (IJAEM)*; 2(6), 545-553: ISSN: 2395-5252: DOI: 10.35629/5252-0206545553.
- Sharma, P.V. (1987). Magnetic Method applied to Mineral Exploration. *Ore Geology Reviews*, 2: 9323-357
- Siddorn, J.P. (2011). Interpreting Aeromagnetic Data for Geological Structure Mapping in the Quest Area. SRK Consulting (Canada) Inc. Geological BC
- Stein, S and Wysession M. (2009). An introduction to Seismology, Earthquakes and Earth Structure chichester: John wiley & Sons ISBN 978-1-4443-1131-0
- Stein, S., and Wysession, M. (2003). An introduction to Seismology, Earthquakes and Earth structure Blackwell Publishing. 1- 52
- Tawey, M. D., Alhassan, D. U., Adetona, A. A., Salako, K. A., Rafiu A. A. and Udensi, E. E (2020). Application of Aeromagnetic Data to Assess the Structures and Solid Mineral Potentials in Part of North Central Nigeria *Journal of Geography, Environment and Earth Science International* 24(5): 11-29, 2020; Article no. JGEESI.58030 ISSN: 2454-7352

- Tawey, M. D., Udensi, E.E., Adetona, A.A and Alhassan, U. D (2019). Identification of Lineaments within Gitata using Derivative, Euler Deconvolution and Centre for Exploration Targeting CET. *International Journal of Science for Global Sustainability* ISSN: 2488-9229
- Telford, W. M., Geldart. L.P. and Sheriff, R.E., (1990). Applied Geophysics, Cambridge: Cambridge University Press, Pp. 64-84.
- Telford, W.M., Geldart, L.P., Sheriff, R.E. and Keys, D.A. (2002). Applied Geophysics. Cambridge University Press, Cambridge
- Thorne, L. and Terry W. C. (1995). Modern Global Seismology. Academic press. Page 535.
- Tsalha, M., Lar, U., Yakubu, T., Kadiri, U and Duncan, U. (2015). The review of the historical and recent seismic activity in Nigeria. *IOSR J Applied Geology Geophysics (IOSRJAGG)*, 3, 48-56.
- Turner, D.C. (1983). Upper proterozoic Schist Belts in the Nigerian sector of the Pan-African province of West Africa. *Precambrian Research*, 21, 55-79.
- Udensi, E. E, Osazuwa, I. B., and Daniyan, M. A. (2003). Trend Analysis of the Total Magnetic Field over the Bida Basin, Nigeria. *Nigerian Journal of Physics*, 15(1), 143-151.
- Udensi, E.E. (2001). Interpretation of the total Magnetic Field over the Nupe Basin Using Aeromagnetic Data. PhD thesis, A.B.U. Zaria, Nigeria
- Udias A, (1999). Principles of Seismology. Cambridge University press. 714
- Verduzco, B., Fairhead, J.D., Green, C.M and Mackenzie C., (2004). New insights into magnetic derivatives for structural mapping, *The Leading Edge*, 116-119.
- Yamusa, I.B., Yamusa, Y.B., Danbatta, U.A., and Najime T., (2018). Geological and Structural analysis using remote sensing for lineament and lithological mapping. IOP Conference Series: *Earth and Environmental Science*, 169, (2018) 012082. Doi:10.1088/1755-1315/169/1/012082

APPENDICES

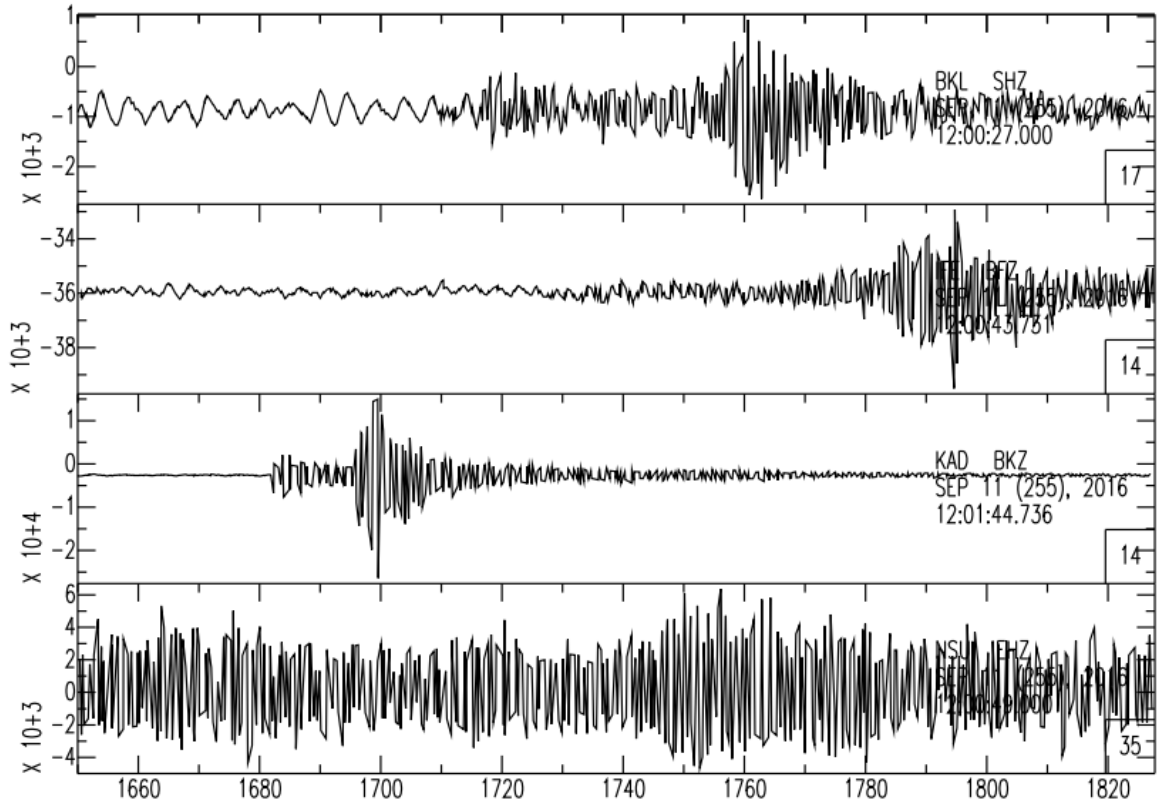
APPENDIX A

SEISMOGRAMS OF LOCAL EARTHQUAKES RECORDED AT THE SEISMOLOGICAL STATIONS USED IN THIS STUDY

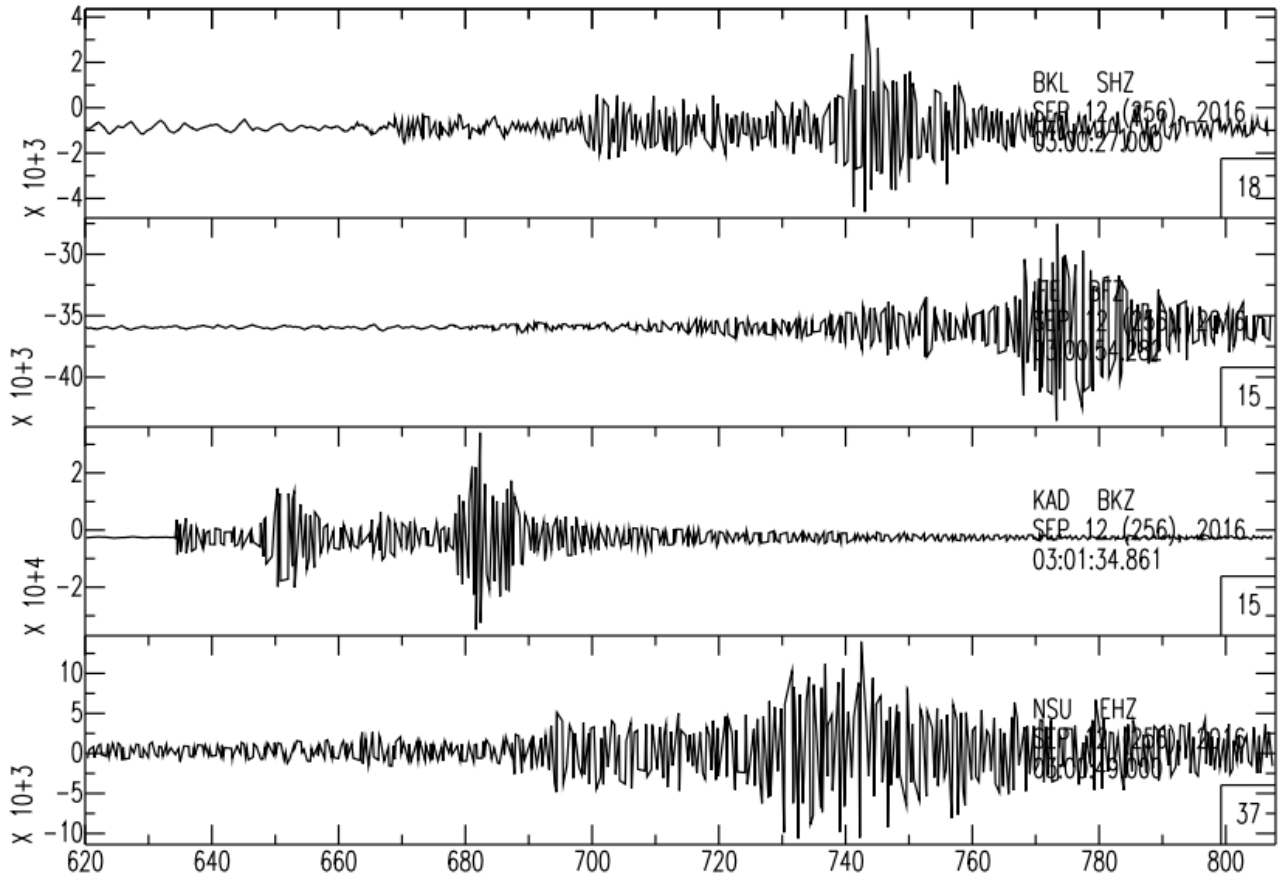


APPENDIX A1: Seismogram of the magnitude 2.8 earthquake of September 11, 2016 (First Kwoi Earthquake).

(BKE represents the east-west component, BKN denotes the north-south component and BKZ designate the vertical component, P is the P-wave and S, the S-wave).

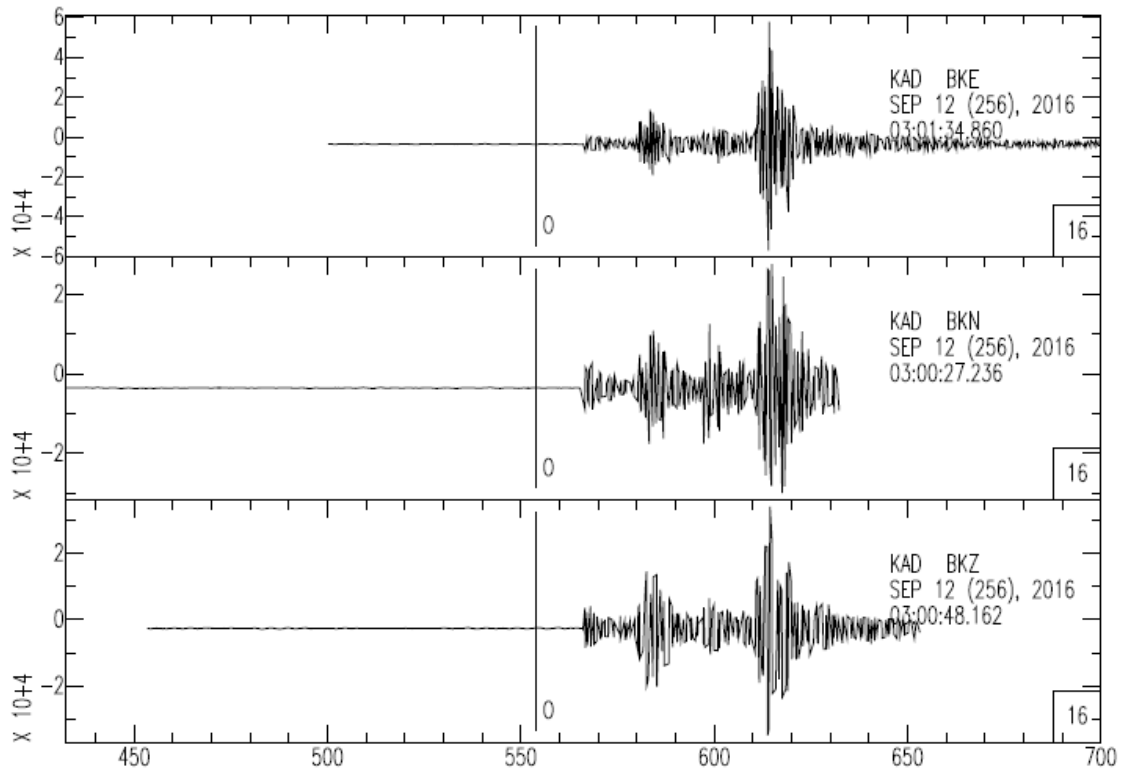


APPENDIX A2: Seismograms of first event (Kwoi earthquakes) recorded by different stations

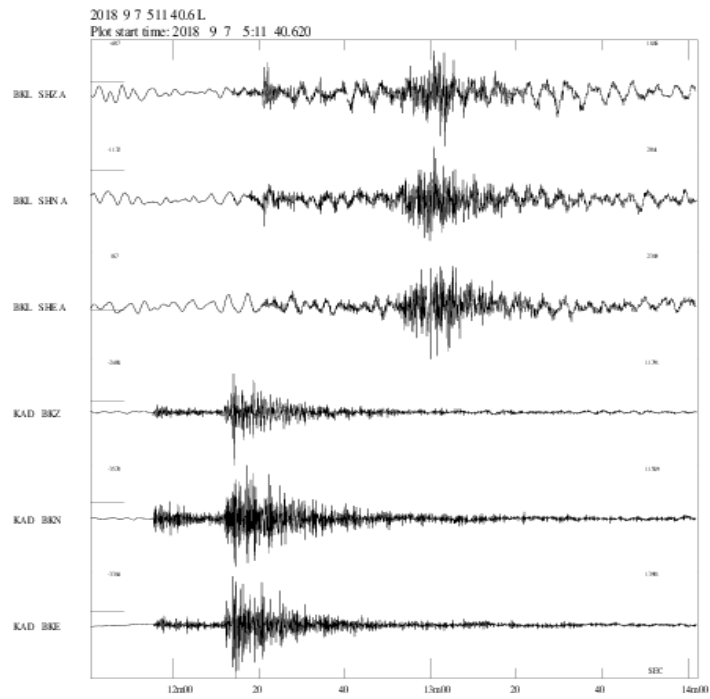


APPENDIX A3: Seismograms of the second and third event (Kwoi earthquakes)

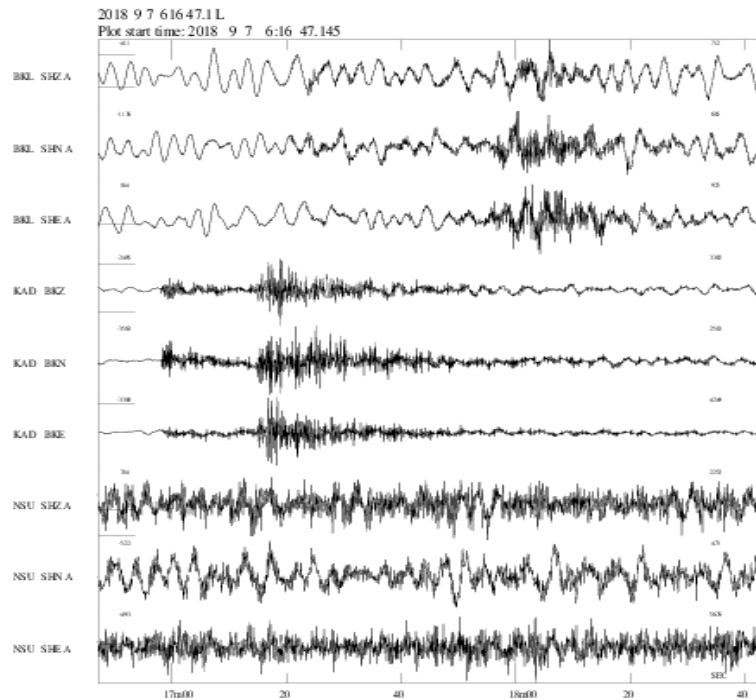
recorded by different stations



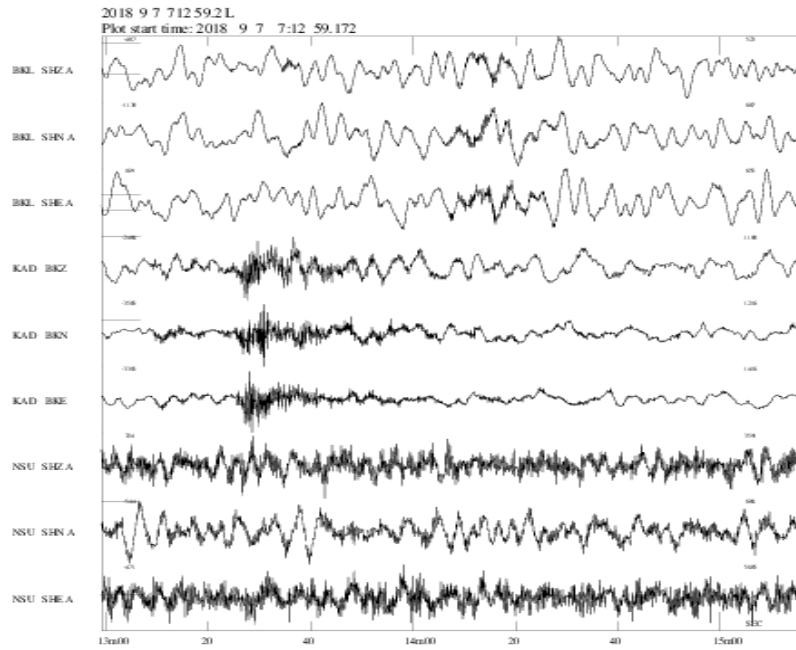
APPENDIX A4: Seismograms of the second and third Kwoi earthquakes recorded by Kaduna station



APPENDIX A5: Seismogram of the magnitude 3.0 Abuja earthquake of September 7 ,
 2018 (main shock) .



APPENDIX A6: Seismogram of Abuja earthquake (First aftershock) on the 7th
 September, 2018



APPENDIX A7: Seismogram of Abuja Earthquake (Second aftershock) on the 7th
September, 2018

APPENDIX B
SOURCE PARAMETERS OF EARTHQUAKES RECORDED AT ALL THE
STATIONS USED IN THIS STUDIES

APPENDIX B1

Source parameters of the Kwoi earthquakes

Date	Origin Time (GMT)	Lat (°N)	Lon (°E)	Depth (km)	Local mag.	Moment mag.
11/09/2016	12:28:16.5	9.570	8.070	10	2.8	3.1
12/09/2016	03:10:48.8	9.640	8.180	10	2.7	3.0
12/09/2016	03:11:20.0	9.590	8.130	10	3.1	3.1

APPENDIX B2

Source parameters and magnitudes of the Abuja earthquake

Date	Event	Origin Time (GMT)	Lat (°N)	Lon (°E)	Depth (km)	Local mag.	Moment mag.
06/09/2018	Mainshock	5:11:32.60	9.14	7.59	15	3.0	2.6
7/09/2018	Aftershock	6:16:17.80	9.03	7.50	12	2.6	2.5
7/09/2018	Aftershock	7:12:18.40	9.16	7.40	10	2.5	2.2